Performance and fatigue analysis of an integrated floating wind-current energy system considering the aero-hydro-servo-elastic coupling effects

Yang YANG[a,*,1], Jianbin FU[a,1], Zhaobin SHI[a], Lu MA[b], Jie YU[c], Fang FANG[d], Shunhua CHEN[e], Zaibin LIN[f], Chun LI[c]

[a]. Faculty of Maritime and Transportation, Ningbo University, Zhejiang province, Ningbo 315211, P.R. China

[b]. China Three Gorges Co., Ltd, Hubei province, Wuhan, 430014

[c]. School of Energy and Power Engineering, University of Shanghai for Science and Technology, Shanghai 200093, P.R. China

[d]. State Key Laboratory of Alternate Electrical Power System with Renewable Energy Source (North China Electric Power University), Beijing 102206, P.R. China

[e]. School of Marine Engineering and Technology, Sun Yat-sen University, Guangdong Province, Zhuhai 519082, P.R China

[f]. School of Engineering, University of Aberdeen, Aberdeen, AB24 3UE, United Kingdom.

*Corresponding author: Yang YANG, yangyang1@nbu.edu.cn

[1] All these authors have made equal contributions to the article

Abstract: Integration of multiple offshore renewable energy converters holds immense promise for achieving cost-effective utilization of marine energy. Integrated Floating Wind-Current Energy Systems (IFESs) have garnered considerable attention as a means to harness the abundant wind and marine resources in deep-sea areas using a single device. However, the dynamic responses of IFESs are significantly influenced by the coupling of aerodynamic and hydrodynamic loads. To assess the performance of a 10MW+ Spar-type IFES under wind-wave-current loadings, this study develops an aero-servo-elastic model within the hydrodynamic analysis tool AQWA. By utilizing the fully coupled model, this study investigates the platform motions, tower loads, and power production of the IFES under various environmental conditions. A comparative analysis is conducted by comparing the results with those obtained for a floating offshore wind turbine (FOWT). Furthermore, fatigue damage at the tower base of both the IFES and FOWT is evaluated. It is found that the presence of current turbines leads to improved platform stability, significant increases in total power production, and reduced fatigue damage at the tower base. These novel findings corroborate the potential and advantages of IFES concepts in enhancing the stability and energy harvest efficiency of floating marine energy converters.

Key worlds: Integrated floating wind-current energy system; Floating offshore wind turbine; Aero-hydro-servo-elastic coupling; Fatigue damage; Dynamic analysis.

1 Introduction

The energy demand is gradually increasing with the rapid development of the worldwide economy. The shortage of the traditional fossil energy resources leads to the acceleration of the pace in exploring and utilizing renewable energy [1-2]. Offshore renewable energy resources, especially the wind energy, have become a major contribution to the promotion of green and low-carbon energy transition because of the abundant resources and the mature technology. The newly-installed global wind power capacity was 94GW in 2021 as reported by the Global Wind Energy Council (GWEC). The accumulated offshore wind capacity is expected to achieve 361GW in 2030, including 6% of floating wind capacity in the deep-sea areas where also contain huge wave and current energy resources [3].

Numerous studies related to floating offshore wind turbines (FOWTs) have recently been carried out. Chen *et al.* [4] utilized a dynamic and sliding mesh coupling technique to study the unsteady aerodynamic properties of a FOWT subjected to single (surge or pitch) and combined motions. It was found that higher amplitudes and frequencies of motion led to increased fluctuations in the overall aerodynamic performance of the turbine. Moreover, the complex platform motions resulted in a negative impact on power generation in FOWT. Cheng *et al.* [5] used the open-source tool OpenFOAM to establish a fully-coupled aero-hydrodynamic model for conducting numerical simulation of FOWTs. The model employed the three-dimensional Reynolds-Averaged Navier-Stokes (RANS) equations and the Pressure-Implicit with Splitting of Operations (PISO) algorithm to solve the pressure-velocity coupling equations. The coupling effects between the semi-submersible platform and the NREL 5MW baseline wind turbine were investigated. Huang *et al.* [6] proposed a novel type of negative stiffness tuned mass damper (TMD-NS) for the stability control of FOWTs. The fixed-point theory was used to obtain the dimensionless optimal parameters of the TMD-NS for achieving a reduction in amplitude ratio and increase in the tuning bandwidth. The TMD-NS was found to be capable of reducing the nacelle displacement and velocity up to 55.87% and 48.18%, respectively. Chuang *et al.* [7] conducted both numerical simulations and scaled experimental tests for a barge 5MW FOWT. The numerical analysis was performed using ANSYS AQWA, while the experimental tests were conducted for a 1:64 scaled-down model. The hydrodynamic model was calibrated based on the results of free-decay tests, and regular and irregular wave model tests were conducted. The results of the tests showed that the fluid sloshing in the damping pool generated an oscillating force reducing the platform motion. Fang *et al*. [8] conducted numerical simulations of a 5MW wind turbine rotor using the improved delayed detached eddy simulation (IDDES) computational fluid dynamics (CFD) method after redesigning the rotor. It revealed that the aerodynamic performance of the FOWT was significantly affected by pitch motion parameters. Specifically, the amplitudes of rotor thrust and torque decreased with the increase of the pitch period, while a larger pitch amplitude could cause the stall phenomenon resulting in larger rotor thrust and torque. Chen *et al.* [9] compared the dynamic responses of a Spar and a semi-submersible scaled FOWT under different operating conditions. It was found that the Spar FOWT was more sensitive to the aerodynamic loads, while the surge and sway motion trajectories were more regular compared to those of the semi-submersible FOWT. Zhou *et al.* [10] examined the impacts of wave type and steepness on the hydrodynamics-aerodynamics responses of a 5MW semi-submersible FOWT. The dynamic response and power output of the FOWT were analyzed using a high-fidelity aero-hydro-mooring CFD solver. The results showed that there were significant differences in the floater motion response prediction between a focused wave and an irregular wave for the same spectrum. The reconstructed focused wave could be used as an alternative for extreme wave studies. Abdelbaky *et al.* [11] introduced a novel controller that utilizes a partial offline quasi-min-max fuzzy model-predictive control approach to analyze and enhance the performance of variable-speed wind turbines. Fleming *et al.* [12] improved the controller of the WindFloat by adding several control modules to the baseline controller. The results of the tests indicated that the use of a coupled linear model significantly improved the overall performance of performance and reduced the bending loads at the tower-base. Kong *et al*. [13-14] proposed an efficient distributed economic model predictive control strategy to enhance load-following capability. The result shows that the control strategy successfully tracks the reference power provided by the transmission system operator. Furthermore, simulation results demonstrate the control strategy's ability to effectively mitigate power pulsations, even in the presence of unbalanced grid voltage conditions.

The above studies mainly focused on the FOWTs with a capacity of up to 5MW. It is noted that adopting 10+MW FOWTs is an effective solution to reducing the levelized cost of electricity. Xue. [15] proposed a Spar-type platform for the application of 10 MW wind turbines in the deep-sea areas. A catenary mooring system was used for station-keeping of the platform. The reliability of the platform heave and pitch were verified by numerical simulations and model tests. Al *et al.* [16] developed a controller for the DTU 10 MW wind turbine supported by a Triple Spar platform to mitigate the rotor speed caused by wave loadings. The mitigation effects under wind and waves condition were examined using a high-fidelity numerical tool. It was found that the novel feedforward controller was capable of narrowing the rotor speed variation range. Ahn *et al*. [17] conducted a scaled model test to verify the performance of a scaled up 10MW FOWT based on the OC4 semisubmersible platform. The test results indicated that the wind turbine exhibited a good performance in terms of the response amplitude and natural period. Zhao *et al*. [18] proposed a conceptual 10MW semi-submersible platform and compared it with the OO-Star platform to validate the numerical model. The dynamic responses of the conceptual FOWT under various fault conditions were examined to confirm the stability of the proposed FOWT concept. In particular, the most significant impact on its heave dynamic behavior was observed under shutdown fault conditions. Xing *et al*. [19] conducted a study on the extreme dynamic responses of a 10MW semi-submersible type FOWT. The average conditional exceedance rate (ACER) and Gumbel methods were used to accurately quantify the FOWT system's extreme dynamic responses and to calculate the ultimate limit state loads.

The studies related to tidal/current energy is being carried out in parallel with the investigations on floating wind technology. Wang *et al*. [20] developed a 2-D vortex panel model based on the potential theory for unsteady hydrodynamics of a tidal turbine. The predicted transient forces on the blades and rotor wake were in good agreement with the test data. Roc *et al*. [21] proposed a new representation of tidal turbine based on an existing momentum and turbulence transport equations, which provided a basis for the development of an array layout optimization tool due to the short computational time. The experimental flume tests showed that the method could accurately predict the momentum and turbulent wake interactions. Badoe *et al*. [22] further employed the generalized actuator disk (GAD) approach to model the fluid structure interactions between multiple tidal energy converters. The physical tests were conducted to validate the numerical simulation results. The results showed that GAD method could effectively evaluate the influence of turbine spacing and arrangement.

Integration of multiple offshore renewable energy convertors is expected to further reduce the energy cost by sharing the floating platform and its seakeeping system [23-24]. Derakhshan *et al.* [25] proposed a method for the design of integrated wind-wave energy system. A case study was conducted for the UK and Syrian sea areas by analyzing the power performance of an integrated wind-wave energy system consisting of a 4.2 MW wind turbine and several wave energy convertors. It was shown that the wave energy devices increased the annual power generation by around 2%. Wan *et al*. [26] proposed the Spar Torus Combination concept composed of a Spar-type FOWT and a circular-shaped wave energy converter (WEC). The positive synergy between the FOWT and the WEC was demonstrated through experimental tests and numerical simulations. Mohanty *et al*. [27] developed a reactive power management method based on Flexible AC Transmission System (FACTS) devices to adjust the power management and stability of an offshore wind-tidal turbine power generation system. The effect of reactive power compensation and its impact on the dynamic stability of an isolated offshore wind and tidal current hybrid system were investigated and validated. Michele *et al*. [28] developed a mathematical model to analyze the hydrodynamic characteristics of an integrated wind-wave energy system under regular and irregular wave conditions. Collazo *et al*. [29-30] experimentally studied the coupling effects between the wave and the pendulous WEC integrated into a Spar FOWT. Lee *et al*. [31] investigated the hydrodynamic loads of a floating wind-wave energy system. A numerical study was conducted to multi-body hydrodynamic interaction between the floating platform and a multi-wavelength energy converter in the frequency domain based on the boundary element method. The analysis revealed that notable variations were observed in the dynamic responses of the WECs if the multi-body hydrodynamic interaction was taken into account.

Li *et al*. [32] developed an unsteady aerodynamic load prediction model within the dynamic analysis tool WEC-Sim for WECs. The coupled effects between the aerodynamic and hydrodynamic loads of the floating wind-wave-current energy system in were investigated. The results indicated that the platform motion response was reduced and the power output was increased compared to the conventional wind turbines. In addition, Li *et al*. [33-34] examined the short-term and long-term responses of the wind-wave-current system under extreme conditions. The findings indicated that the WEC enlarged the fatigue load in mooring lines. However, the interactions of the aerodynamic loads on the wind turbine and the hydrodynamic loads on the tidal turbine were not considered. In addition, the torque-pitch control was ignored for the tidal turbine. Chen *et al*. [35] introduced a new and innovative integrated floating wind-wave generation platform (FWWP), which includes a DeepCwind semi-submersible FOWT and a point absorber WEC. In order to investigate the dynamic responses and power generation capabilities of the FWWP under different operational sea-states, fully coupled analyses were carried out based on the F2A tool. It was found that the incorporation of WECs resulted in increased total power generation when compared to a standalone FOWT. Tian *et al*. [36] conducted research on a 5MW unsupported semi-submersible FOWT and various configurations of annular WECs. They compared the impact of different numbers of WECs on the hydrodynamic performance of the wind turbine. Comparison and discussion of the response amplitude operators (RAOs) and generated power of the studied combination structures in the time domain showed that the combination structure using three WECs has the highest power generation capacity. Yang *et al*. [37] developed a fully coupled model based on FASTv7 and AQWA for floating wind-current energy systems. It was found that the integrated floating wind-current energy system improved the platform motion stability and increased the power production when comparing to the FOWT.

Nonetheless, the interactions between the wind and current energy converters under complexly environmental conditions have not been sufficiently investigated. The major difficulties and challenges in the field of integrated floating energy systems mainly include: i) the need for a numerical simulation model that considers the coupled effects between wind and current energy converters; ii) the development of a pitch-torque control of tidal turbines under dynamic inflow conditions when integrated into a FOWT; iii) the quantitative analysis of the impact of tidal turbines on the dynamic responses of a FOWT under wind-wave-current loadings. Furthermore, a comprehensive evaluation of the fatigue performance of the tower in the presence of current turbines is required.

In order to address these research needs, this paper aims to quantitatively assess the fatigue performance of a 10MW+ Spar-type IFES, considering the effects of aero-hydro-servo-elastic coupling as a continuation of the previous study [37]. In this study, a fully Coupled Analysis Tool for Integrated Floating Energy Systems (CATIFES) was developed to consider the interactions between the FOWT and tidal turbines under different environmental conditions. The proposed case study involves a 10MW Spar-type FOWT integrated with two 550kW tidal turbines. This analysis of a10MW+ IFES is anticipated to provides valuable insights into the interactions of multiple energy converters within the integrated system.

Furthermore, the research evaluates the fatigue damage at the tower-base of the IFES throughout its design service life. This evaluation quantitatively assesses the impact of tidal turbines on extending the tower operational lifespan. These findings obtained from this study are expected to contribute to advancing knowledge in the field and highlight the potential benefits of integrating tidal turbines into FOWT systems.

This paper makes two significant contributions. First, a novel and fully coupled analysis tool (CATIFES) is developed to accurately predict the dynamic responses of an integrated floating wind-current energy system under wind-wave-current loadings. This addresses a significant research gap in the field of coupled analysis for floating wind-wave energy systems. By integrating the aerodynamic and hydrodynamic loads, the CATIFES provides a comprehensive framework for evaluating the performance of these complex systems. Secondly, this study quantitatively evaluates the effect of tidal turbines on the power production, platform motion, and tower fatigue damage of a 10 MW Spar-type FOWT. By comparing the responses of the integrated floating wind-current energy system with those of a standalone FOWT, strong evidence is provided to confirm the benefits derived from integrating multiple types of energy converters on a single floating platform. The evaluation not only highlights the increased power production resulting from the presence of tidal turbines but also demonstrates improved platform stability and reduced fatigue damage at the tower base.

This paper is organized as follows: Section 2 describes the IFES used in this study. The mathematical model of the CATIFES and the validations are presented in Section 3. Section 4 describes the load cases and presents the results and discussions of the IFES under combined wind-wave-current loads. Finally, the conclusions are presented subsequently in Section 5.

2 Introduction of wind-current energy system model

The IFES model proposed in this paper is composed of the DTU 10MW wind turbine, Spar platform up-scaled from the Hywind concept, the mooring system, and two 550kW tidal turbines designed by the Sandia National Laboratory. A preliminary analysis is performed to confirm the best installation position of the tidal turbines. The platform pitch and the overall power production of the IFES are balanced for the best while the tidal turbines are installed at 110m below the sea level. The schematic diagram of the IFES model is presented in Fig. 1.

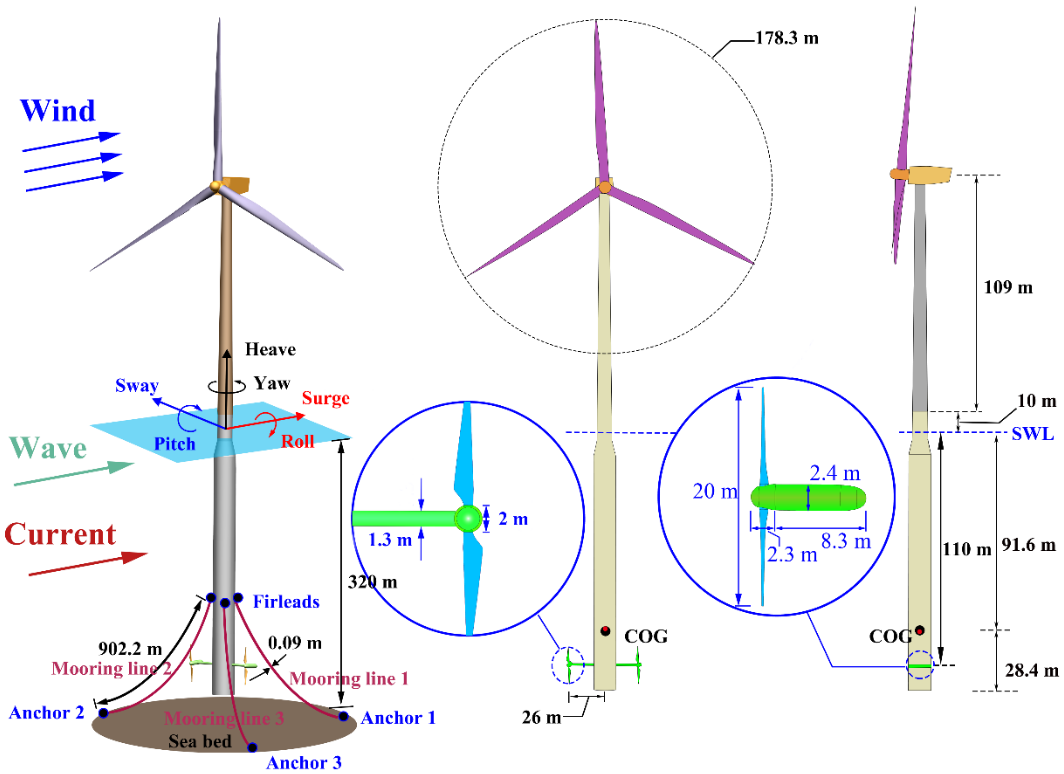

Fig. 1: The schematic diagram of the IFES model

2.1 Introduction to the 10MW wind turbine

The DTU 10MW reference wind turbine is jointly designed by the Technical University of Denmark and Vestas. [38] The full design details in terms of aerodynamic and structural parameters of the wind turbine are released to the public for world-wide researchers to improve offshore wind technology. The rotor diameter is 178.3m and the hub height is 119m. Table 1 presents the main design specifications of the wind turbine.

Table 1: Main design specifications of the DTU 10 MW wind turbine model

Property/Unit	Value	Property/Unit	Value
Rated power/MW	10	Rotor diameter/m	178.3
Rated wind speed/($m \cdot s^{-1}$)	11.4	Hub diameter/m	5.6
Cut-in wind speed/($m \cdot s^{-1}$)	4	Hub height/m	119
Cut-out wind speed/($m \cdot s^{-1}$)	25	Tower height/m	115.63
Cut-in rotor speed/rpm	6	Rotor mass/kg	227962
Rated rotor speed/rpm	9.6	Nacelle mass/kg	446036

2.2 The Spar platform and mooring system

The Spar platform used in this study is up-scaled from the Hywind Spar 5MW model by Shin [39] for supporting the 10MW wind turbine. The draft of the Spar platform is 120m for the application in 320m water depth areas. The platform mass including the ballast is 1.2×10^{7}kg. The mooring system is composed of three suspended chain lines with a length of 902.2m and an equivalent diameter of 0.09m. The properties of the Spar platform and the mooring system are shown in Table 2 and Table 3, respectively.

Table 2: Main properties of Spar platform

Platform property	Value/Unit
Water depth	320/m
Hull thickness	0.06/m
Platform mass including ballast	1.21×10^{7}/kg
Platform length	130/m
Platform diameter above taper	8.3/m
Platform diameter below taper	12/m
Center of mass	-91.96/m
Draft	120/m
Roll inertia	$1.273\times10^{11}/(kg\cdot m^{2})$
Pitch inertia	$1.273\times10^{11}/(kg\cdot m^{2})$
Yaw inertia	$6.056\times10^{10}/(kg\cdot m^{2})$

Table 3: Main properties of mooring system

Mooring property	Value/Unit
Number of mooring lines	3/-
Angel between adjacent lines	120/deg
Fairlead depth	70/m
Anchor depth	320/m
Unstretched length	902.2/m
Equivalent diameter	0.09/m
Equivalent axial stiffness	384.24/MN
Equivalent mass density in air	233.12/(kg/m)

2.3 Introduction of the tidal turbine

The tidal turbine is a 550kW two-blade model designed by the Sandia National Laboratory [40]. The mass of each tidal turbine including the nacelle and connecting beam is 6.13×10^4kg. The rotor and hub diameters are 20m and 2m, respectively. The distance between the platform centerline and hub of the tidal turbine is 26m. The blade shape is optimized by the HARP_Opt tool. The main design parameters are shown in Table 4. The parameters of blade sectional airfoil, twist angle, and relative thickness are shown in Table 5.

Table 4: Main design properties of tidal turbine

Property	Value/Unit
Rated power	550/kW
Cut-in, cut-out current speed	0.5,3.0/(m/s)
Minimum and rated rotor speed	3.0,11.5/rpm
Diameter of the rotor	20.0/m
Diameter of the hub	2.0/m
Rotor mass	1200/kg
Nacelle mass	40100/kg
Cross-beam mass	20000/kg
Drivetrain inertia moment	4.44×10^6/(kg·m^2)
Depth to hub below MSL	46.5/m

Table 5: The blade cross-section properties of the tidal turbine

Local radius/m	Aerofoil-	Twist/deg	Chord/m	Relative thickness/%

1	Cylinder	0.8	12.86	100
1.89	Interpolated	1.243	12.86	53.3
2.7	Interpolated	1.702	12.79	27.55
3.55	NACA 63-424	1.577	9.5	24
4.23	NACA 63-424	1.481	7.85	24
5.01	NACA 63-424	1.371	6.51	24
5.84	NACA 63-424	1.251	5.47	24
6.62	NACA 63-424	1.138	4.71	24
7.23	NACA 63-424	1.046	4.2	24
7.89	NACA 63-424	0.945	3.69	24
8.45	NACA 63-424	0.856	3.28	24
8.92	NACA 63-424	0.781	2.92	24
9.24	NACA 63-424	0.728	2.68	24
9.64	NACA 63-424	0.661	2.35	24
10	NACA 63-424	0.6	2.1	24

3 Fully coupled modeling of the IFES

To consider the coupling effect of the wind turbine and tidal turbines, the aero-servo-elastic simulation capability of OpenFAST for wind turbines is implemented through the external dynamic link library (user_force64.dll) of AQWA, which will be invoked for each determination of the platform responses. In addition, the prediction model of the hydrodynamic loads acting on the tidal turbines is developed based on the blade element momentum theory considering the cavitation. The Coupled Analysis Tool for Integrated Floating Energy Systems (CATIFES) is then developed by integrating the above two models.

3.1 Introduction to OpenFAST

OpenFAST was developed by the National Renewable Energy Laboratory (NREL) to simulate coupled dynamics of horizontal axis wind turbines. OpenFAST is designed to provide a robust software engineering framework for FAST development. The software is not only certified by Germanischer Lloyd but also has the open-source feature [41], therefore it is widely used in the academic research. OpenFAST mainly consists of several modules to consider the interaction effects between loads, control and structural dynamics. OpenFAST is significantly better at predicting the unsteady aerodynamic loadings compared to its previous version (FAST v7). This is why OpenFAST is used instead of FAST v7 to develop the CATIFES model.

The AeroDyn module is responsible for the prediction of aerodynamic loads on the rotor and tower. ElastoDyn is used to determine of structural dynamics of most components including the drivetrain and tower. This paper employs the modal method to examine the tower dynamics, assuming that the tower vibration is linearly represented by several bending modes and neglecting torsional modes. The Spar-type platform used in this paper experiences relatively small yaw moments, resulting in minimal torsional moments on the tower. Therefore, the actual torsional deformation of the tower is considered negligible compared to the variation of inflow wind direction. The assumed modal method has been applied in numerous studies examining the tower dynamics [42-43]. The impact of this assumption on simulation results is anticipated to be insignificant. The control scheme is conducted in the ServoDyn module for the regulation of blade pitch and generator torque. The CATIFES model developed in this study employs these three modules to obtain the aero-servo-elastic responses of the IFES. Specifically, these three modules are compiled as a user defined DLL that can be invoked by AQWA for external force prediction.

3.2 Blade element momentum theory for a tidal turbine

AeroDyn is an open-source tool supported and maintained by NREL [44] for the aerodynamic load prediction of horizontal axis turbine blades. This study employs the Aerodyn v15.04 that is capable of checking the cavitation problem to predict the hydrodynamic loads acting on tidal turbines under unsteady current conditions. The Generalized Dynamic Wake (GDW) model and Blade Element Momentum Theory (BEMT) are used in Aerodyn v15.04. The GDW model is used to calculate the axial induction velocity over the rotor plane under dynamic inflow condition [45]. The tangential induction velocity of each blade section is predicted using the BEMT as the rotation wake is not examined in the GDW model.

The BEM theory is combined by the blade element theory and the momentum theory. The wind turbine blade is treated as finite sections. The lift and drag coefficients of the blade sectional airfoil are used to calculate the aerodynamic force acting on each blade element. Fig. 2 presents the velocity triangle and force acting on an airfoil.

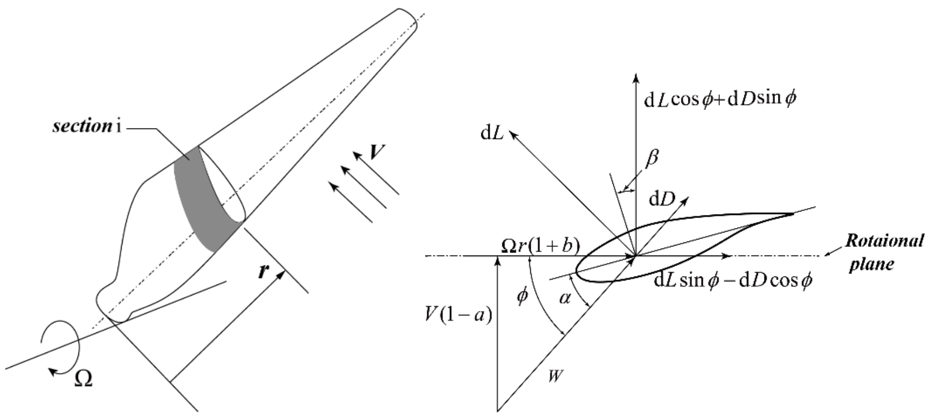

Fig. 2: Illustration of the velocity triangle and force analysis for a blade element

where Ω is the rotational speed of the rotor, r is the local radius of the blade element, V is the inflow velocity, and W denotes the relative inflow speed; a and b are the axial and tangential induction factors; α and β, respectively, the effective angle of attack, twist angle, and inflow angle of the blade element, ϕ is the relative inflow angle of the local element; L and D are, respectively, the lift and drag forces generated by the blade element.

The BEM theory is subsequently applied to compute the loads acting on each blade element, based on the lift and drag coefficients of the local sectional airfoil as represented in Eq. (1) and Eq. (2) [46].

$$\mathrm{d}T = \frac{1}{2}\rho W^2 c(C_l \cos\phi + C_d \sin\phi)\mathrm{d}r \tag{1}$$

$$\mathrm{d}M = \frac{1}{2}\rho W^2 c(C_l \sin\phi - C_d \cos\phi) r\mathrm{d}r \tag{2}$$

where dT and dM are, respectively, the thrust and moment of the local blade element; ρ is the density of the inflow fluid; C_l and C_d are, respectively, the lift and drag coefficients of the sectional airfoil; The Beddoes-Leishman dynamic stall model is used to correct the aerodynamic coefficients under unsteady conditions; c is the chord length of the blade element; $\mathrm{d}r$ is the length of the blade element.

In the analysis, the GDW model first solves the dynamic induction velocity distribution over the rotor. The angle of attack at each blade section is then calculated to call the lift and drag coefficients for the prediction of aerodynamic loads on the blades using Eq. (1) and Eq. (2). It is noted that the floating platform motions will be used to correct the current inflow speed V, which will be further described in the subsequent section. In addition, this study assumes the absence of cavitation when predicting hydrodynamic loads on the tidal turbines. The rated current speed is 2.0 m/s, and the low rated rotor speed of 11.5 rpm corresponds to a blade tip speed of 12.03m/s, making cavitation unlikely [47-49].

This study assumes that the BEM method remains valid for load prediction of the tidal turbines when installed on the platform. The BEM method is commonly employed for calculating the hydrodynamic performance of an individual tidal turbine. In this paper, the tidal turbines are installed on a floating platform. The distance between the blade tip and platform is not substantial, but a 50% blade tip clearance is maintained relative to the rotor diameter. Recent studies suggested that a tip clearance of 10% of the rotor diameter has no significant impacts on the blade's aerodynamic performance of wind turbines, and this conclusion can be extrapolated to tidal turbines [50-52]. Thus, this assumption is not expected to significantly influence on the results.

3.3 Introduction to AQWA and integration of the sub-models

The CATIFES model is developed within the hydrodynamic analysis software package, namely AQWA. AQWA that is a commonly-used tool for hydrodynamic analysis of marine and offshore structures [53]. The potential theory is employed by AQWA to solve the radiation and diffraction problems of a large size floater for obtaining the added mass, radiation damping, and wave excitation forces in frequency domain analysis. Potential flow assumption neglects the viscous effects of sea water when calculating the hydrodynamic loads on the platform. However, it is a widely accepted method in the field of marine engineering [54-55]. The influence of this assumption on the final results is relatively minor since an additional damping is introduced to account for the viscous effects.

Based on the frequency domain solutions, the platform responses can be calculated using a prediction-correction time-marching method in the AQWA solver, while mooring restoring forces and external loads calculated by the user defined DLL (user_force64.dll).

This paper assumes that the platform acts as a rigid body with six degrees of freedom since the restoring stiffness provided by the mooring system and ballast is significantly smaller than the structural bending stiffness. The participation rate of the platform bending modes is relatively minor compared to the translational and rational modes. This aligns with the typical modelling approach for dynamic analysis of Spar-type platforms. The assumption is expected to have a minimal impact on the results [56-58]. The governing equation of motion of the platform is given as:

$$(\boldsymbol{m}+\boldsymbol{A}_{\mathrm{wv}})\ddot{\boldsymbol{X}}(t)+\boldsymbol{C}\dot{\boldsymbol{X}}(t)+\boldsymbol{K}\boldsymbol{X}(t)+\int_0^t \boldsymbol{h}(t-\tau)\ddot{\boldsymbol{X}}(\tau)\mathrm{d}\tau=\boldsymbol{F}_{\mathrm{h}}(t)+\boldsymbol{F}_{\mathrm{t}}(t)+\boldsymbol{F}_{\mathrm{e}}(t) \tag{3}$$

where m is the platform inertial mass, $\boldsymbol{A}_{\mathrm{wv}}$ is the added mass; K and C are, respectively, the total stiffness and damping matrices; $\boldsymbol{X}(t)$, $\dot{\boldsymbol{X}}(t)$, and $\ddot{\boldsymbol{X}}(t)$ are, respectively, the displacement, velocity, and acceleration vectors of the platform; $\boldsymbol{h}(t)$ is the acceleration impulse function used to consider the radiation memory effect; $\boldsymbol{F}_{\mathrm{h}}(t)$ is the hydrodynamic load and $\boldsymbol{F}_{\mathrm{t}}(t)$ is the mooring restoring force; $\boldsymbol{F}_{\mathrm{e}}(t)$ denotes the external force including the aerodynamic load of the wind turbine and the hydrodynamic load of the tidal turbines. It should be noted that the external forces acting on the platform comprise not only the aerodynamic forces of the wind turbine but also the hydrodynamic forces generated by the tidal turbines.

Fig. 3 presents the logical flow of CATIFES. As can observed from Fig. 3, the dynamic responses of the wind turbine and the tidal turbine are solved by the external force DLL (user_force64.dll), while AQWA solves the platform responses based on the hydrodynamic loads and the external force on the platform. The user_force64.dll is invoked by AQWA at each time step to calculate the aerodynamic loads on the wind turbine and hydrodynamic loads on the tidal turbines. The platform displacement, velocity, and acceleration will be transferred to the DLL and used to for the calculation of the dynamic response of tower, nacelle, and blade structure and aerodynamic load. The shear force and bending moment at the tower-base are fed back to the DLL for the solution of platform motions.

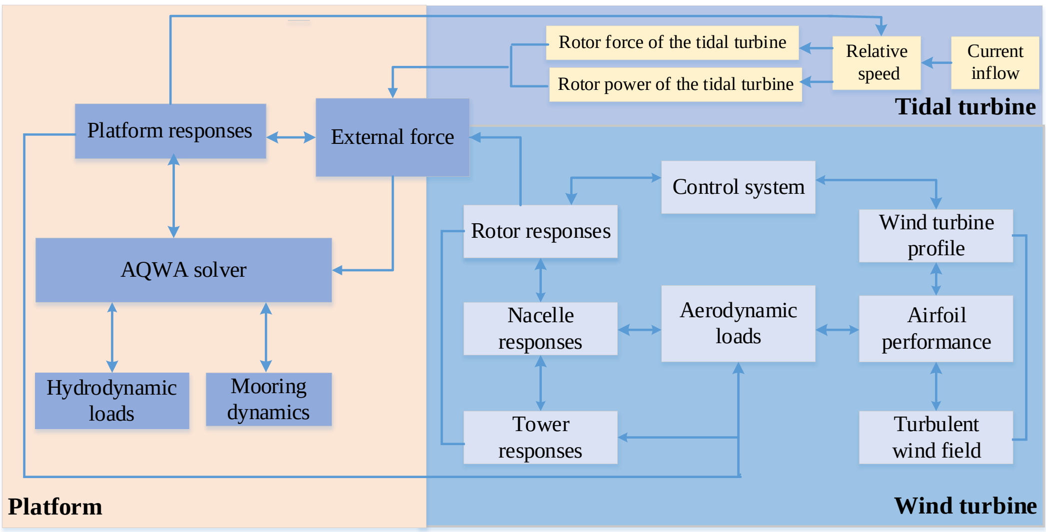

Fig. 3: Schematic of the coupling logic of CATIFES modules

Similarly, the hydrodynamic forces on the tidal turbines are calculated using the method presented in Section 3.2, which takes into account the contribution of platform motions to the current inflow speed $U_{curr,rel}$ using Eq. (4). The hydrodynamic load of the tidal turbines will be transferred back into AQWA acting as an external force for the prediction of platform motions. It is apparently that the aerodynamic load of the wind turbine or the hydrodynamic load of the tidal turbine is affected by the platform response, and vice versa.

$$U_{curr,rel} = U_{curr} - U_{ptfm,surge} - (Z_{tidal} - Z_{ptfm})U_{ptfm,pitch} + (Y_{tidal} - Y_{ptfm})U_{ptfm,yaw} \quad (4)$$

where U_{curr} is the defined inflow current speed at the tidal hub depth. $U_{ptfm,surge}$, $U_{ptfm,pitch}$

and $U_{ptfm,yaw}$ are the surge, pitch and yaw velocities of the platform, respectively. Z_{tidal} and Z_{ptfm} are the vertical coordinates of the CMs of the tidal turbine and platform, respectively. Y_{tidal} and Y_{ptfm} are the lateral coordinates of the CMs of the tidal turbine and platform, respectively.

Since the AQWA solver only accepts the external force applying at the mass center of the platform, transformations must be made to the aerodynamic loads calculated in the DLL. Taking the coupling between the platform and the wind turbine as the example, the platform motions generated by the AQWA solver is the response at the mass center of the platform, while the platform motion accepted by the DLL for updating the kinematics of the wind turbine is at a specific reference point that is usually the tower-base. Therefore, the Euler angle transformation matrix given below is used for the data transfer between the AQWA solver and DLL [59].

$$\boldsymbol{E} = \begin{bmatrix} \cos\theta_2\cos\theta_3 & \sin\theta_1\sin\theta_2\cos\theta_3 - \cos\theta_2\sin\theta_3 & \cos\theta_1\sin\theta_2\cos\theta_3 + \sin\theta_1\sin\theta_3 \\ \cos\theta_2\sin\theta_3 & \sin\theta_1\sin\theta_2\cos\theta_3 + \cos\theta_2\sin\theta_3 & \cos\theta_1\sin\theta_2\cos\theta_3 - \sin\theta_1\sin\theta_3 \\ -\sin\theta_2 & \sin\theta_1\cos\theta_2 & \cos\theta_1\cos\theta_2 \end{bmatrix} \quad (5)$$

where θ_1, θ_2, and θ_3 are, respectively, the roll, pitch, and yaw angles of the platform.

The platform motion output from AQWA is transformed as follows:

$$\boldsymbol{D}_{DLL} = \boldsymbol{D}_{AQWA} - \boldsymbol{E} \bullet \boldsymbol{P} \quad (6)$$

where $\boldsymbol{P}$ is the position vector from the platform reference point to the mass center of platform, $\boldsymbol{D}_{AQWA}$ and $\boldsymbol{D}_{DLL}$ are, respectively, the platform displacement vectors obtained at AQWA and the incoming DLL.

The velocity of the platform is transformed as follows:

$$\boldsymbol{U}_{DLL} = \boldsymbol{U}_{AQWA} - \boldsymbol{E} \bullet \boldsymbol{P} \times \boldsymbol{\omega} \quad (7)$$

where $\boldsymbol{U}_{AQWA}$ and $\boldsymbol{U}_{DLL}$ are the platform velocity vectors obtained in AQWA and the one used in the DLL, respectively; $\boldsymbol{\omega}$ is the rotational velocity vector of the platform obtained in

AQWA.

The platform acceleration is not available for transfer between the solver and the DLL. Therefore, the first-order forward difference of the velocity is used to denote the acceleration as follows:

$$\boldsymbol{a}_{DLL} = \frac{\boldsymbol{U}_{DLL} - \boldsymbol{U}'_{DLL}}{\Delta t} \tag{8}$$

where $\boldsymbol{a}_{DLL}$ is the platform acceleration and $\boldsymbol{U}'_{DLL}$ is the platform velocity at the last time step, Δt is the time step of the simulation.

The tower-base loads calculated in the DLL will be transferred to the AQWA solver as a external force for the prediction of the platform motion. It is noted the tower-base loads are referred to the local platform coordinate system, however, the external force applying at the mass center of platform is referred to the inertial coordinate system. The loads are corrected as follows:

$$\boldsymbol{F}_{AQWA} = \boldsymbol{E}^{-1} \bullet \boldsymbol{F}_{DLL} \tag{9}$$

$$\boldsymbol{M}_{AQWA} = \boldsymbol{E}^{-1} \bullet (\boldsymbol{M}_{DLL} - \boldsymbol{P} \times \boldsymbol{F}_{DLL}) \tag{10}$$

where $\boldsymbol{F}_{AQWA}$ and $\boldsymbol{F}_{DLL}$ are the translational force vectors fed back into in AQWA and calculated in the DLL, respectively; $\boldsymbol{E}^{-1}$ is the inverse of the transformation matrix $\boldsymbol{E}$; $\boldsymbol{M}_{AQWA}$ is the moment vector applying at the mass center of the platform referred to the inertial coordinate system; $\boldsymbol{M}_{DLL}$ is the moment vector at the tower-base referred to the local platform coordinate system.

3.4 Validation of the CATIFES

Since there is no published experimental or numerical simulation data for the wind-current type IFES, the validation of the CATIFES model is examined by verifying its capability in performing coupled analysis of a FOWT and in predicting performance of tidal turbines, respectively.

The dynamic responses of the DTU 10MW wind turbine supported by the Spar platform under 9m/s turbulent wind condition are calculated using CATIFES and OpenFAST v3.2, respectively. The results during 800s to 3600s is selected for the comparison to avoid the influence of the transient behavior. Fig. 4 shows the comparison of the platform motions. It can be observed that the results calculated by CATIFES and OpenFAST agree very well in trends and magnitudes. More specifically, the mean values of the pitch predicted by OpenFAST v3.2 and CAT4IFES are respectively 8.3 degrees and 8.5 degrees, meaning the difference is 2.4%. The difference between the maximum pitch predicted by the present model and OpenFAST is 0.7 degrees, equivalent to a relative error of 4.8%. The platform surge motions obtained by CATIFES and OpenFAST are almost identical in the domain variations. The comparison of the platform motions indicates that CATIFES could produce acceptable dynamic responses of a FOWT under turbulent wind conditions.

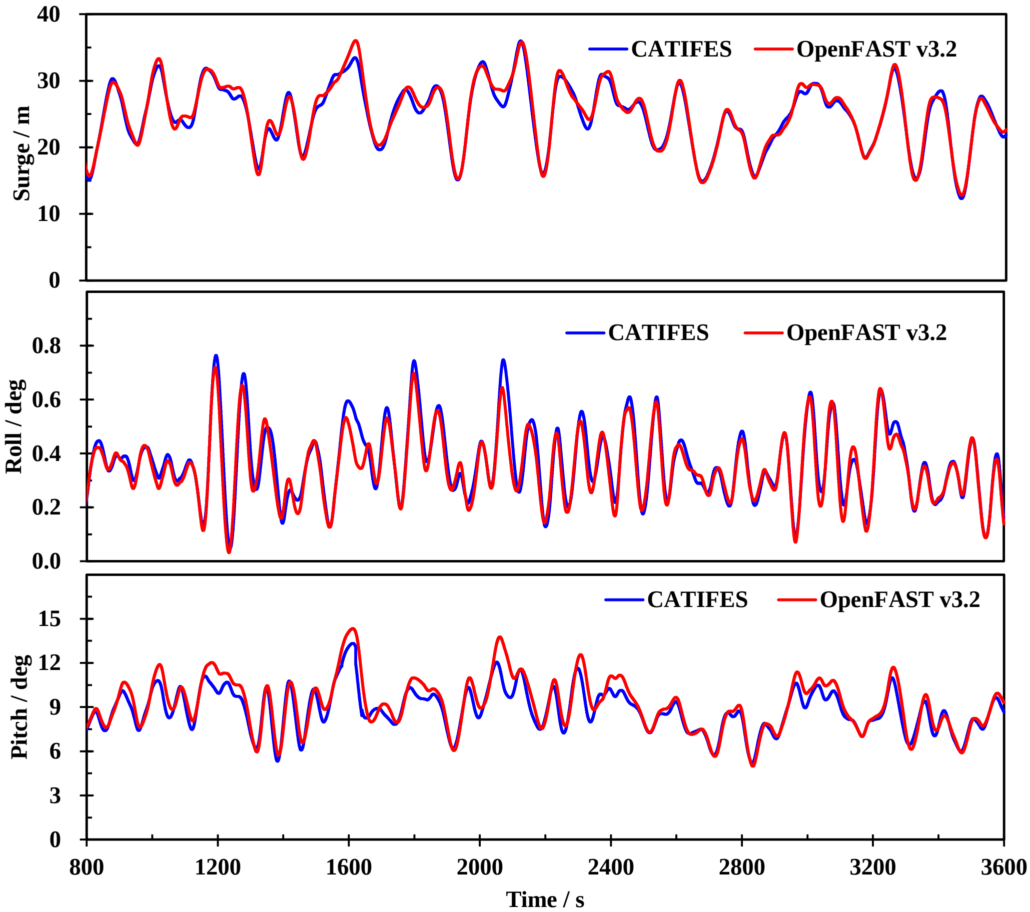

Fig. 4: Comparison between the platform motions predicted by the present CATIFES model

and OpenFAST

Fig. 5 presents the fairlead tension in the mooring lines. Good agreements between the fairlead tensions in each mooring line predicted by CATIFES and OepnFAST are observed. There is only a small difference for the maximum values. More specifically, the mean value and standard deviation of the fairlead tension in mooring line #2 predicted by CATIFES are 2.55MN and 0.12MN, while the corresponding results obtained using OpenFAST are 2.58MN and 0.13MN. The maximum tensions in mooring line #2 calculated by CATIFES and OpenFAST are 2.90MN and 2.92MN, respectively. The relative error is only 0.68%.

The main reason producing the difference between the simulation results of the present model and OpenFAST is that there is a minor difference between the mooring modeling theories of OpenFAST and AQWA. AQWA uses the finite element method to consider the dynamic mooring effects and calculates the hydrodynamic loads acting on the mooring based on the wave velocity at the current position of the mooring. OpenFAST, on the other hand, considers the dynamic effects of the mooring using the lumped mass approach, and the hydrodynamic loads applied to the mooring are based on the wave motion at the initial position of the platform. Although a minor difference between the results is observed, the overall agreement is good enough, indicating that the CAT4IFES model can consider the coupling effect between the aero-elasticity and hydrodynamics of the FOWT.

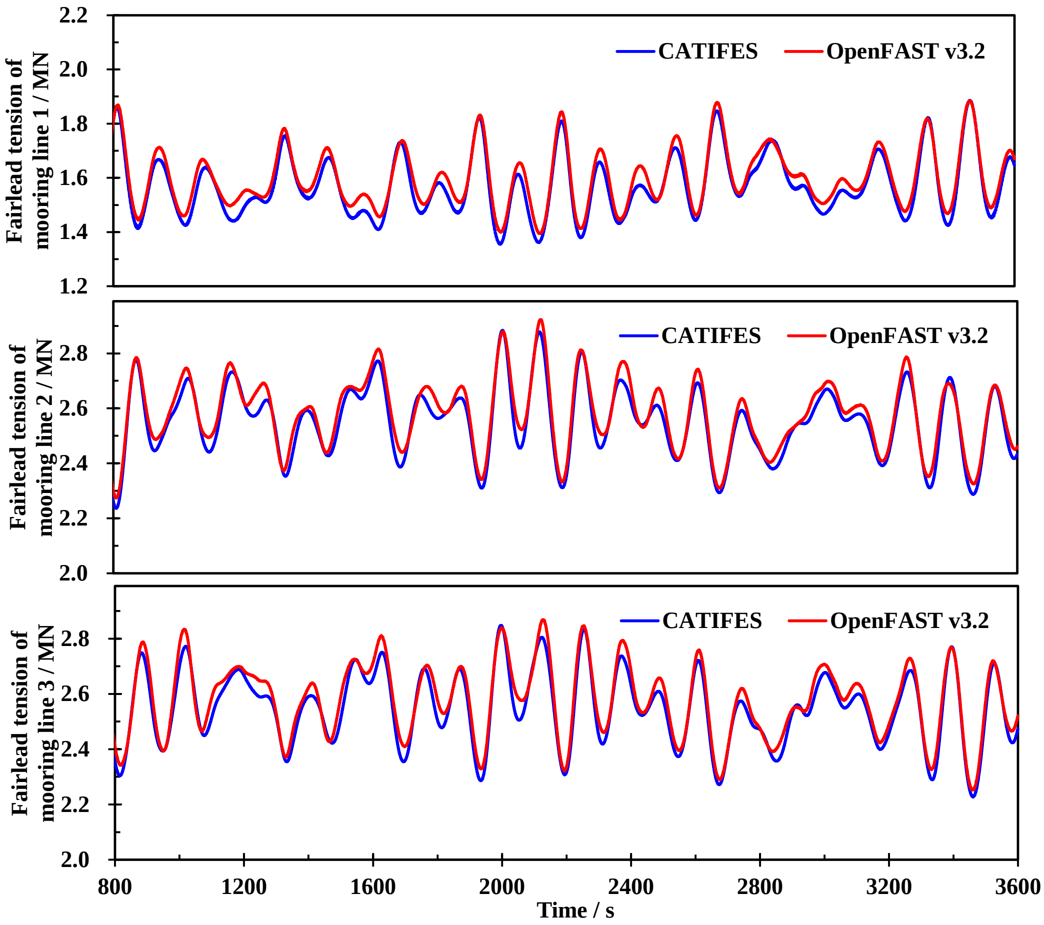

Fig. 5: Fairlead tension of CATIFES and OpenFAST v3.2

The experimental data from the model test conducted by Bahaj et al [47]. and Doman et al [48]. is used to validate CATIFES for predicting the hydrodynamic performance of a tidal turbine. The test data and numerical simulation results are presented in Fig. 6. In model test 1, the numerical simulation predicted power and thrust coefficients that are consistent with the trends in the test data, although the power coefficient is slightly overestimated for high tip-speed ratios (TSR). In model test 2, the numerical results at low TSR are slightly higher than the test data due to the cavitation effect. However, within the common operating range of TSR 4-6, the power and thrust coefficients predicted by the present CATIFES agree well with the test results. Overall, the consistency between the numerical simulation results and the model tests is good, confirming the accuracy of the numerical model in predicting the response of tidal turbines is acceptable.

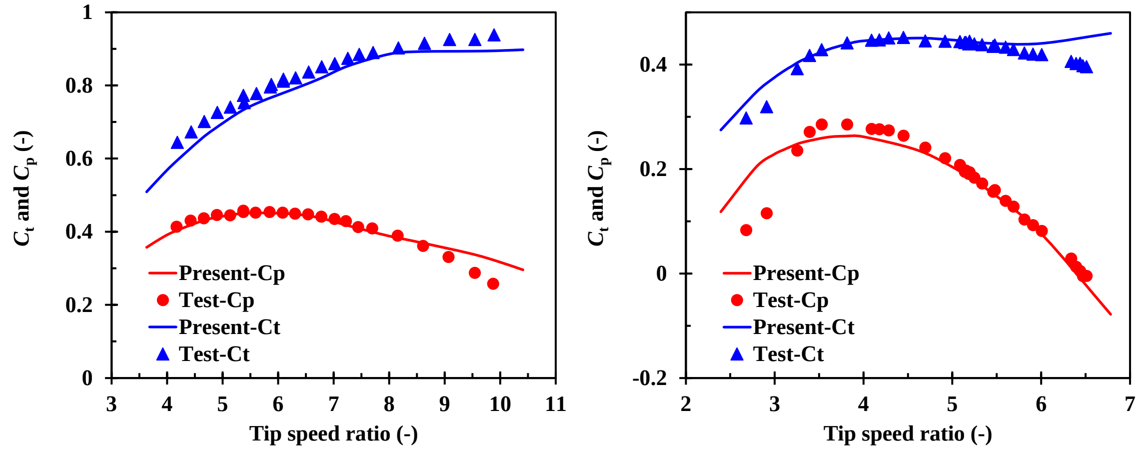

(a) Model test 1 (b) Model test 2

Fig. 6: Comparison between tidal turbine responses obtained from the present numerical simulations and model tests; (a) model test 1 conducted by Bahaj *et al.* [47] for a 0.8 m diameter rotor, (b) model test 2 conducted by Doman *et al.* [48] for a 0.762 m diameter rotor.

A pitch-torque controller is developed to adjust the power production of the tidal turbine. In order to validated the controller, the simulation of the tidal turbine suffering a step current speed condition is conducted. The duration of each step speed is 50s. Fig. 7 presents the generator power, rotor speed and blade pitch angle of the tidal turbine under the step current speed condition. It is observed that a steady state is quickly achieved after a quite short transient period between each two speeds. The power and rotor speed in the steady states are compared with the design parameters as presented in Fig. 8. It can be observed that the numerical results are identical to the design parameters for each inflow current speed. The comparison indicates that the controller implemented in this study is efficient in adjusting rotor speed and blade pitch to achieve a target power.

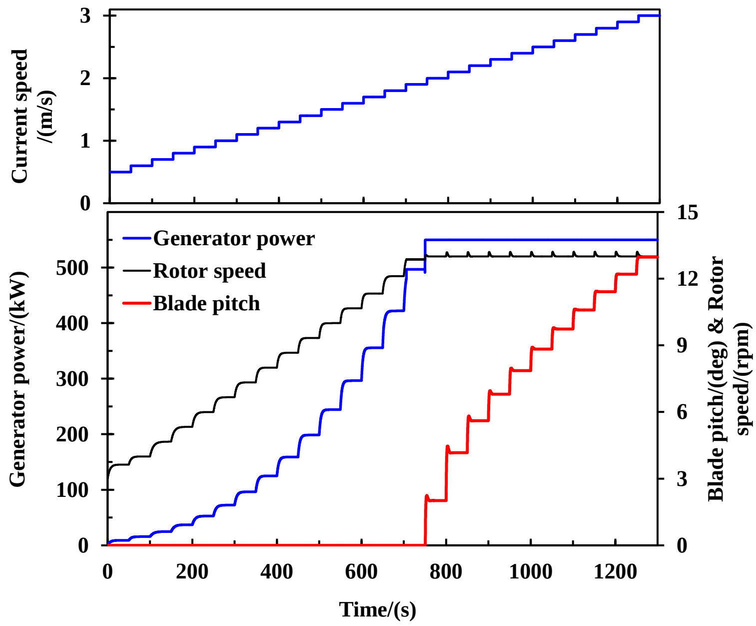

Fig. 7: Controller performance under an unsteady inflow condition

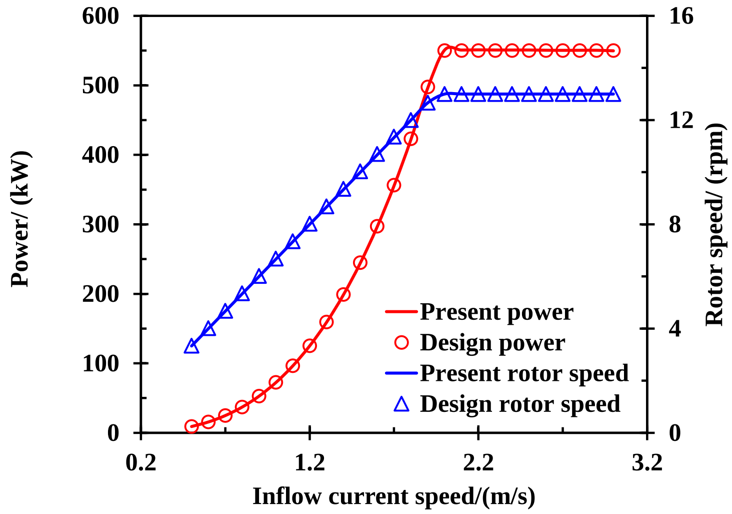

Fig. 8: Comparisons of power and rotor speed under steady conditions

4 Results and discussions

4.1 Definition of load cases

Table 6 presents the definitions of the environmental conditions of the load cases examined in this study. The wind speed gradually increases from 3m/s to 25m/s. The three-dimensional wind field of each load case is generated using TurbSim based on the Kaimal spectrum. The significant wave height and spectral peak period corresponding to each wind speed are defined according to the met-ocean data measured from an Eastern coastal site of the USA [53]. The JONSWAP wave spectrum with a peak shape parameter of 3.3 is applied for the irregular waves.

Table 6: Load cases for different environmental conditions

	Wind speed/(m/s)	Significant Wave Height/m	Peak Spectral Period/s	Current speed at MSL/(m/s)	Probability
LC1	3	1.089	8.569	0.61	2.34%
LC2	4	1.108	8.496	0.65	3.57%
LC3	5	1.146	8.392	0.68	4.13%
LC4	6	1.198	8.264	0.73	5.56%
LC5	7	1.269	8.103	0.92	6.98%
LC6	8	1.359	7.923	1.06	7.78%
LC7	9	1.478	7.724	1.22	8.24%
LC8	10	1.617	7.569	1.31	7.66%
LC9	11	1.779	7.451	1.46	7.00%
LC10	12	1.954	7.443	1.52	6.77%
LC11	13	2.144	7.457	1.66	6.32%
LC12	14	2.350	7.508	1.70	5.99%
LC13	15	2.573	7.629	1.81	5.24%
LC14	16	2.808	7.810	2.01	4.70%
LC15	17	3.062	8.047	2.12	4.17%
LC16	18	3.361	8.294	2.23	3.24%
LC17	19	3.645	8.549	2.42	2.89%
LC18	20	3.860	8.796	2.51	2.13%
LC19	21	4.081	9.042	2.66	1.83%
LC20	22	4.335	9.288	2.71	1.15%
LC21	23	4.610	9.534	2.81	1.00%
LC22	24	4.905	9.779	2.86	0.72%
LC23	25	5.216	10.025	2.98	0.66%

The dynamic responses of the IFES with two tidal turbines installed at 110m below the sea level calculated using CAT4IFES and compared with those of the FOWT for the load cases presented in Table 6.

The simulation duration of each load case is set to 4400s and time step is 0.005s. To avoid the influence of transient response, the statistical analysis is performed for the responses in 2000s to 4400s.

4.2 Time-varying responses in the rated condition

In order to obtain a preliminary understanding of the dynamic behavior of the IFES and the efficacy of integrating tidal turbines within the FOWT system, the dynamic responses of the IFES under a specific load case are compared with those of the FOWT. Fig. 9 presents the platform motions of the IFES and the FOWT under LC9 in which the wind speed is 11m/s and the current speed is 1.46m/s. Due to the presence of the tidal turbines, the average platform surge of the IFES is larger than that of the FOWT, while the maximum value decreases. More specifically, the maximum platform surge motions of the IFES and the FOWT are respectively 32.51m and 35.50m, implying a reduction of 8.42% is obtained. Moreover, the fluctuation in the surge motion is alleviated. The standard deviation of the platform surge corresponding to the IFES is 4.38m, while the value of the FOWT is 6.56m. The reason is that the hydrodynamic thrust on the tidal turbines prevents the platform from excessively moving back against the wind when the aerodynamic damping is decreased duo to the increase of blade pitch angle.

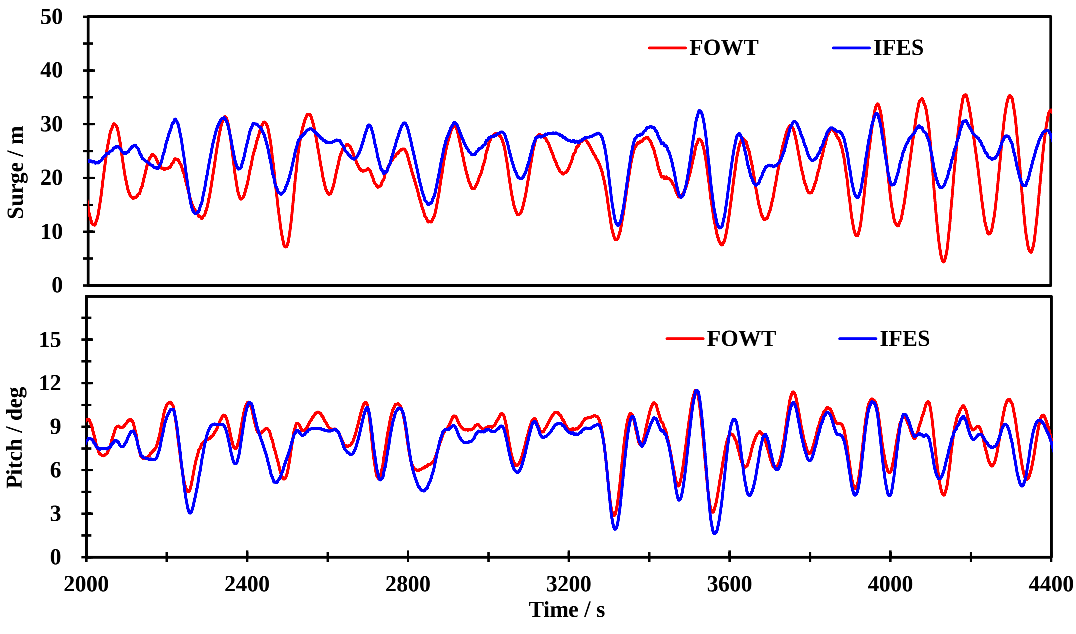

Fig. 9: Platform motion of the IFES and FOWT under LC9

As aforementioned in this paper, the tidal turbines are installed at 110m below the mean sea level which is 18.4m lower than the mass center of the platform. The hydrodynamic thrust of the tidal turbines produces a bending moment reverse to that generated by the wind turbine. Therefore, the IFES has a relatively smaller platform pitch than the FOWT as observed from Fig. 9 (b). The average platform pitch of the IFES is reduced by 6.42% compared to that of the FOWT, from 8.25 degrees to 7.72 degrees.

Fig. 10 presents the mooring tension of the FOWT and IFES. The mooring line #1 (windward) of the IFES experiences higher tension due to the more stretched state caused by the relatively larger horizontal thrust. As the platform approaches the leeward mooring, the mooring line #2 and #3 become loose and therefore experience a relatively smaller tension.

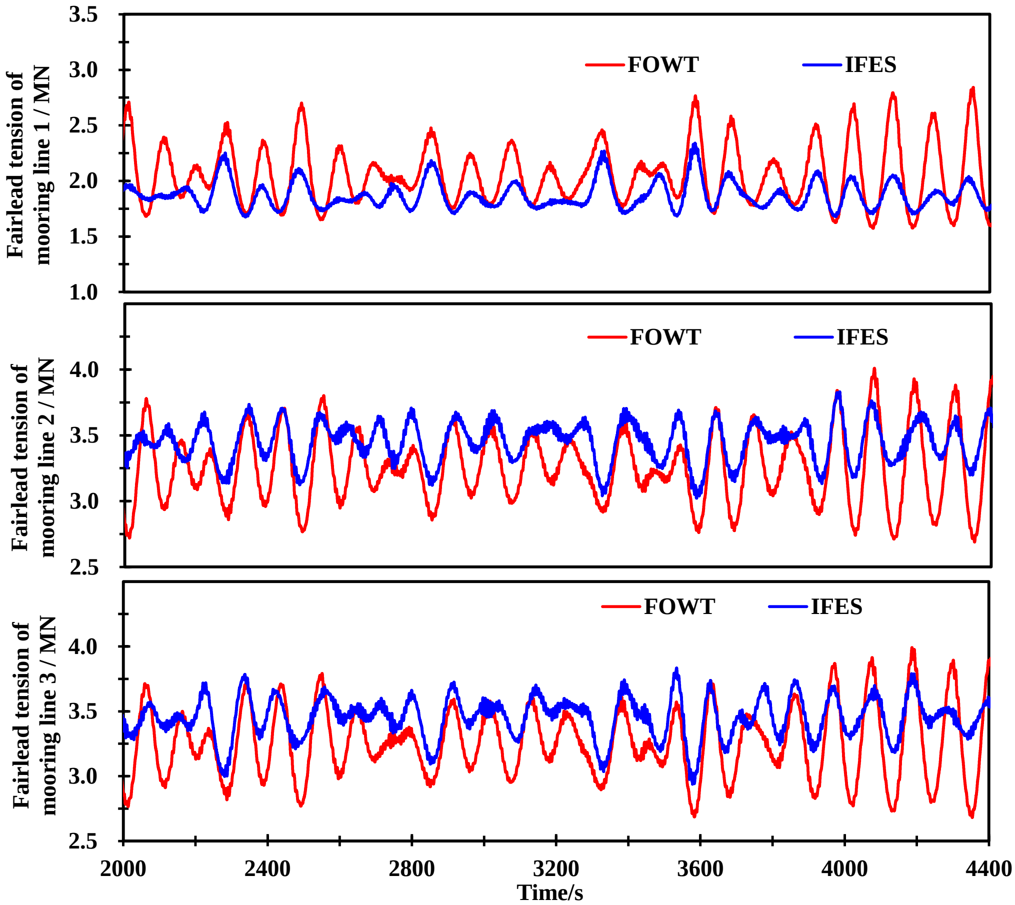

Fig. 10: Fairlead tensions of the mooring line under LC9

Table 7 presents the statistical values of tensions in the three mooring lines of the IFES and FOWT. Error means the difference between the results of the IFES and FOWT. It shows that the maximum tension of each mooring line of the IFES is smaller than that of the FOWT, especially for mooring line #1 placed in the downwind direction. The maximum tension is reduced by 17.61%. The average tension in mooring lines #2 and #3 of the IFES is 5.83% relatively larger than that of the FOWT. Nonetheless, the standard deviation of the tension in each mooring line is significantly reduced. The reductions in mooring line #1, #2 and #3 are respectively55.56%, 44.44% and 40.74%

Table 7: Statistical values of mooring tensions / MN

		FOWT	IFES	Error/%
Mooring line #1	Max	2.84	2.34	-17.61
	Average	2.06	1.87	-9.22
	Std.dev	0.27	0.12	-55.56
Mooring line #2	Max	4.01	3.83	-4.49
	Average	3.26	3.45	5.83
	Std.dev	0.27	0.15	-44.44
Mooring line #3	Max	3.99	3.83	-4.01
	Average	3.26	3.45	5.83
	Std.dev	0.27	0.16	-40.74

Fig. 11 presents the output power of the IFES and FOWT. The average power generated by the wind turbine of the IFES is 8.63MW and the FOWT produces a mean power of 8.59MW. In addition, the generator power of the wind turbine in the IFES is smoother compared to the FOWT due to the more stable platform motions. As a result, the average output power increases by 0.47% and the corresponding standard deviation decreases by 6.82%. Moreover, the two tidal turbines produce an average power of 0.30MW that is slightly lower than the expectation due to the influence of the platform motions. The total power of the IFES is 8.93MW that is 3.96% higher than the FOWT. The above results indicate that the integration of wind and current energy devices not only increases the total power of the whole system, but also improves the wind turbine's power performance.

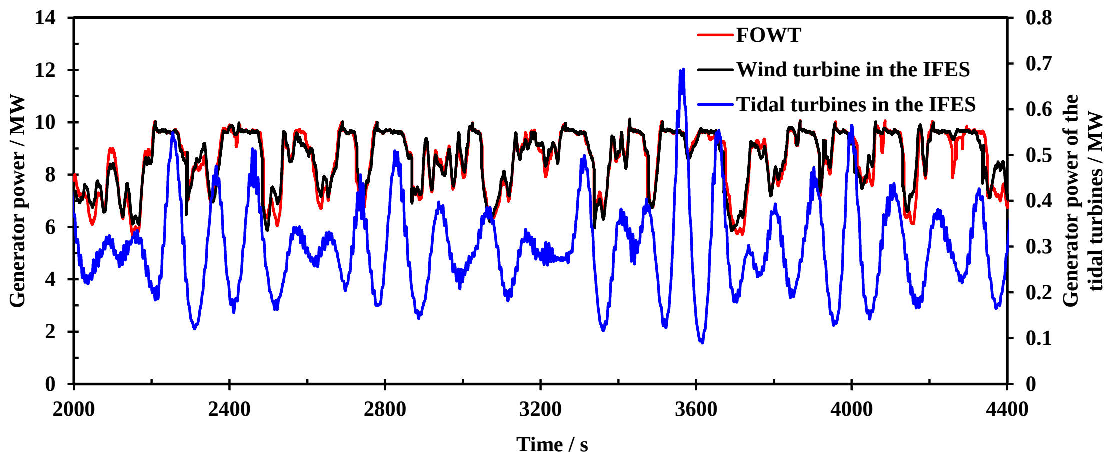

Fig. 11: Generator power of the IFES and FOWT under LC9

4.3 Statistical values of the results

Fig. 12 presents the average output power of the FOWT and IFES under various environmental conditions. The IFES shows higher power output compared to the FOWT for all load cases due to the contribution of the tidal turbines. When wind speed below 11m/s, the corresponding current speeds are smaller than 1.46m/s, resulting in an increase rate of approximately 3% of the total power due to tidal turbines. For load cases with a current speed higher than 2.01m/s, the two tidal turbines produce about 0.9MW power, which increases the total power by around 10% compared to the FOWT. Notably, the tidal turbines do not negatively affect the power performance of the wind turbine in the IFES. The average power output of the wind turbine in the IFES is almost the same as that of the FOWT in all load cases, and even slightly higher than that of the FOWT for wind speeds below 18m/s. This is mainly due to the fact that tidal turbines mitigate the fluctuation of the platform motions, thereby improving the performance of the wind turbine.

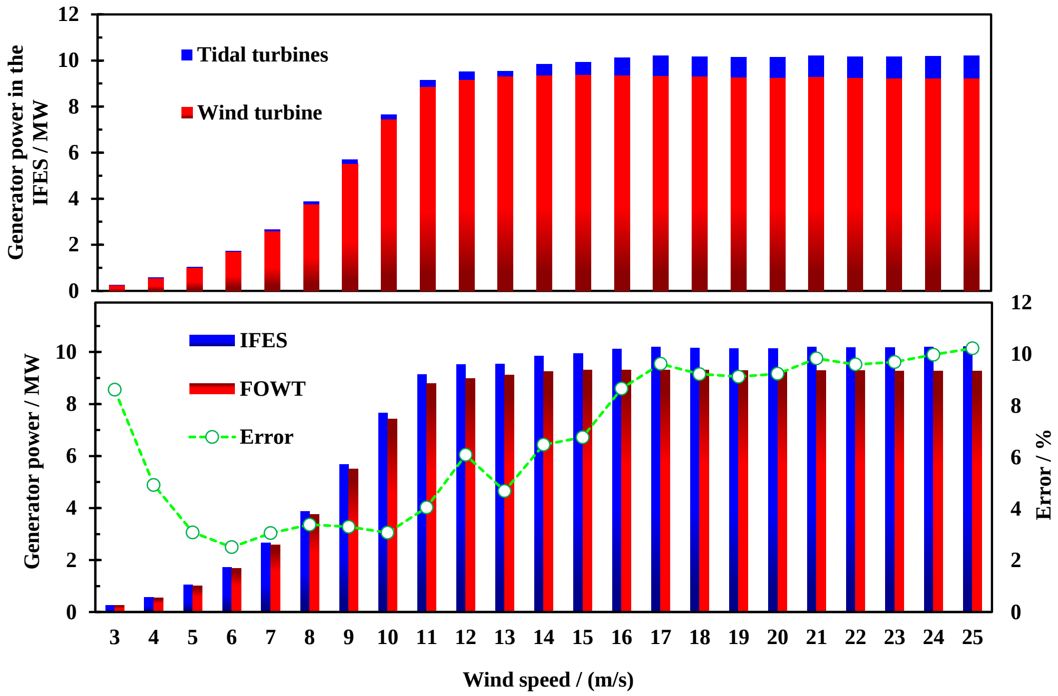

Fig. 12: The average output power of the IFES and FOWT under all load cases

The average and standard deviation of the surge and pitch motions of the FOWT and the IFES under all the load cases are presented in Fig. 13. The pitch motion of the IFES is smaller than that of the FOWT for each of the examined load cases. It is noteworthy that when the speed exceeds 16m/s, the pitch reduction ratio is more than 20%. This reduction is particularly evident at a wind speed of 25m/s, where the pitch motion decrease from 3.36 degrees to 2.45 degrees, resulting in a reduction proportion of up to 27.08%. This is mainly because the tidal turbine is located below the mass center of the platform, which produces a bending moment on the platform inverse to the bending moment generated by the wind turbine.

For the same reason, the horizontal force acting on the platform is increased by the tidal turbines, leading to a lager surge motion of the platform as observed from Fig. 13(a). In addition, the standard deviation of the surge motion of the IFES is much smaller in the rated-around wind speed conditions. The standard deviation of the surge motion of the FOWT under LC10 and LC11 are 14.39m and 16.76m, respectively. The corresponding values of the IFES are respectively reduced to 6.17m and 5.90m. The wind speed in these two is over rated wind speed. The pitch control activated to reduce the aerodynamic efficiency for the regulation of generator torque. As a result, the fluctuation in the aerodynamic thrust is triggered, resulting a large standard deviation of surge motion. While the tidal turbines provide a hydrodynamic thrust that counteracts a certain of the fluctuations of the aerodynamic thrust. Therefore, the variation of the surge motion in these conditions is much smoother as evidenced by the significantly smaller standard deviation. In the LC14~LC23, the tidal turbines operate in the rated-above conditions. The pitch control is activated to maintain the generator power, resulting in a notable fluctuation in the hydrodynamic loads due to platform motions. Meanwhile, the aerodynamic thrust provided by the wind turbine is relatively small. The fluctuation in the hydrodynamic thrust of the tidal turbines significantly affects the platform surge motion. This implies that the coupling between the tidal turbines and the wind turbine must be considered for the control of the IFES, for improving the stability and safety of the system.

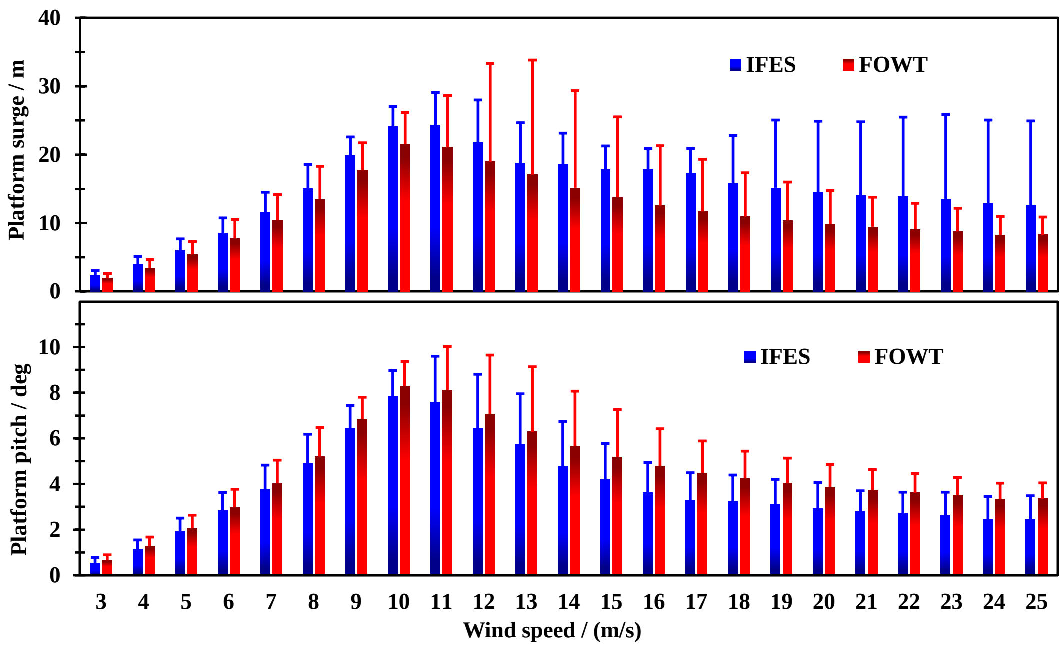

Fig. 13: Platform motion of the IFES and FPWT under load cases

Fig. 14 presents the average mooring tensions of the IFES and FOWT under all load cases.

Mooring line #1 is located in the downwind position, while moorings line #2 and #3 are situated in the windward position as shown in Fig. 1. In the IFES, the horizontal thrust generated by the tidal turbine causes a more significant longitudinal movement displacement of the platform, leading to a more significant stretching of the windward mooring. Thus, the tension in this mooring becomes notably high. When the wind speed is 17m/s, the corresponding current speeds are 2.12m/s. This leads to a decrease in the tension of mooring line #1 from 2.37MN to 1.97MN, resulting in a reduction rate of up to 16.88%. The reduction in tension of mooring line #1 in the IFES is greater than 10% compared to the average value in the FOWT under LC10 to LC18.

Furthermore, as the platform approaches the downwind mooring line anchor point, mooring #1 experiencing a relaxed state consequently has a less tension. It is worth noting that the reduction in tension of mooring #1 of the IFES is more substantial than that of the FOWT due to the presence of the tidal turbines. The results suggest that the installation of tidal turbines can result in significant differences in the mooring tension distribution, particularly in the windward moorings. Under LC10 and LC11, the mean value of mooring line #2 increased from 3.29MN and 3.27MN for the FOWT to 3.39MN and 3.28MN for the IFES, respectively. However, the increase ratios were only 3.04% and 0.31%, respectively. On the other hand, the mooring line #1 decreased significantly from 2.23MN and 2.35MN for the FOWT to 1.94MN and 2.04MN for the IFES, resulting in decrease proportions of 13.00% and 13.19%, respectively.

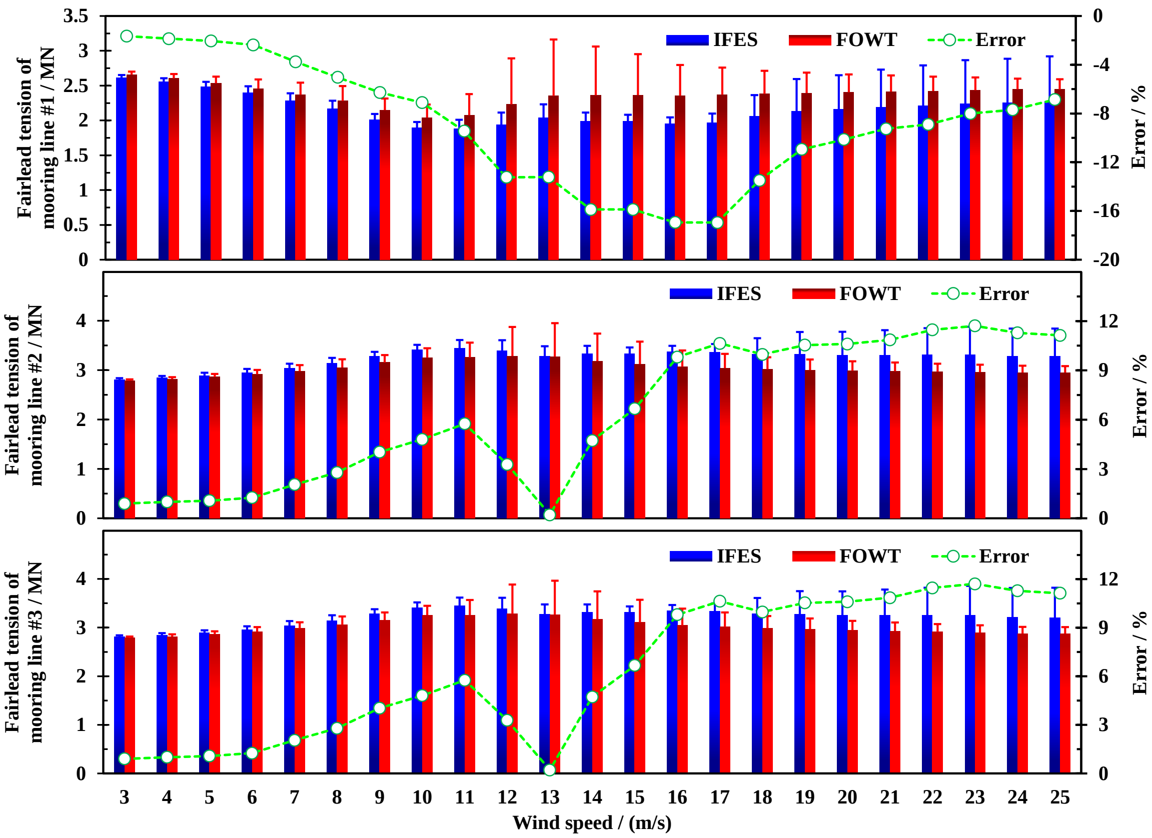

Fig. 14: Average of fairlead tension in the mooring lines under load cases

4.4 Tower fatigue damage

In this paper, the fatigue assessment is performed int the domain using the rainflow counting method for cycles. To ensure that the tower remains free from fatigue damage during its design service life, the estimation of the tower fatigue damage is required [60]. According to the Palmgren-Miner theory, individual stresses under cyclic loading are independent of each other, implying that the fatigue damage can accumulate linearly. Once the accumulated damage reaches a specific threshold value, fatigue damage occurs in the member [61]. The total fatigue damage is calculated by summing up the damage caused by each design sea state as given in Eq. (11). The damage for each sea state is computed by adding the damage for each stress or tension level using the rainflow counting method.

$$D = \sum_{j}^{N_{total}} \frac{n_j}{N_j} \tag{11}$$

where n_j is the number of cycles in the j^{th} stress range in the time history and N_j is the number of cycles to failure in the corresponding stress range according to the design S-N curve.

The fatigue damage at the tower base is evaluated. The stress at the tower base is converted from the bending moment and axial force as follows.

$$\sigma = \frac{M_y}{I_y} r \cdot \cos\theta - \frac{F_z}{A} - \frac{M_x}{I_x} r \cdot \sin\theta \tag{12}$$

where F_z is the axial force, M_x and M_y are the bending moments about the x-axis and y-axis, θ is the angle of the fatigue analysis point. A is the cross-section area. The coordinate system of the tower-base loads is presented in Fig. 15.

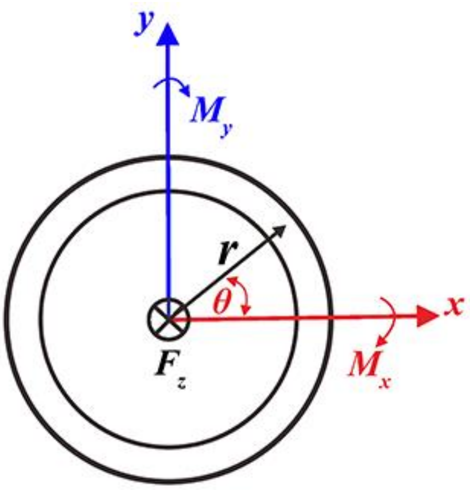

Fig. 15: Tower-base coordinate system

The S-N curve suggested in the DNV standard [62] for fatigue assessment of offshore steel structure is selected. The number of cycles to failure N is calculated using Eq. (13).

$$\log N = \log a - m \log\left(\Delta\sigma \left(\frac{t}{t_{ref}} \right)^k \right) \tag{13}$$

where $\Delta\sigma$ represents the stress range, and t is the thickness at the tower-base. Table 8 gives the values of other parameters for the fatigue assessment.

Table 8: S-N curve parameter for tower base

$N \leq 10^7$ cycles		$N > 10^7$ cycles		Fatigue time at 10^7 cycles [MPa]	k	t_{ref} [mm]
m	$\log a$	m	$\log a$			
3	12.164	5	15.606	52.63	0.2	25

As revealed in the above sections, the average value and standard deviation of the platform pitch motion are reduced by the tidal turbines. The installation of the tidal turbines is expected to reduce the loads at the tower-base, potentially decrease the fatigue damage. In order to quantitatively evaluate the effect of the tidal turbines on the tower fatigue damage, the equivalent stress of the tower is obtained using Eq. (13) for a specific orientation angle based on the bending moments and axial force eight orientation angles.

The equivalent tower-base stress at the 0° orientation (see Fig. 15) of IFES and FOWT under LC5, LC9 and LC18 are presented in Fig. 16. It is found that the mean stress of the IFES is lower than that of the FOWT for each of the load cases. At a wind speed of 7m/s, The maximum stress values of the FOWT and IFES under LC5 are respectively 3.48MPa and 3.42MPa. This indicates a stress reduction of 1.72% with the IFES model. Furthermore, the average stress value is reduced from 1.86MPa to 1.78MPa in the IFES model, meaning that a reduction of 4.30% is obtained. This stress reduction is attributed to the tidal turbines that alleviate the impact force of the current on the tower.

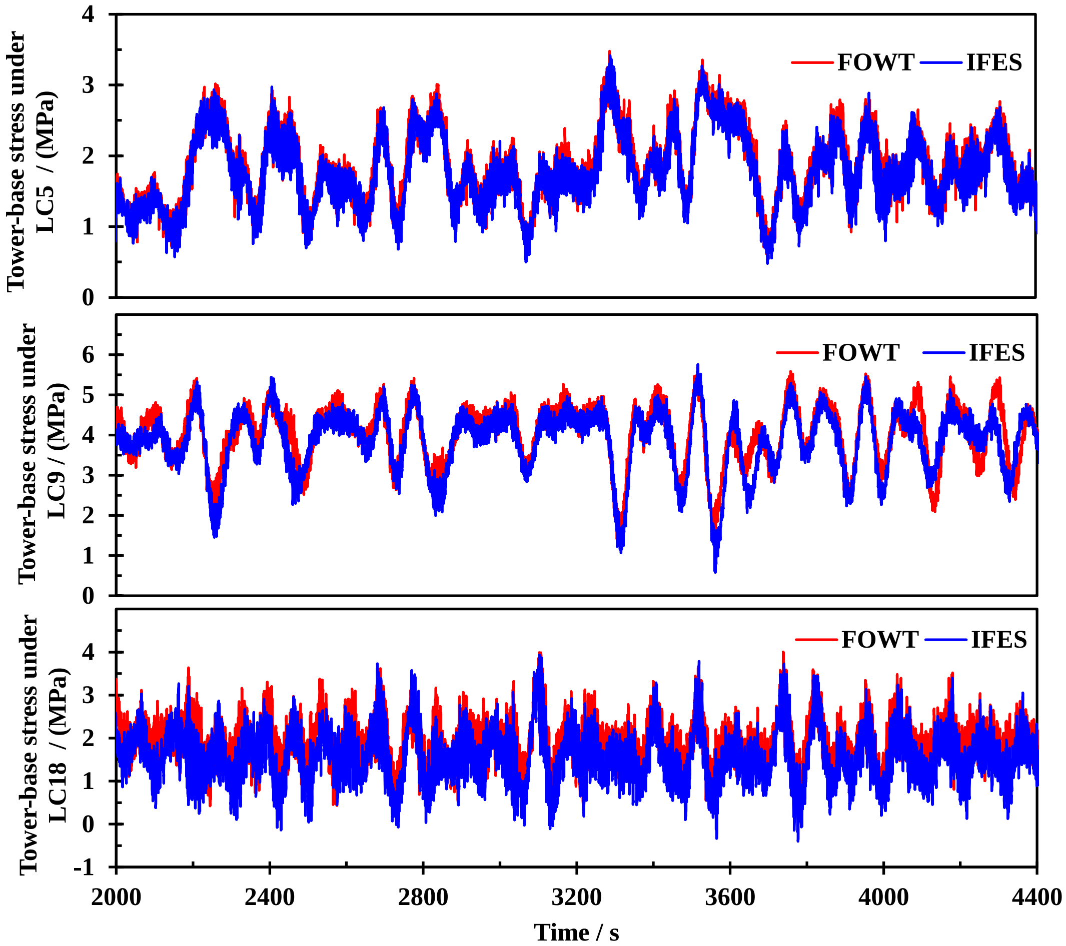

Fig 16: Tower-base stress at the 0° orientation under LC5, LC9 and LC18, respectively

Considering the occurrence probability, the weighting fatigue damage at the tower-base of the IFES and FOWT contributed by each of the load case is presented in Fig. 17. It is evident that the FOWT model experiences higher fatigue damage when the wind speed ranges between 12m/s and 15m/s. The IFES model exhibits significant reduction in the fatigue damage value. Notably, the fatigue damage decreases from 0.1447 to 0.0729 in IFES under the condition with a wind speed of 13m/s, denoting a remarkable reduction of 49.62%.

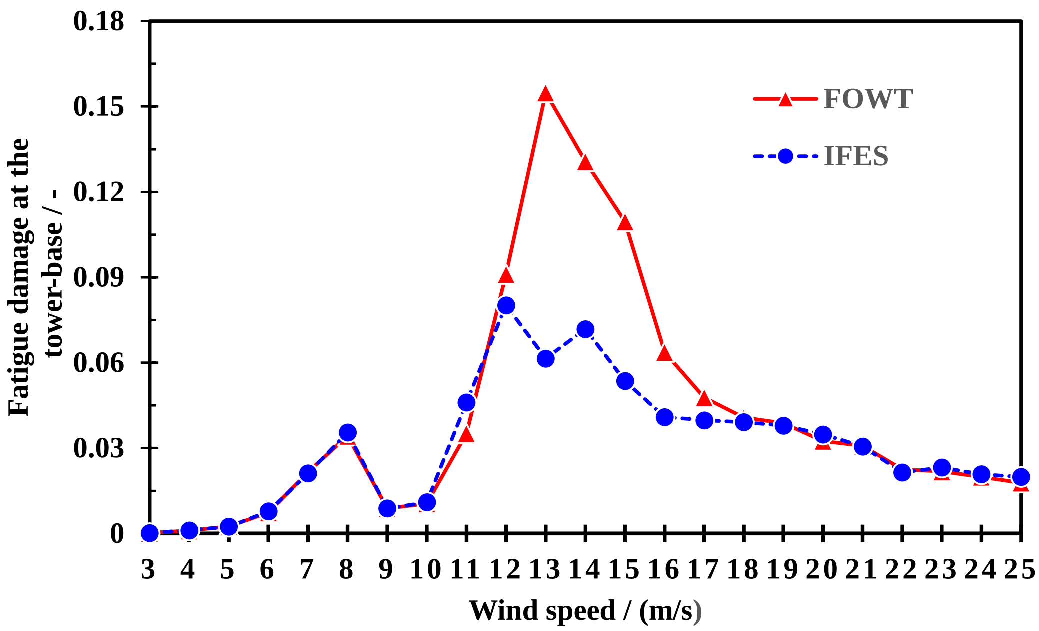

Fig. 17: Fatigue damage at the tower-base of the IFES and FOWT under all the load cases

The fatigue damage induced by each load case at the critical location is evaluated first and subsequently cumulated to obtain the total fatigue damage at the tower-base.

Fig. 18 presents the fatigue damage at the tower-base of the IFES and FOWT. It is evident that the FOWT experiences the highest fatigue damage at 0° and 180° orientations of the tower-base section with a value of 0.9345 and 0.9288, respectively. However, the introduction of two tidal turbines has led to a significant reduction in the corresponding damage for the IFES. The fatigue damage for IFES reduced by 13.91% and 14.14% at 0° and 180° orientations. Moreover, the IFES is successful in reducing the fatigue damage in other orientations at the tower-base section compared to the FOWT.

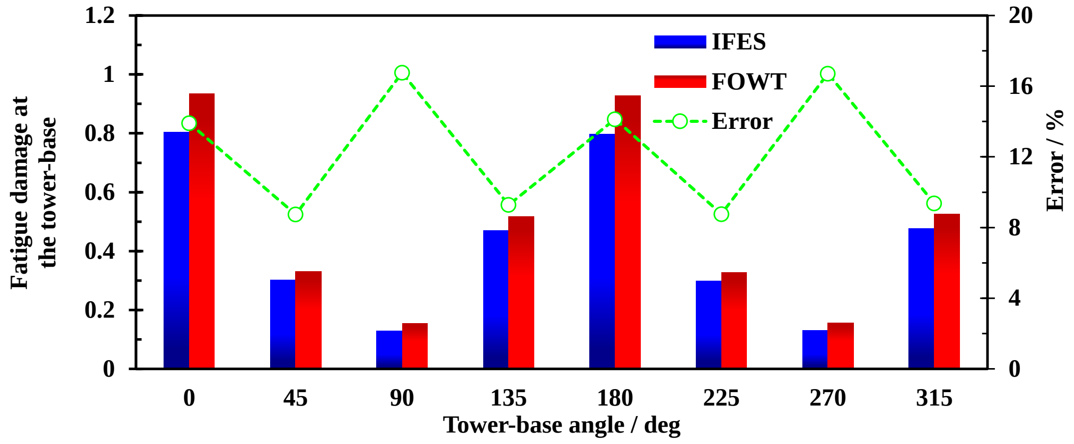

Fig. 18: Fatigue damage at the tower-base of the IFES and FOWT

5 Conclusions

This study investigates the performance and fatigue damage of an IFES consisting of a 10MW wind turbine and two 550kW tidal turbines. The validation against the OpenFAST and model test data confirms the suitability of CATIFES for multi-physics field coupled simulations of IFES. Integrating tidal turbines with a FOWT is able to improve the platform stability by introducing an additional reverse overturning bending moment. Consequently, the generator power of the wind turbine is improved in magnitude and smoothness.

Furthermore, the integration of tidal turbines into the FOWT significantly mitigates the tension fluctuation in the mooring lines by over 40.74%, primarily due to the narrower surge motion range. Compared to the FOWT, the maximum tension in each mooring line of the IFES is relatively smaller. Moreover, the fatigue damage at the tower-base of the IFES is significantly reduced compared to the FOWT. Specifically, the fatigue damage in the longitudinal points at the tower-base section decreased by around 14% due to the reverse bending moment produced by the tidal turbines.

It should be noted that the variable-speed-variable-pitch control of the wind and tidal turbines are examined separately, since developing a synergistic control strategy between the wind and tidal turbines is beyond the scope of this study. Future research can focus on developing a synergic control algorithm to improve the power production and motion performance of the whole system by incorporating additional control objectives into the conventional pitch-torque controllers. Another limitation of this paper is the omission of the structural flexibility of the tidal turbine's blades. Future studies can address this limitation by developing a fully coupled hydro-servo-elastic model to more accurately analyze the dynamic responses of the IFES.

Acknowledgements

The authors are grateful for the financial support from the National Key R&D Program of China (No. 2023YFE0102000), National Natural Science Foundation of China (Grant No.: 52101317), China Three Gorges Group Co., LTD (Contract No.: 202303059), Natural Science Foundation of Zhejiang Province (Grant No.: LQ22E090001), and the State Key Laboratory of Alternate Electrical Power System with Renewable Energy Sources (Grant No.: LAPS22009).

References

[1] Tahiri, F. E., Chikh, K., & Khafallah, M. (2021). Optimal management energy system and control strategies for isolated hybrid solar-wind-battery-diesel power system. *Emerging Science Journal*, 5(2), 111-124.

[2] Adanta, D., Sari, D. P., Syofii, I., Prakoso, A. P., Saputra, M. A. A., & Thamrin, I. (2023). Performance comparison of crossflow turbine configuration upper blade convex and curvature by computational method. *Civil Engineering Journal*, 9(1), 154-165.

[3] Council, G. W. E. (2022). Floating offshore wind—a global opportunity. *The Global Wind Energy Council*.

[4] Chen, Z., Wang, X., Guo, Y., & Kang, S. (2021). Numerical analysis of unsteady aerodynamic performance of floating offshore wind turbine under platform surge and pitch motions. *Renewable Energy*, 163, 1849-1870.

[5] Cheng, P., Huang, Y., & Wan, D. (2019). A numerical model for fully coupled aero-hydrodynamic analysis of floating offshore wind turbine. *Ocean Engineering*, 173, 183-196.

[6] Huang, Z., Qian, Y., Wang, Y., Mu, A., Yang, B., & Wang, J. (2022). Numerical analysis of floating wind turbines stability control strategy based on a novel tuned mass damper. *Journal of Renewable and Sustainable Energy*, 14(5).

[7] Chuang, T. C., Yang, W. H., & Yang, R. Y. (2021). Experimental and numerical study of a barge-type FOWT platform under wind and wave load. *Ocean Engineering*, 230, 109015.

[8] Fang, Y., Duan, L., Han, Z., Zhao, Y., & Yang, H. (2020). Numerical analysis of

aerodynamic performance of a floating offshore wind turbine under pitch motion. *Energy*, 192, 116621.

[9] Chen, J., Hu, Z., & Duan, F. (2018). Comparisons of dynamical characteristics of a 5 MW floating wind turbine supported by a spar-buoy and a semi-submersible using model testing methods. *Journal of Renewable and Sustainable Energy*, *10*(5).

[10] Zhou, Y., Xiao, Q., Peyrard, C., & Pan, G. (2021). Assessing focused wave applicability on a coupled aero-hydro-mooring FOWT system using CFD approach. *Ocean Engineering*, 240, 109987.

[11] Abdelbaky, M. A., Liu, X., & Jiang, D. (2020). Design and implementation of partial offline fuzzy model-predictive pitch controller for large-scale wind-turbines. *Renewable Energy*, 145, 981-996.

[12] Fleming, P. A., Peiffer, A., & Schlipf, D. (2019). Wind turbine controller to mitigate structural loads on a floating wind turbine platform. *Journal of Offshore Mechanics and Arctic Engineering*, 141(6), 061901.

[13] Kong, X., Ma, L., Wang, C., Guo, S., Abdelbaky, M. A., Liu, X., & Lee, K. Y. (2022). Large-scale wind farm control using distributed economic model predictive scheme. *Renewable Energy*, 181, 581-591.

[14] Kong, X., Wang, X., Abdelbaky, M. A., Liu, X., & Lee, K. Y. (2022). Nonlinear MPC for DFIG-based wind power generation under unbalanced grid conditions. *International Journal of Electrical Power & Energy Systems*, 134, 107416.

[15] Xue, W. (2016). *Design, numerical modelling and analysis of a spar floater supporting the DTU 10MW wind turbine* (Master's thesis, NTNU).

[16] Al, M., Fontanella, A., van der Hoek, D., Liu, Y., Belloli, M., & van Wingerden, J. W. (2020, September). Feedforward control for wave disturbance rejection on floating offshore wind turbines. *In Journal of Physics: Conference Series (Vol. 1618, No. 2, p. 022048)*. IOP Publishing.

[17] Ahn, H., & Shin, H. (2020). Experimental and numerical analysis of a 10 MW floating offshore wind turbine in regular waves. *Energies*, 13(10), 2608.

[18] Zhao, Z., Shi, W., Wang, W., Qi, S., & Li, X. (2021). Dynamic analysis of a novel semi-submersible platform for a 10 MW wind turbine in intermediate water depth. *Ocean Engineering*, 237, 109688.

[19] Xing, Y., Wang, S., Karuvathil, A., Balakrishna, R., & Gaidai, O. (2023). Characterisation of extreme load responses of a 10-MW floating semi-submersible type wind turbine. *Heliyon*, 9(2).

[20] Wang, L. B., Zhang, L., & Zeng, N. D. (2007). A potential flow 2-D vortex panel model: Applications to vertical axis straight blade tidal turbine. *Energy Conversion and Management*, *48*(2), 454-461.

[21] Roc, T., Greaves, D., Thyng, K. M., & Conley, D. C. (2014). Tidal turbine representation in an ocean circulation model: Towards realistic applications. *Ocean engineering*, *78*, 95-111.

[22] Badoe, C. E., Edmunds, M., Williams, A. J., Nambiar, A., Sellar, B., Kiprakis, A., & Masters, I. (2022). Robust validation of a generalised actuator disk CFD model for tidal turbine analysis using the FloWave ocean energy research facility. *Renewable Energy*, *190*, 232-250.

[23] Diab, H., Amara, Y., Hlioui, S., & Paulides, J. J. (2021). Design and realization of a hybrid excited flux switching Vernier machine for renewable energy conversion. *Energies*, 14(19), 6060.

[24] Osman, P., Hayward, J. A., Penesis, I., Marsh, P., Hemer, M. A., Griffin, D., ... & Herzfeld, M. (2021). Dispatchability, energy security, and reduced capital cost in tidal-wind and tidal-solar energy farms. *Energies*, 14(24), 8504.

[25] Derakhshan, S., Moghimi, M., & Motawej, H. (2018). Development of a mathematical model to design an offshore wind and wave hybrid energy system. *Energy Equipment and Systems*, *6*(2), 181-200.

[26] Wan, L., Gao, Z., & Moan, T. (2015). Experimental and numerical study of hydrodynamic responses of a combined wind and wave energy converter concept in survival modes. *Coastal Engineering*, *104*, 151-169.

[27] Mohanty, A., Viswavandya, M., Ray, P. K., & Mohanty, S. (2016). Reactive power control and optimisation of hybrid off shore tidal turbine with system uncertainties. *Journal of Ocean Engineering and Science*, 1(4), 256-267.

[28] Michele, S., Renzi, E., Perez-Collazo, C., Greaves, D., & Iglesias, G. (2019). Power extraction in regular and random waves from an OWC in hybrid wind-wave energy systems. *Ocean Engineering*, *191*, 106519.

[29] Perez-Collazo, C., Pemberton, R., Greaves, D., & Iglesias, G. (2019). Monopile-mounted wave energy converter for a hybrid wind-wave system. *Energy Conversion and Management*, 199, 111971.

[30] Perez-Collazo, C., Greaves, D., & Iglesias, G. (2018). A novel hybrid wind-wave energy converter for jacket-frame substructures. *Energies*, 11(3), 637.

[31] Lee, H., Poguluri, S. K., & Bae, Y. H. (2018). Performance analysis of multiple wave energy converters placed on a floating platform in the frequency domain. *Energies*, 11(2), 406.

[32] Li L., Gao Y., Yuan Z., Day, S., & Hu, Z. (2018). Dynamic response and power production of a floating integrated wind, wave and tidal energy system. *Renewable Energy*, 116, 412-422.

[33] Li L., Cheng Z., Yuan Z., & Gao, Y. (2018). Short-term Extreme Response and Fatigue Damage of an Integrated Offshore Renewable Energy System. *Renewable Energy*, 126, 617-629.

[34] Li L., Yuan Z M., Gao Y., Zhang, X., & Tezdogan, T. (2019). Investigation on long-term extreme response of an integrated offshore renewable energy device with a modified environmental contour method. *Renewable Energy*, 132, 33-42.

[35] Chen, M., Xiao, P., Zhou, H., Li, C. B., & Zhang, X. (2022). Fully Coupled Analysis of an Integrated Floating Wind-Wave Power Generation Platform in Operational Sea-states. *Frontiers in Energy Research*, *10*, 931057.

[36] Tian, W., Wang, Y., Shi, W., Michailides, C., Wan, L., & Chen, M. (2023). Numerical study of hydrodynamic responses for a combined concept of semisubmersible wind turbine and different layouts of a wave energy converter. *Ocean Engineering*, 272, 113824.

[37] Yang, Y., Bashir, M., Wang, J., Yu, J., & Li, C. (2020). Performance evaluation of an integrated floating energy system based on coupled analysis. *Energy Conversion and Management*, 223, 113308.

[38] Bayati, I., Belloli, M. A. R. C. O., Bernini, L. U. C. A., Mikkelsen, R., & Zasso, A. L. B. E. R. T. O. (2016, September). On the aero-elastic design of the DTU 10MW wind turbine blade for the LIFES50+ wind tunnel scale model. *In Journal of Physics: Conference Series* (Vol. 753, No. 2, p. 022028). IOP Publishing.

[39] Shin, H. (2011, June). Model test of the OC3-Hywind floating offshore wind turbine. In *ISOPE International Ocean and Polar Engineering Conference* (pp. ISOPE-I). ISOPE.

[40] Topper, M. B., Olson, S. S., & Roberts, J. D. (2021). On the benefits of negative hydrodynamic interactions in small tidal energy arrays. *Applied Energy*, *297*, 117091.

[41] Jonkman, J., Branlard, E., Hall, M., Hayman, G., Platt, A., & Robertson, A. (2020). Implementation of substructure flexibility and member-level load capabilities for floating offshore wind turbines in OpenFAST *(No. NREL/TP-5000-76822). National Renewable Energy Lab. (NREL)*, Golden, CO (United States).

[42] Zhang, Z., & Høeg, C. (2021). Inerter-enhanced tuned mass damper for vibration damping of floating offshore wind turbines. *Ocean Engineering*, 223, 108663.

[43] Dinh, V. N., & Basu, B. (2013). On the modeling of spar-type floating offshore wind turbines. *Key Engineering Materials*, 569, 636-643.

[44] Molland, A. F., Bahaj, A. S., Chaplin, J. R., & Batten, W. M. J. (2004). Measurements and predictions of forces, pressures and cavitation on 2-D sections suitable for marine current turbines. Proceedings of the Institution of Mechanical Engineers, Part M: *Journal of Engineering for the Maritime Environment*, 218(2), 127-138.

[45] Yang, Y., Bashir, M., Michailides, C., Li, C., & Wang, J. (2020). Development and application of an aero-hydro-servo-elastic coupling framework for analysis of floating offshore wind turbines. *Renewable Energy*, 161, 606-625.

[46] Yang, Y., Li, C., Zhang, W., Yang, J., Ye, Z., Miao, W., & Ye, K. (2016). A multi-objective optimization for HAWT blades design by considering structural strength. *Journal of Mechanical Science and Technology*, 30, 3693-3703.

[47] Bahaj, A. S., Molland, A. F., Chaplin, J. R., & Batten, W. M. J. (2007). Power and thrust measurements of marine current turbines under various hydrodynamic flow conditions in a cavitation tunnel and a towing tank. *Renewable energy*, 32(3), 407-426.

[48] Doman, D. A., Murray, R. E., Pegg, M. J., Gracie, K., Johnstone, C. M., & Nevalainen, T. (2015). Tow-tank testing of a 1/20th scale horizontal axis tidal turbine with uncertainty analysis. *International Journal of Marine Energy*, 11, 105-119.

[49] Nicholls-Lee, R. F., Turnock, S. R., & Boyd, S. W. (2013). Application of bend-twist coupled blades for horizontal axis tidal turbines. *Renewable Energy*, *50*, 541-550.

[50] Bastankhah, M., & Abkar, M. (2019). Multirotor wind turbine wakes. *Physics of Fluids*, 31(8).

[51] Ghaisas, N. S., Ghate, A. S., & Lele, S. K. (2020). Effect of tip spacing, thrust coefficient and turbine spacing in multi-rotor wind turbines and farms. *Wind Energy Science*, 5(1), 51-72.

[52] Hebbar, U., Rane, J. D., Gandhi, F., & Sahni, O. (2020). Analysis of interactional aerodynamics in multi-rotor wind turbines using large eddy simulations. *In AIAA Scitech 2020 Forum* (p. 1489).

[53] Stewart, G. M., Robertson, A., Jonkman, J., & Lackner, M. A. (2016). The creation of a comprehensive metocean data set for offshore wind turbine simulations. *Wind Energy*, 19(6), 1151-1159.

[54] Lee, D. H., & Jeong, Y. J. (2011). Integrated analysis of hydrodynamic motions and structural behavior of large-scaled floating structures using AQWA-ANSYS coupling. *Journal of the computational structural engineering institute of Korea*, 24(6), 601-608.

[55] Zou, Q., Lu, Z., & Shen, Y. (2023). Short-term prediction of hydrodynamic response of a novel semi-submersible FOWT platform under wind, current and wave loads. *Ocean Engineering*, 278, 114471.

[56] Ding, Q., Li, C., Yu, N., Hao, W., & Ji, J. (2018). Numerical and experimental investigation into the dynamic response of a floating wind turbine spar array platform. *Journal of Mechanical Science and Technology*, 32, 1106-1116.

[57] Jeon, S. H., Cho, Y. U., Seo, M. W., Cho, J. R., & Jeong, W. B. (2013). Dynamic response of floating substructure of spar-type offshore wind turbine with catenary mooring cables. *Ocean Engineering*, 72, 356-364.

[58] Matha, D., Sandner, F., Molins, C., Campos, A., & Cheng, P. W. (2015). Efficient preliminary floating offshore wind turbine design and testing methodologies and application to a concrete spar design. *Philosophical Transactions of the Royal Society A: Mathematical, Physical and Engineering Sciences*, 373(2035), 20140350.

[59] Yang, Y., Bashir, M., Michailides, C., Li, C., & Wang, J. (2020). Development and

application of an aero-hydro-servo-elastic coupling framework for analysis of floating offshore wind turbines. *Renewable Energy*, 161, 606-625.

[60] Ismaiel, A. (2023). Wind turbine blade dynamics simulation under the effect of atmospheric turbulence. *Emerging Science Journal*, 7(1), 162-176.

[61] Ye, X. W., Ni, Y. Q., & Ko, J. M. (2012). Experimental evaluation of stress concentration factor of welded steel bridge T-joints. *Journal of Constructional Steel Research*, 70, 78-85.

[62] Veritas, D. N. (2004). Design of Offshore Wind Turbine Structure. O*ffshore Standard DNV-OS-J101*.

Performance and fatigue analysis of an integrated floating wind-current energy system considering the aero-hydro-servo-elastic coupling effects

Yang YANG[a,*,1], Jianbin FU[a,1], Zhaobin SHI[a], Lu MA[b], Jie YU[c], Fang FANG[d], Shunhua CHEN[e], Zaibin LIN[f], Chun LI[c]

[a]. Faculty of Maritime and Transportation, Ningbo University, Zhejiang province, Ningbo 315211, P.R. China

[b]. China Three Gorges Co., Ltd, Hubei province, Wuhan, 430014

[c]. School of Energy and Power Engineering, University of Shanghai for Science and Technology, Shanghai 200093, P.R. China

[d]. State Key Laboratory of Alternate Electrical Power System with Renewable Energy Source (North China Electric Power University), Beijing 102206, P.R. China

[e]. School of Marine Engineering and Technology, Sun Yat-sen University, Guangdong Province, Zhuhai 519082, P.R China

[f]. School of Engineering, University of Aberdeen, Aberdeen, AB24 3UE, United Kingdom.

*Corresponding author: Yang YANG, yangyang1@nbu.edu.cn

[1] All these authors have made equal contributions to the article

Abstract: Integration of multiple offshore renewable energy converters holds immense promise for achieving cost-effective utilization of marine energy. Integrated Floating Wind-Current Energy Systems (IFESs) have garnered considerable attention as a means to harness the abundant wind and marine resources in deep-sea areas using a single device. However, the dynamic responses of IFESs are significantly influenced by the coupling of aerodynamic and hydrodynamic loads. To assess the performance of a 10MW+ Spar-type IFES under wind-wave-current loadings, this study develops an aero-servo-elastic model within the hydrodynamic analysis tool AQWA. By utilizing the fully coupled model, this study investigates the platform motions, tower loads, and power production of the IFES under various environmental conditions. A comparative analysis is conducted by comparing the results with those obtained for a floating offshore wind turbine (FOWT). Furthermore, fatigue damage at the tower base of both the IFES and FOWT is evaluated. It is found that the presence of current turbines leads to improved platform stability, significant increases in total power production, and reduced fatigue damage at the tower base. These novel findings corroborate the potential and advantages of IFES concepts in enhancing the stability and energy harvest efficiency of floating marine energy converters.

Key worlds: Integrated floating wind-current energy system; Floating offshore wind turbine; Aero-hydro-servo-elastic coupling; Fatigue damage; Dynamic analysis.

1 Introduction

The energy demand is gradually increasing with the rapid development of the worldwide economy. The shortage of the traditional fossil energy resources leads to the acceleration of the pace in exploring and utilizing renewable energy [1-2]. Offshore renewable energy resources, especially the wind energy, have become a major contribution to the promotion of green and low-carbon energy transition because of the abundant resources and the mature technology. The newly-installed global wind power capacity was 94GW in 2021 as reported by the Global Wind Energy Council (GWEC). The accumulated offshore wind capacity is expected to achieve 361GW in 2030, including 6% of floating wind capacity in the deep-sea areas where also contain huge wave and current energy resources [3].

Numerous studies related to floating offshore wind turbines (FOWTs) have recently been carried out. Chen *et al.* [4] utilized a dynamic and sliding mesh coupling technique to study the unsteady aerodynamic properties of a FOWT subjected to single (surge or pitch) and combined motions. It was found that higher amplitudes and frequencies of motion led to increased fluctuations in the overall aerodynamic performance of the turbine. Moreover, the complex platform motions resulted in a negative impact on power generation in FOWT. Cheng *et al.* [5] used the open-source tool OpenFOAM to establish a fully-coupled aero-hydrodynamic model for conducting numerical simulation of FOWTs. The model employed the three-dimensional Reynolds-Averaged Navier-Stokes (RANS) equations and the Pressure-Implicit with Splitting of Operations (PISO) algorithm to solve the pressure-velocity coupling equations. The coupling effects between the semi-submersible platform and the NREL 5MW baseline wind turbine were investigated. Huang *et al.* [6] proposed a novel type of negative stiffness tuned mass damper (TMD-NS) for the stability control of FOWTs. The fixed-point theory was used to obtain the dimensionless optimal parameters of the TMD-NS for achieving a reduction in amplitude ratio and increase in the tuning bandwidth. The TMD-NS was found to be capable of reducing the nacelle displacement and velocity up to 55.87% and 48.18%, respectively. Chuang *et al.* [7] conducted both numerical simulations and scaled experimental tests for a barge 5MW FOWT. The numerical analysis was performed using ANSYS AQWA, while the experimental tests were conducted for a 1:64 scaled-down model. The hydrodynamic model was calibrated based on the results of free-decay tests, and regular and irregular wave model tests were conducted. The results of the tests showed that the fluid sloshing in the damping pool generated an oscillating force reducing the platform motion. Fang *et al*. [8] conducted numerical simulations of a 5MW wind turbine rotor using the improved delayed detached eddy simulation (IDDES) computational fluid dynamics (CFD) method after redesigning the rotor. It revealed that the aerodynamic performance of the FOWT was significantly affected by pitch motion parameters. Specifically, the amplitudes of rotor thrust and torque decreased with the increase of the pitch period, while a larger pitch amplitude could cause the stall phenomenon resulting in larger rotor thrust and torque. Chen *et al.* [9] compared the dynamic responses of a Spar and a semi-submersible scaled FOWT under different operating conditions. It was found that the Spar FOWT was more sensitive to the aerodynamic loads, while the surge and sway motion trajectories were more regular compared to those of the semi-submersible FOWT. Zhou *et al.* [10] examined the impacts of wave type and steepness on the hydrodynamics-aerodynamics responses of a 5MW semi-submersible FOWT. The dynamic response and power output of the FOWT were analyzed using a high-fidelity aero-hydro-mooring CFD solver. The results showed that there were significant differences in the floater motion response prediction between a focused wave and an irregular wave for the same spectrum. The reconstructed focused wave could be used as an alternative for extreme wave studies. Abdelbaky *et al.* [11] introduced a novel controller that utilizes a partial offline quasi-min-max fuzzy model-predictive control approach to analyze and enhance the performance of variable-speed wind turbines. Fleming *et al.* [12] improved the controller of the WindFloat by adding several control modules to the baseline controller. The results of the tests indicated that the use of a coupled linear model significantly improved the overall performance of performance and reduced the bending loads at the tower-base. Kong *et al.* [13-14] proposed an efficient distributed economic model predictive control strategy to enhance load-following capability. The result shows that the control strategy successfully tracks the reference power provided by the transmission system operator. Furthermore, simulation results demonstrate the control strategy's ability to effectively mitigate power pulsations, even in the presence of unbalanced grid voltage conditions.

The above studies mainly focused on the FOWTs with a capacity of up to 5MW. It is noted that adopting 10+MW FOWTs is an effective solution to reducing the levelized cost of electricity. Xue. [15] proposed a Spar-type platform for the application of 10 MW wind turbines in the deep-sea areas. A catenary mooring system was used for station-keeping of the platform. The reliability of the platform heave and pitch were verified by numerical simulations and model tests. Al *et al.* [16] developed a controller for the DTU 10 MW wind turbine supported by a Triple Spar platform to mitigate the rotor speed caused by wave loadings. The mitigation effects under wind and waves condition were examined using a high-fidelity numerical tool. It was found that the novel feedforward controller was capable of narrowing the rotor speed variation range. Ahn *et al.* [17] conducted a scaled model test to verify the performance of a scaled up 10MW FOWT based on the OC4 semisubmersible platform. The test results indicated that the wind turbine exhibited a good performance in terms of the response amplitude and natural period. Zhao *et al.* [18] proposed a conceptual 10MW semi-submersible platform and compared it with the OO-Star platform to validate the numerical model. The dynamic responses of the conceptual FOWT under various fault conditions were examined to confirm the stability of the proposed FOWT concept. In particular, the most significant impact on its heave dynamic behavior was observed under shutdown fault conditions. Xing *et al.* [19] conducted a study on the extreme dynamic responses of a 10MW semi-submersible type FOWT. The average conditional exceedance rate (ACER) and Gumbel methods were used to accurately quantify the FOWT system's extreme dynamic responses and to calculate the ultimate limit state loads.

The studies related to tidal/current energy is being carried out in parallel with the investigations on floating wind technology. Wang *et al*. [20] developed a 2-D vortex panel model based on the potential theory for unsteady hydrodynamics of a tidal turbine. The predicted transient forces on the blades and rotor wake were in good agreement with the test data. Roc *et al*. [21] proposed a new representation of tidal turbine based on an existing momentum and turbulence transport equations, which provided a basis for the development of an array layout optimization tool due to the short computational time. The experimental flume tests showed that the method could accurately predict the momentum and turbulent wake interactions. Badoe *et al*. [22] further employed the generalized actuator disk (GAD) approach to model the fluid structure interactions between multiple tidal energy converters. The physical tests were conducted to validate the numerical simulation results. The results showed that GAD method could effectively evaluate the influence of turbine spacing and arrangement.

Integration of multiple offshore renewable energy convertors is expected to further reduce the energy cost by sharing the floating platform and its seakeeping system [23-24]. Derakhshan *et al.* [25] proposed a method for the design of integrated wind-wave energy system. A case study was conducted for the UK and Syrian sea areas by analyzing the power performance of an integrated wind-wave energy system consisting of a 4.2 MW wind turbine and several wave energy convertors. It was shown that the wave energy devices increased the annual power generation by around 2%. Wan *et al*. [26] proposed the Spar Torus Combination concept composed of a Spar-type FOWT and a circular-shaped wave energy converter (WEC). The positive synergy between the FOWT and the WEC was demonstrated through experimental tests and numerical simulations. Mohanty *et al*. [27] developed a reactive power management method based on Flexible AC Transmission System (FACTS) devices to adjust the power management and stability of an offshore wind-tidal turbine power generation system. The effect of reactive power compensation and its impact on the dynamic stability of an isolated offshore wind and tidal current hybrid system were investigated and validated. Michele *et al*. [28] developed a mathematical model to analyze the hydrodynamic characteristics of an integrated wind-wave energy system under regular and irregular wave conditions. Collazo *et al*. [29-30] experimentally studied the coupling effects between the wave and the pendulous WEC integrated into a Spar FOWT. Lee *et al*. [31] investigated the hydrodynamic loads of a floating wind-wave energy system. A numerical study was conducted to multi-body hydrodynamic interaction between the floating platform and a multi-wavelength energy converter in the frequency domain based on the boundary element method. The analysis revealed that notable variations were observed in the dynamic responses of the WECs if the multi-body hydrodynamic interaction was taken into account.

Li *et al*. [32] developed an unsteady aerodynamic load prediction model within the dynamic analysis tool WEC-Sim for WECs. The coupled effects between the aerodynamic and hydrodynamic loads of the floating wind-wave-current energy system in were investigated. The results indicated that the platform motion response was reduced and the power output was increased compared to the conventional wind turbines. In addition, Li *et al*. [33-34] examined the short-term and long-term responses of the wind-wave-current system under extreme conditions. The findings indicated that the WEC enlarged the fatigue load in mooring lines. However, the interactions of the aerodynamic loads on the wind turbine and the hydrodynamic loads on the tidal turbine were not considered. In addition, the torque-pitch control was ignored for the tidal turbine. Chen *et al*. [35] introduced a new and innovative integrated floating wind-wave generation platform (FWWP), which includes a DeepCwind semi-submersible FOWT and a point absorber WEC. In order to investigate the dynamic responses and power generation capabilities of the FWWP under different operational sea-states, fully coupled analyses were carried out based on the F2A tool. It was found that the incorporation of WECs resulted in increased total power generation when compared to a standalone FOWT. Tian *et al*. [36] conducted research on a 5MW unsupported semi-submersible FOWT and various configurations of annular WECs. They compared the impact of different numbers of WECs on the hydrodynamic performance of the wind turbine. Comparison and discussion of the response amplitude operators (RAOs) and generated power of the studied combination structures in the time domain showed that the combination structure using three WECs has the highest power generation capacity. Yang *et al*. [37] developed a fully coupled model based on FASTv7 and AQWA for floating wind-current energy systems. It was found that the integrated floating wind-current energy system improved the platform motion stability and increased the power production when comparing to the FOWT.

Nonetheless, the interactions between the wind and current energy converters under complexly environmental conditions have not been sufficiently investigated. The major difficulties and challenges in the field of integrated floating energy systems mainly include: i) the need for a numerical simulation model that considers the coupled effects between wind and current energy converters; ii) the development of a pitch-torque control of tidal turbines under dynamic inflow conditions when integrated into a FOWT; iii) the quantitative analysis of the impact of tidal turbines on the dynamic responses of a FOWT under wind-wave-current loadings. Furthermore, a comprehensive evaluation of the fatigue performance of the tower in the presence of current turbines is required.

In order to address these research needs, this paper aims to quantitatively assess the fatigue performance of a 10MW+ Spar-type IFES, considering the effects of aero-hydro-servo-elastic coupling as a continuation of the previous study [37]. In this study, a fully Coupled Analysis Tool for Integrated Floating Energy Systems (CATIFES) was developed to consider the interactions between the FOWT and tidal turbines under different environmental conditions. The proposed case study involves a 10MW Spar-type FOWT integrated with two 550kW tidal turbines. This analysis of a10MW+ IFES is anticipated to provides valuable insights into the interactions of multiple energy converters within the integrated system.

Furthermore, the research evaluates the fatigue damage at the tower-base of the IFES throughout its design service life. This evaluation quantitatively assesses the impact of tidal turbines on extending the tower operational lifespan. These findings obtained from this study are expected to contribute to advancing knowledge in the field and highlight the potential benefits of integrating tidal turbines into FOWT systems.

This paper makes two significant contributions. First, a novel and fully coupled analysis tool (CATIFES) is developed to accurately predict the dynamic responses of an integrated floating wind-current energy system under wind-wave-current loadings. This addresses a significant research gap in the field of coupled analysis for floating wind-wave energy systems. By integrating the aerodynamic and hydrodynamic loads, the CATIFES provides a comprehensive framework for evaluating the performance of these complex systems. Secondly, this study quantitatively evaluates the effect of tidal turbines on the power production, platform motion, and tower fatigue damage of a 10 MW Spar-type FOWT. By comparing the responses of the integrated floating wind-current energy system with those of a standalone FOWT, strong evidence is provided to confirm the benefits derived from integrating multiple types of energy converters on a single floating platform. The evaluation not only highlights the increased power production resulting from the presence of tidal turbines but also demonstrates improved platform stability and reduced fatigue damage at the tower base.

This paper is organized as follows: Section 2 describes the IFES used in this study. The mathematical model of the CATIFES and the validations are presented in Section 3. Section 4 describes the load cases and presents the results and discussions of the IFES under combined wind-wave-current loads. Finally, the conclusions are presented subsequently in Section 5.

2 Introduction of wind-current energy system model

The IFES model proposed in this paper is composed of the DTU 10MW wind turbine, Spar platform up-scaled from the Hywind concept, the mooring system, and two 550kW tidal turbines designed by the Sandia National Laboratory. A preliminary analysis is performed to confirm the best installation position of the tidal turbines. The platform pitch and the overall power production of the IFES are balanced for the best while the tidal turbines are installed at 110m below the sea level. The schematic diagram of the IFES model is presented in Fig. 1.

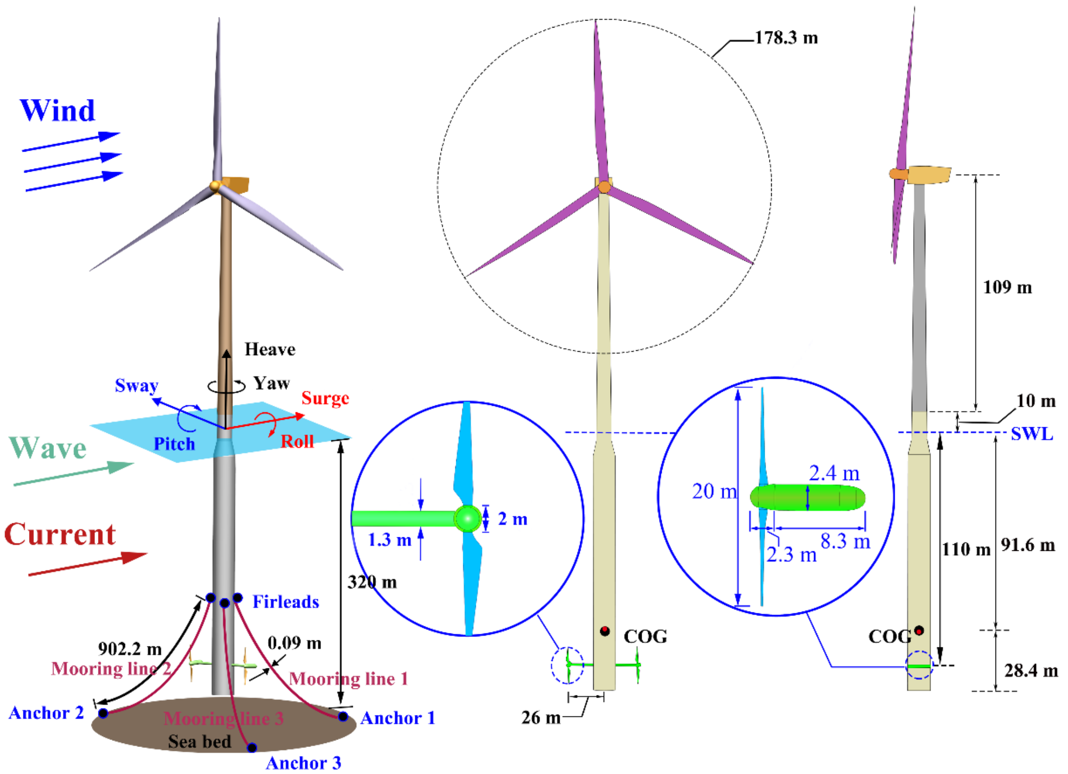

Fig. 1: The schematic diagram of the IFES model

2.1 Introduction to the 10MW wind turbine

The DTU 10MW reference wind turbine is jointly designed by the Technical University of Denmark and Vestas. [38] The full design details in terms of aerodynamic and structural parameters of the wind turbine are released to the public for world-wide researchers to improve offshore wind technology. The rotor diameter is 178.3m and the hub height is 119m. Table 1 presents the main design specifications of the wind turbine.

Table 1: Main design specifications of the DTU 10 MW wind turbine model

Property/Unit	**Value**	**Property/Unit**	**Value**
Rated power/MW	10	Rotor diameter/m	178.3
Rated wind speed/($m \cdot s^{-1}$)	11.4	Hub diameter/m	5.6
Cut-in wind speed/($m \cdot s^{-1}$)	4	Hub height/m	119
Cut-out wind speed/($m \cdot s^{-1}$)	25	Tower height/m	115.63
Cut-in rotor speed/rpm	6	Rotor mass/kg	227962
Rated rotor speed/rpm	9.6	Nacelle mass/kg	446036

2.2 The Spar platform and mooring system

The Spar platform used in this study is up-scaled from the Hywind Spar 5MW model by Shin [39] for supporting the 10MW wind turbine. The draft of the Spar platform is 120m for the application in 320m water depth areas. The platform mass including the ballast is 1.2×10^{7}kg. The mooring system is composed of three suspended chain lines with a length of 902.2m and an equivalent diameter of 0.09m. The properties of the Spar platform and the mooring system are shown in Table 2 and Table 3, respectively.

Table 2: Main properties of Spar platform

Platform property	**Value/Unit**
Water depth	320/m
Hull thickness	0.06/m
Platform mass including ballast	1.21×10^{7}/kg
Platform length	130/m
Platform diameter above taper	8.3/m
Platform diameter below taper	12/m
Center of mass	-91.96/m
Draft	120/m
Roll inertia	1.273×10^{11}/($kg \cdot m^{2}$)
Pitch inertia	1.273×10^{11}/($kg \cdot m^{2}$)
Yaw inertia	6.056×10^{10}/($kg \cdot m^{2}$)

Table 3: Main properties of mooring system

Mooring property	**Value/Unit**
Number of mooring lines	3/-
Angel between adjacent lines	120/deg
Fairlead depth	70/m
Anchor depth	320/m
Unstretched length	902.2/m
Equivalent diameter	0.09/m
Equivalent axial stiffness	384.24/MN
Equivalent mass density in air	233.12/(kg/m)

2.3 Introduction of the tidal turbine

The tidal turbine is a 550kW two-blade model designed by the Sandia National Laboratory [40]. The mass of each tidal turbine including the nacelle and connecting beam is 6.13×10^4kg. The rotor and hub diameters are 20m and 2m, respectively. The distance between the platform centerline and hub of the tidal turbine is 26m. The blade shape is optimized by the HARP_Opt tool. The main design parameters are shown in Table 4. The parameters of blade sectional airfoil, twist angle, and relative thickness are shown in Table 5.

Table 4: Main design properties of tidal turbine

Property	**Value/Unit**
Rated power	550/kW
Cut-in, cut-out current speed	0.5,3.0/(m/s)
Minimum and rated rotor speed	3.0,11.5/rpm
Diameter of the rotor	20.0/m
Diameter of the hub	2.0/m
Rotor mass	1200/kg
Nacelle mass	40100/kg
Cross-beam mass	20000/kg
Drivetrain inertia moment	4.44×10^6/(kg·m^2)
Depth to hub below MSL	46.5/m

Table 5: The blade cross-section properties of the tidal turbine

Local radius/m	**Aerofoil-**	**Twist/deg**	**Chord/m**	**Relative thickness/%**

1	Cylinder	0.8	12.86	100
1.89	Interpolated	1.243	12.86	53.3
2.7	Interpolated	1.702	12.79	27.55
3.55	NACA 63-424	1.577	9.5	24
4.23	NACA 63-424	1.481	7.85	24
5.01	NACA 63-424	1.371	6.51	24
5.84	NACA 63-424	1.251	5.47	24
6.62	NACA 63-424	1.138	4.71	24
7.23	NACA 63-424	1.046	4.2	24
7.89	NACA 63-424	0.945	3.69	24
8.45	NACA 63-424	0.856	3.28	24
8.92	NACA 63-424	0.781	2.92	24
9.24	NACA 63-424	0.728	2.68	24
9.64	NACA 63-424	0.661	2.35	24
10	NACA 63-424	0.6	2.1	24

3 Fully coupled modeling of the IFES

To consider the coupling effect of the wind turbine and tidal turbines, the aero-servo-elastic simulation capability of OpenFAST for wind turbines is implemented through the external dynamic link library (user_force64.dll) of AQWA, which will be invoked for each determination of the platform responses. In addition, the prediction model of the hydrodynamic loads acting on the tidal turbines is developed based on the blade element momentum theory considering the cavitation. The Coupled Analysis Tool for Integrated Floating Energy Systems (CATIFES) is then developed by integrating the above two models.

3.1 Introduction to OpenFAST

OpenFAST was developed by the National Renewable Energy Laboratory (NREL) to simulate coupled dynamics of horizontal axis wind turbines. OpenFAST is designed to provide a robust software engineering framework for FAST development. The software is not only certified by Germanischer Lloyd but also has the open-source feature [41], therefore it is widely used in the academic research. OpenFAST mainly consists of several modules to consider the interaction effects between loads, control and structural dynamics. OpenFAST is significantly better at predicting the unsteady aerodynamic loadings compared to its previous version (FAST v7). This is why OpenFAST is used instead of FAST v7 to develop the CATIFES model.

The AeroDyn module is responsible for the prediction of aerodynamic loads on the rotor and tower. ElastoDyn is used to determine of structural dynamics of most components including the drivetrain and tower. This paper employs the modal method to examine the tower dynamics, assuming that the tower vibration is linearly represented by several bending modes and neglecting torsional modes. The Spar-type platform used in this paper experiences relatively small yaw moments, resulting in minimal torsional moments on the tower. Therefore, the actual torsional deformation of the tower is considered negligible compared to the variation of inflow wind direction. The assumed modal method has been applied in numerous studies examining the tower dynamics [42-43]. The impact of this assumption on simulation results is anticipated to be insignificant. The control scheme is conducted in the ServoDyn module for the regulation of blade pitch and generator torque. The CATIFES model developed in this study employs these three modules to obtain the aero-servo-elastic responses of the IFES. Specifically, these three modules are compiled as a user defined DLL that can be invoked by AQWA for external force prediction.

3.2 Blade element momentum theory for a tidal turbine

AeroDyn is an open-source tool supported and maintained by NREL [44] for the aerodynamic load prediction of horizontal axis turbine blades. This study employs the Aerodyn v15.04 that is capable of checking the cavitation problem to predict the hydrodynamic loads acting on tidal turbines under unsteady current conditions. The Generalized Dynamic Wake (GDW) model and Blade Element Momentum Theory (BEMT) are used in Aerodyn v15.04. The GDW model is used to calculate the axial induction velocity over the rotor plane under dynamic inflow condition [45]. The tangential induction velocity of each blade section is predicted using the BEMT as the rotation wake is not examined in the GDW model.

The BEM theory is combined by the blade element theory and the momentum theory. The wind turbine blade is treated as finite sections. The lift and drag coefficients of the blade sectional airfoil are used to calculate the aerodynamic force acting on each blade element. Fig. 2 presents the velocity triangle and force acting on an airfoil.

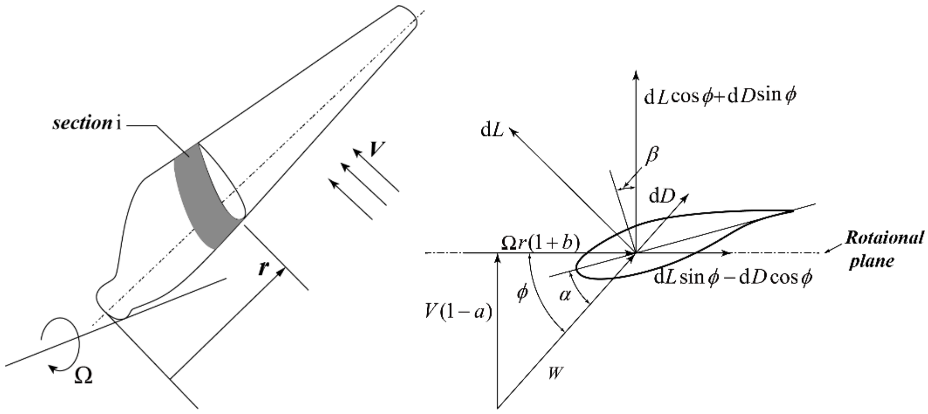

Fig. 2: Illustration of the velocity triangle and force analysis for a blade element

where Ω is the rotational speed of the rotor, r is the local radius of the blade element, V is the inflow velocity, and W denotes the relative inflow speed; a and b are the axial and tangential induction factors; α and β, respectively, the effective angle of attack, twist angle, and inflow angle of the blade element, ϕ is the relative inflow angle of the local element; L and D are, respectively, the lift and drag forces generated by the blade element.

The BEM theory is subsequently applied to compute the loads acting on each blade element, based on the lift and drag coefficients of the local sectional airfoil as represented in Eq. (1) and Eq. (2) [46].

$$\mathrm{d}T = \frac{1}{2}\rho W^2 c(C_l \cos\phi + C_d \sin\phi)\mathrm{d}r \tag{1}$$

$$\mathrm{d}M = \frac{1}{2}\rho W^2 c(C_l \sin\phi - C_d \cos\phi) r\mathrm{d}r \tag{2}$$

where dT and dM are, respectively, the thrust and moment of the local blade element; ρ is the density of the inflow fluid; C_l and C_d are, respectively, the lift and drag coefficients of the sectional airfoil; The Beddoes-Leishman dynamic stall model is used to correct the aerodynamic coefficients under unsteady conditions; c is the chord length of the blade element; $\mathrm{d}r$ is the length of the blade element.

In the analysis, the GDW model first solves the dynamic induction velocity distribution over the rotor. The angle of attack at each blade section is then calculated to call the lift and drag coefficients for the prediction of aerodynamic loads on the blades using Eq. (1) and Eq. (2). It is noted that the floating platform motions will be used to correct the current inflow speed V, which will be further described in the subsequent section. In addition, this study assumes the absence of cavitation when predicting hydrodynamic loads on the tidal turbines. The rated current speed is 2.0 m/s, and the low rated rotor speed of 11.5 rpm corresponds to a blade tip speed of 12.03m/s, making cavitation unlikely [47-49].

This study assumes that the BEM method remains valid for load prediction of the tidal turbines when installed on the platform. The BEM method is commonly employed for calculating the hydrodynamic performance of an individual tidal turbine. In this paper, the tidal turbines are installed on a floating platform. The distance between the blade tip and platform is not substantial, but a 50% blade tip clearance is maintained relative to the rotor diameter. Recent studies suggested that a tip clearance of 10% of the rotor diameter has no significant impacts on the blade's aerodynamic performance of wind turbines, and this conclusion can be extrapolated to tidal turbines [50-52]. Thus, this assumption is not expected to significantly influence on the results.

3.3 Introduction to AQWA and integration of the sub-models

The CATIFES model is developed within the hydrodynamic analysis software package, namely AQWA. AQWA that is a commonly-used tool for hydrodynamic analysis of marine and offshore structures [53]. The potential theory is employed by AQWA to solve the radiation and diffraction problems of a large size floater for obtaining the added mass, radiation damping, and wave excitation forces in frequency domain analysis. Potential flow assumption neglects the viscous effects of sea water when calculating the hydrodynamic loads on the platform. However, it is a widely accepted method in the field of marine engineering [54-55]. The influence of this assumption on the final results is relatively minor since an additional damping is introduced to account for the viscous effects.

Based on the frequency domain solutions, the platform responses can be calculated using a prediction-correction time-marching method in the AQWA solver, while mooring restoring forces and external loads calculated by the user defined DLL (user_force64.dll).

This paper assumes that the platform acts as a rigid body with six degrees of freedom since the restoring stiffness provided by the mooring system and ballast is significantly smaller than the structural bending stiffness. The participation rate of the platform bending modes is relatively minor compared to the translational and rational modes. This aligns with the typical modelling approach for dynamic analysis of Spar-type platforms. The assumption is expected to have a minimal impact on the results [56-58]. The governing equation of motion of the platform is given as:

$$(\boldsymbol{m}+\boldsymbol{A}_{\mathrm{wv}})\ddot{\boldsymbol{X}}(t)+\boldsymbol{C}\dot{\boldsymbol{X}}(t)+\boldsymbol{K}\boldsymbol{X}(t)+\int_0^t \boldsymbol{h}(t-\tau)\ddot{\boldsymbol{X}}(\tau)\mathrm{d}\tau=\boldsymbol{F}_{\mathrm{h}}(t)+\boldsymbol{F}_{\mathrm{t}}(t)+\boldsymbol{F}_{\mathrm{e}}(t) \tag{3}$$

where *m* is the platform inertial mass, $\boldsymbol{A}_{\mathrm{wv}}$ is the added mass; *K* and *C* are, respectively, the total stiffness and damping matrices; $\boldsymbol{X}(t)$, $\dot{\boldsymbol{X}}(t)$, and $\ddot{\boldsymbol{X}}(t)$ are, respectively, the displacement, velocity, and acceleration vectors of the platform; $\boldsymbol{h}(t)$ is the acceleration impulse function used to consider the radiation memory effect; $\boldsymbol{F}_{\mathrm{h}}(t)$ is the hydrodynamic load and $\boldsymbol{F}_{\mathrm{t}}(t)$ is the mooring restoring force; $\boldsymbol{F}_{\mathrm{e}}(t)$ denotes the external force including the aerodynamic load of the wind turbine and the hydrodynamic load of the tidal turbines. It should be noted that the external forces acting on the platform comprise not only the aerodynamic forces of the wind turbine but also the hydrodynamic forces generated by the tidal turbines.

Fig. 3 presents the logical flow of CATIFES. As can observed from Fig. 3, the dynamic responses of the wind turbine and the tidal turbine are solved by the external force DLL (user_force64.dll), while AQWA solves the platform responses based on the hydrodynamic loads and the external force on the platform. The user_force64.dll is invoked by AQWA at each time step to calculate the aerodynamic loads on the wind turbine and hydrodynamic loads on the tidal turbines. The platform displacement, velocity, and acceleration will be transferred to the DLL and used to for the calculation of the dynamic response of tower, nacelle, and blade structure and aerodynamic load. The shear force and bending moment at the tower-base are fed back to the DLL for the solution of platform motions.

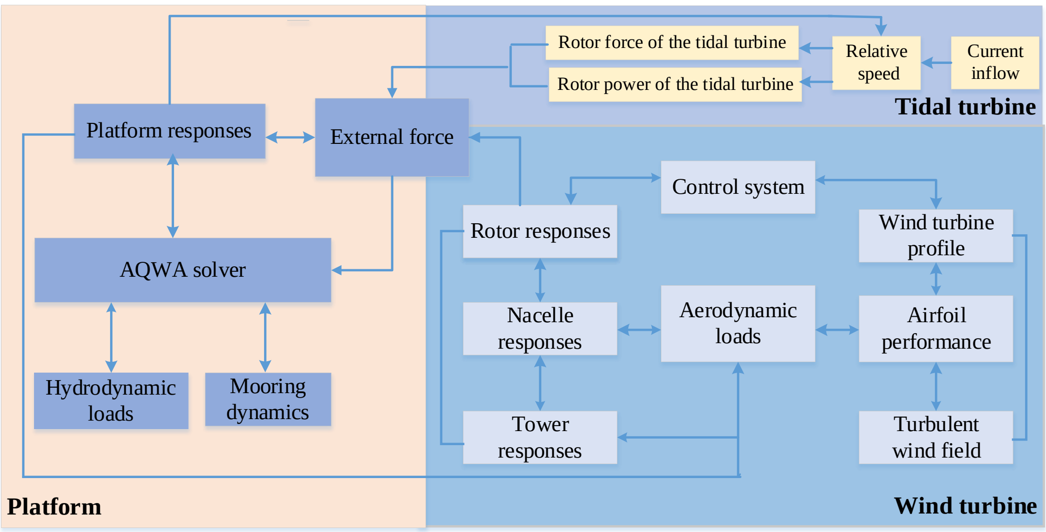

Fig. 3: Schematic of the coupling logic of CATIFES modules

Similarly, the hydrodynamic forces on the tidal turbines are calculated using the method presented in Section 3.2, which takes into account the contribution of platform motions to the current inflow speed $U_{curr,rel}$ using Eq. (4). The hydrodynamic load of the tidal turbines will be transferred back into AQWA acting as an external force for the prediction of platform motions. It is apparently that the aerodynamic load of the wind turbine or the hydrodynamic load of the tidal turbine is affected by the platform response, and vice versa.

$$U_{curr,rel} = U_{curr} - U_{ptfm,surge} - (Z_{tidal} - Z_{ptfm})U_{ptfm,pitch} + (Y_{tidal} - Y_{ptfm})U_{ptfm,yaw} \qquad (4)$$

where U_{curr} is the defined inflow current speed at the tidal hub depth. $U_{ptfm,surge}$, $U_{ptfm,pitch}$

and $U_{ptfm,yaw}$ are the surge, pitch and yaw velocities of the platform, respectively. Z_{tidal} and Z_{ptfm} are the vertical coordinates of the CMs of the tidal turbine and platform, respectively. Y_{tidal} and Y_{ptfm} are the lateral coordinates of the CMs of the tidal turbine and platform, respectively.

Since the AQWA solver only accepts the external force applying at the mass center of the platform, transformations must be made to the aerodynamic loads calculated in the DLL. Taking the coupling between the platform and the wind turbine as the example, the platform motions generated by the AQWA solver is the response at the mass center of the platform, while the platform motion accepted by the DLL for updating the kinematics of the wind turbine is at a specific reference point that is usually the tower-base. Therefore, the Euler angle transformation matrix given below is used for the data transfer between the AQWA solver and DLL [59].

$$\boldsymbol{E}=\begin{bmatrix} \cos\theta_2\cos\theta_3 & \sin\theta_1\sin\theta_2\cos\theta_3-\cos\theta_2\sin\theta_3 & \cos\theta_1\sin\theta_2\cos\theta_3+\sin\theta_1\sin\theta_3 \\ \cos\theta_2\sin\theta_3 & \sin\theta_1\sin\theta_2\cos\theta_3+\cos\theta_2\sin\theta_3 & \cos\theta_1\sin\theta_2\cos\theta_3-\sin\theta_1\sin\theta_3 \\ -\sin\theta_2 & \sin\theta_1\cos\theta_2 & \cos\theta_1\cos\theta_2 \end{bmatrix} \quad (5)$$

where θ_1, θ_2, and θ_3 are, respectively, the roll, pitch, and yaw angles of the platform.

The platform motion output from AQWA is transformed as follows:

$$\boldsymbol{D}_{DLL}=\boldsymbol{D}_{AQWA}-\boldsymbol{E}\bullet\boldsymbol{P} \quad (6)$$

where $\boldsymbol{P}$ is the position vector from the platform reference point to the mass center of platform, $\boldsymbol{D}_{AQWA}$ and $\boldsymbol{D}_{DLL}$ are, respectively, the platform displacement vectors obtained at AQWA and the incoming DLL.

The velocity of the platform is transformed as follows:

$$\boldsymbol{U}_{DLL}=\boldsymbol{U}_{AQWA}-\boldsymbol{E}\bullet\boldsymbol{P}\times\boldsymbol{\omega} \quad (7)$$

where $\boldsymbol{U}_{AQWA}$ and $\boldsymbol{U}_{DLL}$ are the platform velocity vectors obtained in AQWA and the one used in the DLL, respectively; $\boldsymbol{\omega}$ is the rotational velocity vector of the platform obtained in

AQWA.

The platform acceleration is not available for transfer between the solver and the DLL. Therefore, the first-order forward difference of the velocity is used to denote the acceleration as follows:

$$\boldsymbol{a}_{DLL} = \frac{\boldsymbol{U}_{DLL} - \boldsymbol{U}'_{DLL}}{\Delta t} \tag{8}$$

where $\boldsymbol{a}_{DLL}$ is the platform acceleration and $\boldsymbol{U}'_{DLL}$ is the platform velocity at the last time step, Δt is the time step of the simulation.

The tower-base loads calculated in the DLL will be transferred to the AQWA solver as a external force for the prediction of the platform motion. It is noted the tower-base loads are referred to the local platform coordinate system, however, the external force applying at the mass center of platform is referred to the inertial coordinate system. The loads are corrected as follows:

$$\boldsymbol{F}_{AQWA} = \boldsymbol{E}^{-1} \bullet \boldsymbol{F}_{DLL} \tag{9}$$

$$\boldsymbol{M}_{AQWA} = \boldsymbol{E}^{-1} \bullet (\boldsymbol{M}_{DLL} - \boldsymbol{P} \times \boldsymbol{F}_{DLL}) \tag{10}$$

where $\boldsymbol{F}_{AQWA}$ and $\boldsymbol{F}_{DLL}$ are the translational force vectors fed back into in AQWA and calculated in the DLL, respectively; $\boldsymbol{E}^{-1}$ is the inverse of the transformation matrix $\boldsymbol{E}$; $\boldsymbol{M}_{AQWA}$ is the moment vector applying at the mass center of the platform referred to the inertial coordinate system; $\boldsymbol{M}_{DLL}$ is the moment vector at the tower-base referred to the local platform coordinate system.

3.4 Validation of the CATIFES

Since there is no published experimental or numerical simulation data for the wind-current type IFES, the validation of the CATIFES model is examined by verifying its capability in performing coupled analysis of a FOWT and in predicting performance of tidal turbines, respectively.

The dynamic responses of the DTU 10MW wind turbine supported by the Spar platform under 9m/s turbulent wind condition are calculated using CATIFES and OpenFAST v3.2, respectively. The results during 800s to 3600s is selected for the comparison to avoid the influence of the transient behavior. Fig. 4 shows the comparison of the platform motions. It can be observed that the results calculated by CATIFES and OpenFAST agree very well in trends and magnitudes. More specifically, the mean values of the pitch predicted by OpenFAST v3.2 and CAT4IFES are respectively 8.3 degrees and 8.5 degrees, meaning the difference is 2.4%. The difference between the maximum pitch predicted by the present model and OpenFAST is 0.7 degrees, equivalent to a relative error of 4.8%. The platform surge motions obtained by CATIFES and OpenFAST are almost identical in the domain variations. The comparison of the platform motions indicates that CATIFES could produce acceptable dynamic responses of a FOWT under turbulent wind conditions.

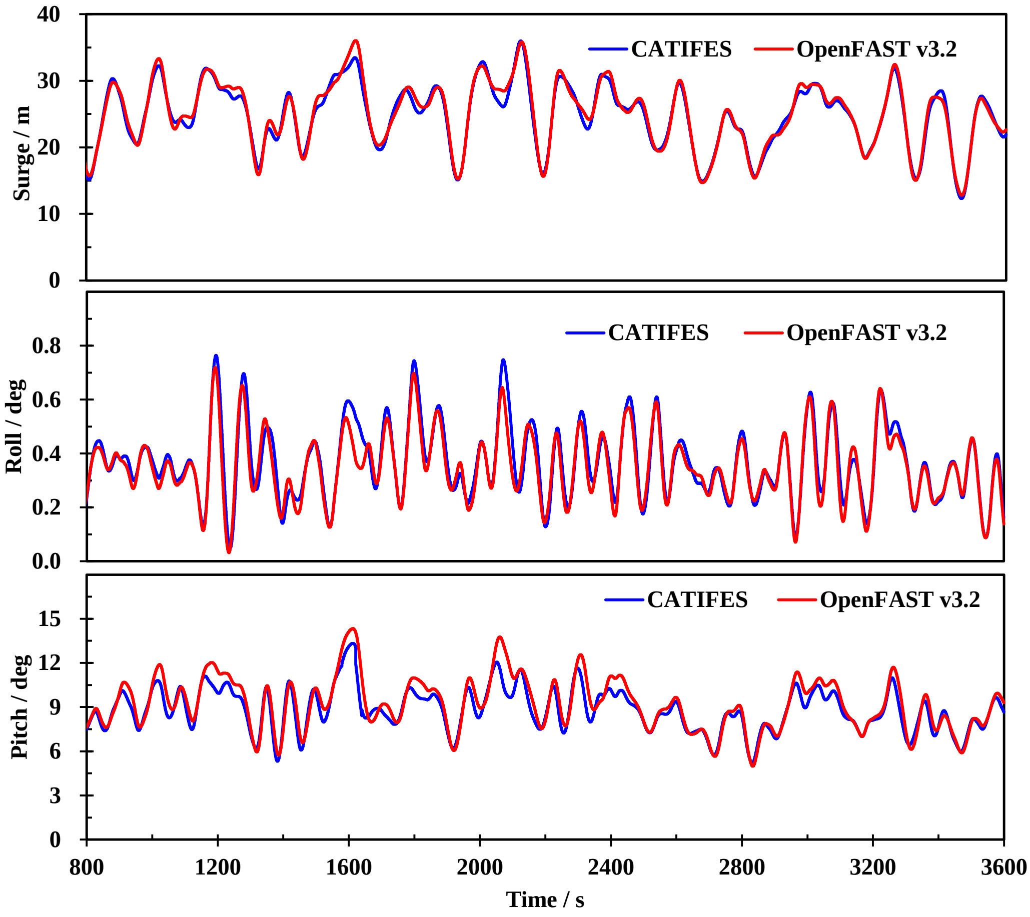

Fig. 4: Comparison between the platform motions predicted by the present CATIFES model

and OpenFAST

Fig. 5 presents the fairlead tension in the mooring lines. Good agreements between the fairlead tensions in each mooring line predicted by CATIFES and OepnFAST are observed. There is only a small difference for the maximum values. More specifically, the mean value and standard deviation of the fairlead tension in mooring line #2 predicted by CATIFES are 2.55MN and 0.12MN, while the corresponding results obtained using OpenFAST are 2.58MN and 0.13MN. The maximum tensions in mooring line #2 calculated by CATIFES and OpenFAST are 2.90MN and 2.92MN, respectively. The relative error is only 0.68%.

The main reason producing the difference between the simulation results of the present model and OpenFAST is that there is a minor difference between the mooring modeling theories of OpenFAST and AQWA. AQWA uses the finite element method to consider the dynamic mooring effects and calculates the hydrodynamic loads acting on the mooring based on the wave velocity at the current position of the mooring. OpenFAST, on the other hand, considers the dynamic effects of the mooring using the lumped mass approach, and the hydrodynamic loads applied to the mooring are based on the wave motion at the initial position of the platform. Although a minor difference between the results is observed, the overall agreement is good enough, indicating that the CAT4IFES model can consider the coupling effect between the aero-elasticity and hydrodynamics of the FOWT.

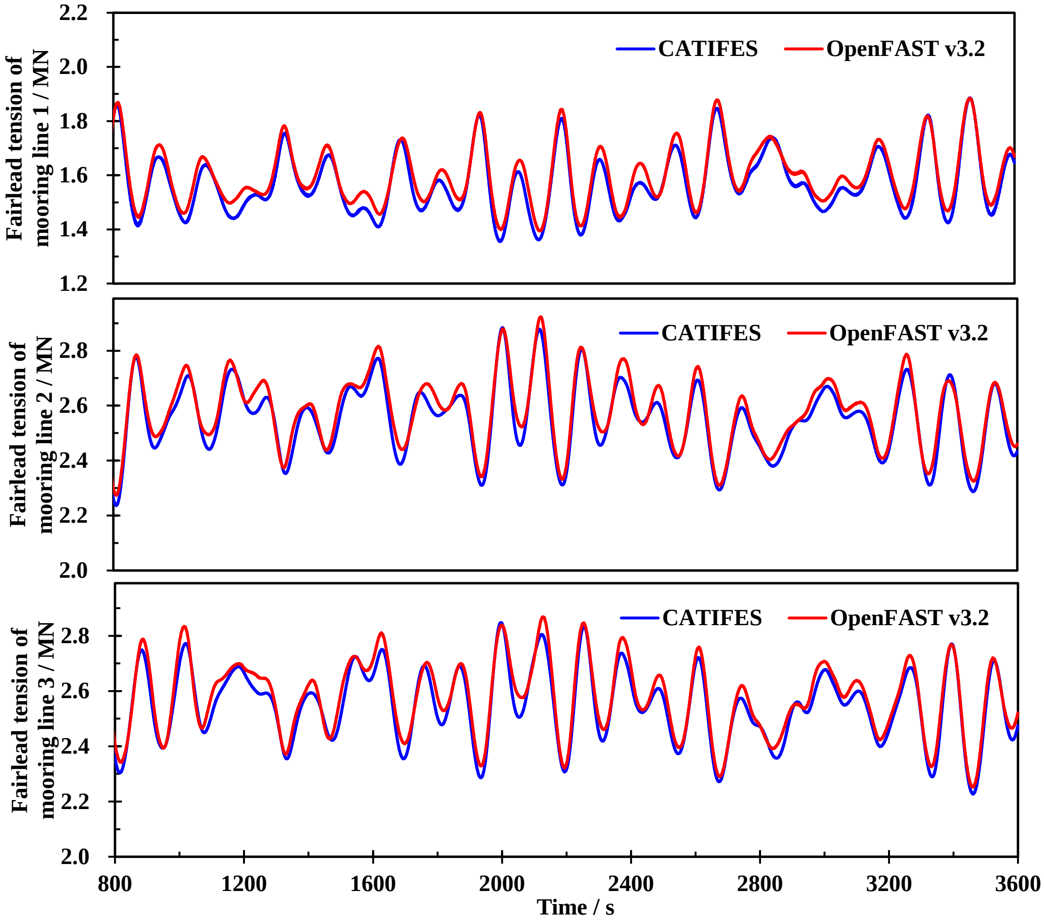

Fig. 5: Fairlead tension of CATIFES and OpenFAST v3.2

The experimental data from the model test conducted by Bahaj et al [47]. and Doman et al [48]. is used to validate CATIFES for predicting the hydrodynamic performance of a tidal turbine. The test data and numerical simulation results are presented in Fig. 6. In model test 1, the numerical simulation predicted power and thrust coefficients that are consistent with the trends in the test data, although the power coefficient is slightly overestimated for high tip-speed ratios (TSR). In model test 2, the numerical results at low TSR are slightly higher than the test data due to the cavitation effect. However, within the common operating range of TSR 4-6, the power and thrust coefficients predicted by the present CATIFES agree well with the test results. Overall, the consistency between the numerical simulation results and the model tests is good, confirming the accuracy of the numerical model in predicting the response of tidal turbines is acceptable.

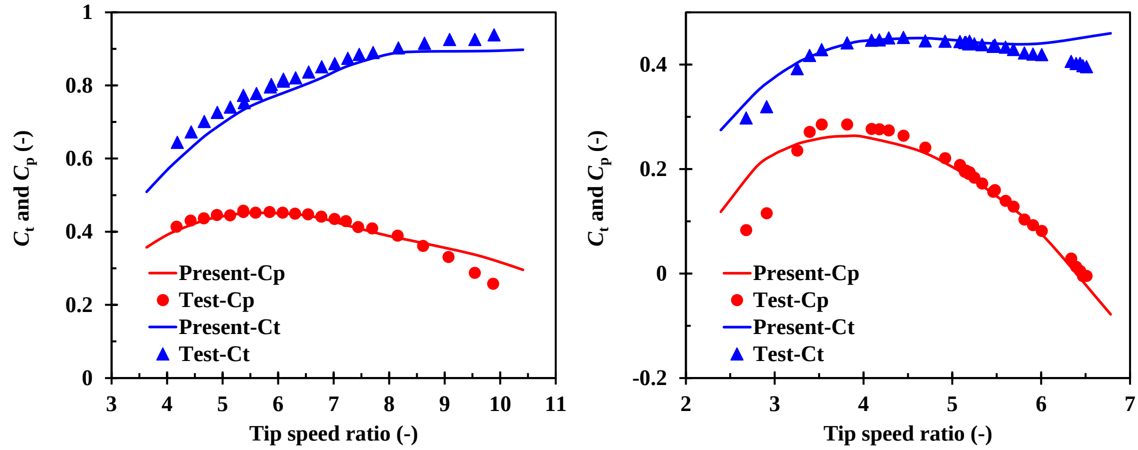

(a) Model test 1 (b) Model test 2

Fig. 6: Comparison between tidal turbine responses obtained from the present numerical simulations and model tests; (a) model test 1 conducted by Bahaj *et al.* [47] for a 0.8 m diameter rotor, (b) model test 2 conducted by Doman *et al.* [48] for a 0.762 m diameter rotor.

A pitch-torque controller is developed to adjust the power production of the tidal turbine. In order to validated the controller, the simulation of the tidal turbine suffering a step current speed condition is conducted. The duration of each step speed is 50s. Fig. 7 presents the generator power, rotor speed and blade pitch angle of the tidal turbine under the step current speed condition. It is observed that a steady state is quickly achieved after a quite short transient period between each two speeds. The power and rotor speed in the steady states are compared with the design parameters as presented in Fig. 8. It can be observed that the numerical results are identical to the design parameters for each inflow current speed. The comparison indicates that the controller implemented in this study is efficient in adjusting rotor speed and blade pitch to achieve a target power.

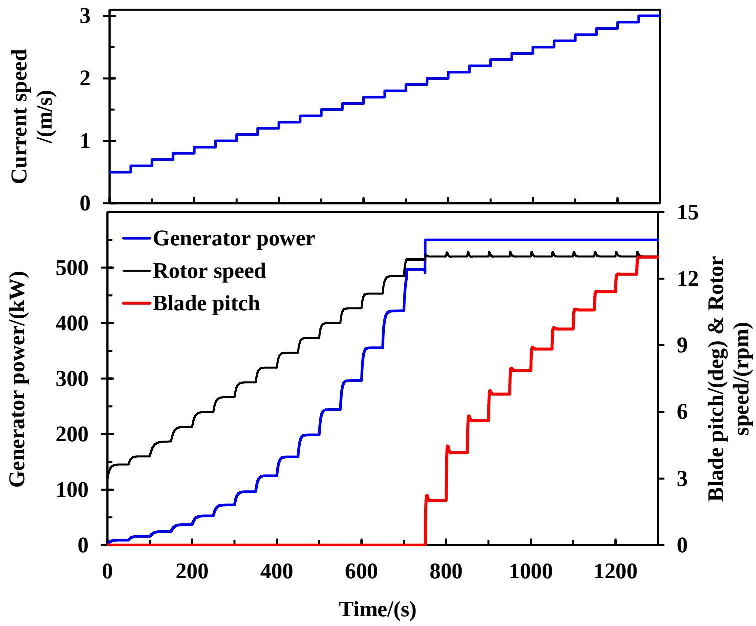

Fig. 7: Controller performance under an unsteady inflow condition

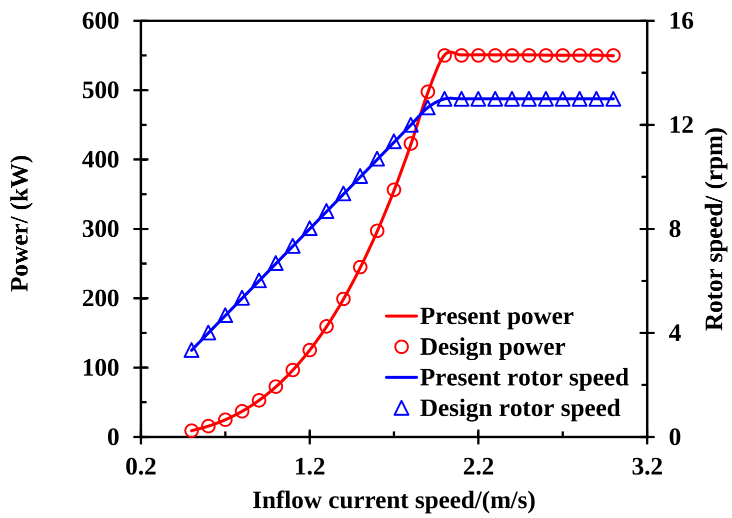

Fig. 8: Comparisons of power and rotor speed under steady conditions

4 Results and discussions

4.1 Definition of load cases

Table 6 presents the definitions of the environmental conditions of the load cases examined in this study. The wind speed gradually increases from 3m/s to 25m/s. The three-dimensional wind field of each load case is generated using TurbSim based on the Kaimal spectrum. The significant wave height and spectral peak period corresponding to each wind speed are defined according to the met-ocean data measured from an Eastern coastal site of the USA [53]. The JONSWAP wave spectrum with a peak shape parameter of 3.3 is applied for the irregular waves.

Table 6: Load cases for different environmental conditions

	Wind speed/(m/s)	Significant Wave Height/m	Peak Spectral Period/s	Current speed at MSL/(m/s)	Probability
LC1	3	1.089	8.569	0.61	2.34%
LC2	4	1.108	8.496	0.65	3.57%
LC3	5	1.146	8.392	0.68	4.13%
LC4	6	1.198	8.264	0.73	5.56%
LC5	7	1.269	8.103	0.92	6.98%
LC6	8	1.359	7.923	1.06	7.78%
LC7	9	1.478	7.724	1.22	8.24%
LC8	10	1.617	7.569	1.31	7.66%
LC9	11	1.779	7.451	1.46	7.00%
LC10	12	1.954	7.443	1.52	6.77%
LC11	13	2.144	7.457	1.66	6.32%
LC12	14	2.350	7.508	1.70	5.99%
LC13	15	2.573	7.629	1.81	5.24%
LC14	16	2.808	7.810	2.01	4.70%
LC15	17	3.062	8.047	2.12	4.17%
LC16	18	3.361	8.294	2.23	3.24%
LC17	19	3.645	8.549	2.42	2.89%
LC18	20	3.860	8.796	2.51	2.13%
LC19	21	4.081	9.042	2.66	1.83%
LC20	22	4.335	9.288	2.71	1.15%
LC21	23	4.610	9.534	2.81	1.00%
LC22	24	4.905	9.779	2.86	0.72%
LC23	25	5.216	10.025	2.98	0.66%

The dynamic responses of the IFES with two tidal turbines installed at 110m below the sea level calculated using CAT4IFES and compared with those of the FOWT for the load cases presented in Table 6.

The simulation duration of each load case is set to 4400s and time step is 0.005s. To avoid the influence of transient response, the statistical analysis is performed for the responses in 2000s to 4400s.

4.2 Time-varying responses in the rated condition

In order to obtain a preliminary understanding of the dynamic behavior of the IFES and the efficacy of integrating tidal turbines within the FOWT system, the dynamic responses of the IFES under a specific load case are compared with those of the FOWT. Fig. 9 presents the platform motions of the IFES and the FOWT under LC9 in which the wind speed is 11m/s and the current speed is 1.46m/s. Due to the presence of the tidal turbines, the average platform surge of the IFES is larger than that of the FOWT, while the maximum value decreases. More specifically, the maximum platform surge motions of the IFES and the FOWT are respectively 32.51m and 35.50m, implying a reduction of 8.42% is obtained. Moreover, the fluctuation in the surge motion is alleviated. The standard deviation of the platform surge corresponding to the IFES is 4.38m, while the value of the FOWT is 6.56m. The reason is that the hydrodynamic thrust on the tidal turbines prevents the platform from excessively moving back against the wind when the aerodynamic damping is decreased duo to the increase of blade pitch angle.

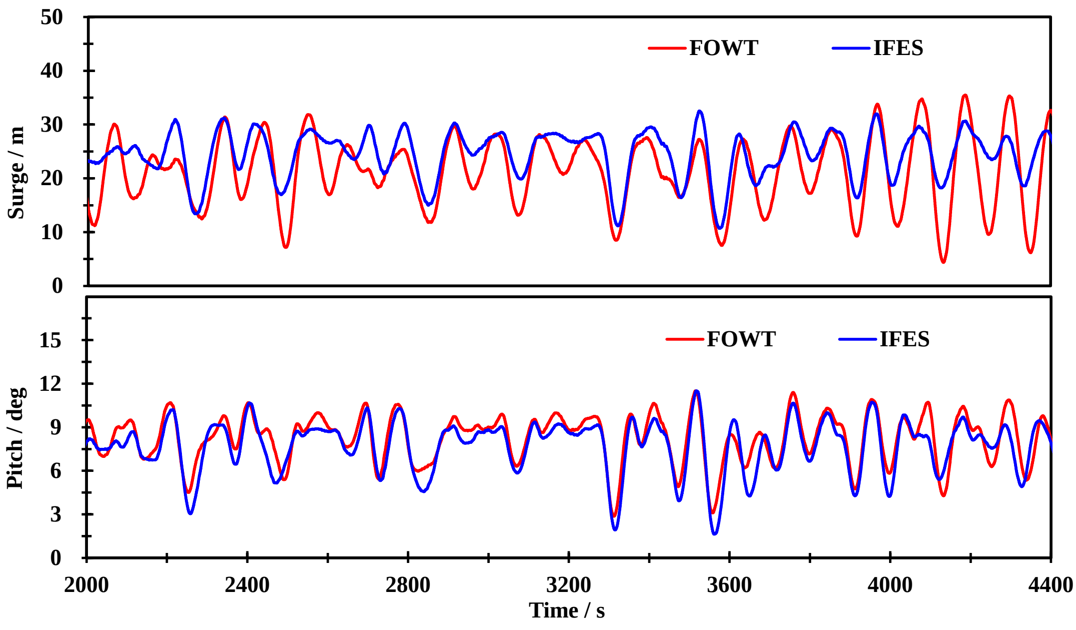

Fig. 9: Platform motion of the IFES and FOWT under LC9

As aforementioned in this paper, the tidal turbines are installed at 110m below the mean sea level which is 18.4m lower than the mass center of the platform. The hydrodynamic thrust of the tidal turbines produces a bending moment reverse to that generated by the wind turbine. Therefore, the IFES has a relatively smaller platform pitch than the FOWT as observed from Fig. 9 (b). The average platform pitch of the IFES is reduced by 6.42% compared to that of the FOWT, from 8.25 degrees to 7.72 degrees.

Fig. 10 presents the mooring tension of the FOWT and IFES. The mooring line #1 (windward) of the IFES experiences higher tension due to the more stretched state caused by the relatively larger horizontal thrust. As the platform approaches the leeward mooring, the mooring line #2 and #3 become loose and therefore experience a relatively smaller tension.

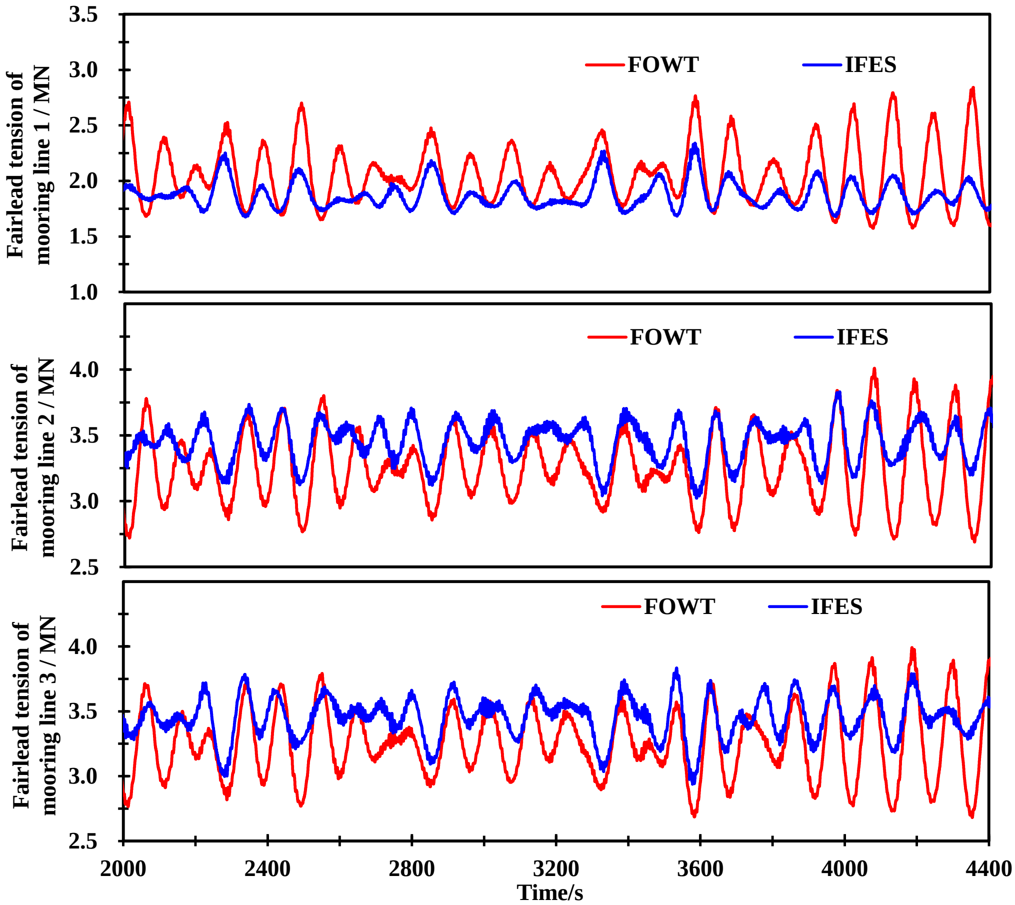

Fig. 10: Fairlead tensions of the mooring line under LC9

Table 7 presents the statistical values of tensions in the three mooring lines of the IFES and FOWT. Error means the difference between the results of the IFES and FOWT. It shows that the maximum tension of each mooring line of the IFES is smaller than that of the FOWT, especially for mooring line #1 placed in the downwind direction. The maximum tension is reduced by 17.61%. The average tension in mooring lines #2 and #3 of the IFES is 5.83% relatively larger than that of the FOWT. Nonetheless, the standard deviation of the tension in each mooring line is significantly reduced. The reductions in mooring line #1, #2 and #3 are respectively55.56%, 44.44% and 40.74%

Table 7: Statistical values of mooring tensions / MN

		FOWT	IFES	Error/%
Mooring line #1	Max	2.84	2.34	-17.61
	Average	2.06	1.87	-9.22
	Std.dev	0.27	0.12	-55.56
Mooring line #2	Max	4.01	3.83	-4.49
	Average	3.26	3.45	5.83
	Std.dev	0.27	0.15	-44.44
Mooring line #3	Max	3.99	3.83	-4.01
	Average	3.26	3.45	5.83
	Std.dev	0.27	0.16	-40.74

Fig. 11 presents the output power of the IFES and FOWT. The average power generated by the wind turbine of the IFES is 8.63MW and the FOWT produces a mean power of 8.59MW. In addition, the generator power of the wind turbine in the IFES is smoother compared to the FOWT due to the more stable platform motions. As a result, the average output power increases by 0.47% and the corresponding standard deviation decreases by 6.82%. Moreover, the two tidal turbines produce an average power of 0.30MW that is slightly lower than the expectation due to the influence of the platform motions. The total power of the IFES is 8.93MW that is 3.96% higher than the FOWT. The above results indicate that the integration of wind and current energy devices not only increases the total power of the whole system, but also improves the wind turbine's power performance.

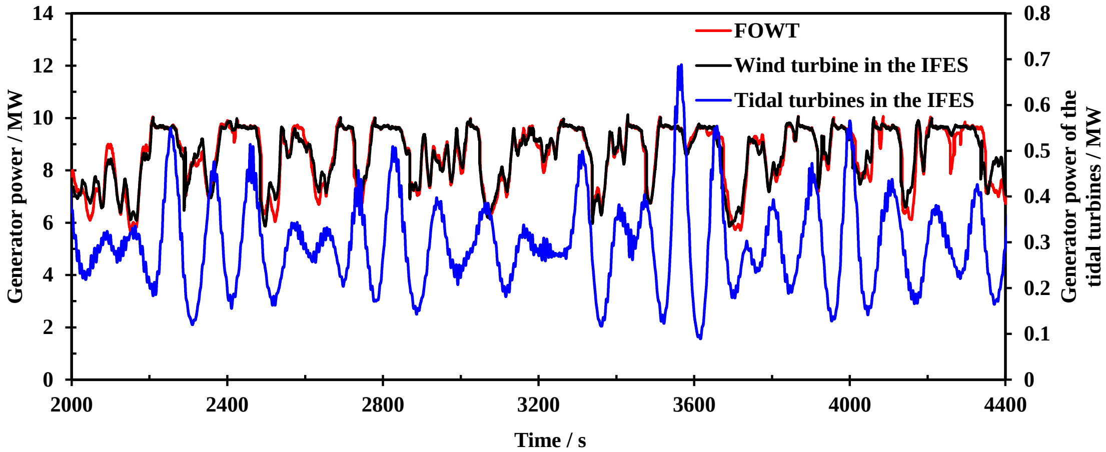

Fig. 11: Generator power of the IFES and FOWT under LC9

4.3 Statistical values of the results

Fig. 12 presents the average output power of the FOWT and IFES under various environmental conditions. The IFES shows higher power output compared to the FOWT for all load cases due to the contribution of the tidal turbines. When wind speed below 11m/s, the corresponding current speeds are smaller than 1.46m/s, resulting in an increase rate of approximately 3% of the total power due to tidal turbines. For load cases with a current speed higher than 2.01m/s, the two tidal turbines produce about 0.9MW power, which increases the total power by around 10% compared to the FOWT. Notably, the tidal turbines do not negatively affect the power performance of the wind turbine in the IFES. The average power output of the wind turbine in the IFES is almost the same as that of the FOWT in all load cases, and even slightly higher than that of the FOWT for wind speeds below 18m/s. This is mainly due to the fact that tidal turbines mitigate the fluctuation of the platform motions, thereby improving the performance of the wind turbine.

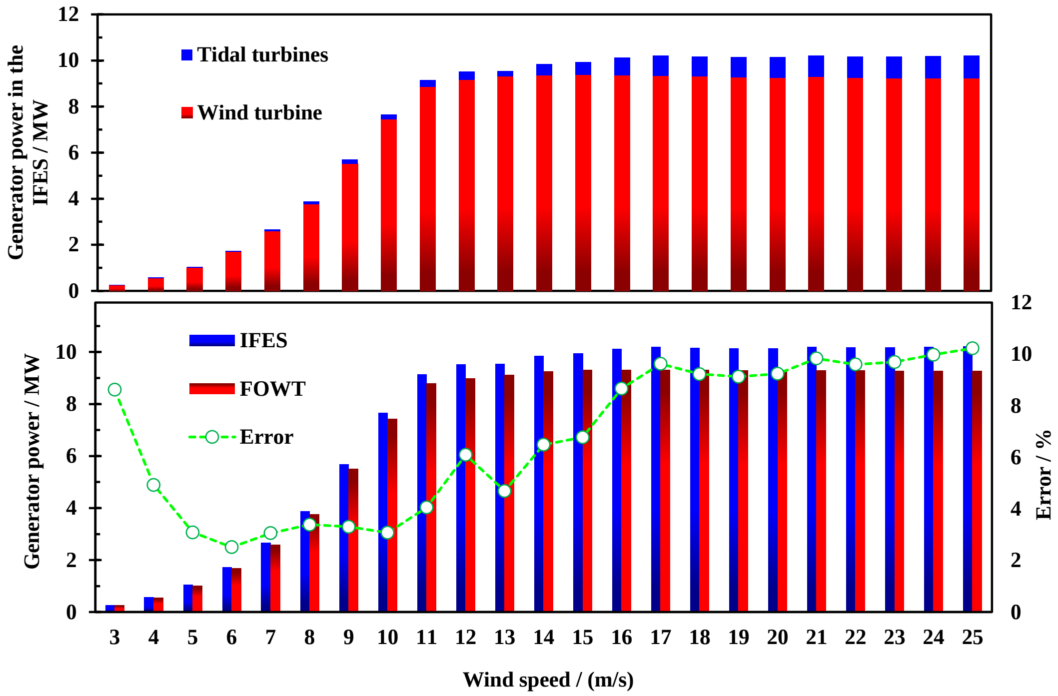

Fig. 12: The average output power of the IFES and FOWT under all load cases

The average and standard deviation of the surge and pitch motions of the FOWT and the IFES under all the load cases are presented in Fig. 13. The pitch motion of the IFES is smaller than that of the FOWT for each of the examined load cases. It is noteworthy that when the speed exceeds 16m/s, the pitch reduction ratio is more than 20%. This reduction is particularly evident at a wind speed of 25m/s, where the pitch motion decrease from 3.36 degrees to 2.45 degrees, resulting in a reduction proportion of up to 27.08%. This is mainly because the tidal turbine is located below the mass center of the platform, which produces a bending moment on the platform inverse to the bending moment generated by the wind turbine.

For the same reason, the horizontal force acting on the platform is increased by the tidal turbines, leading to a lager surge motion of the platform as observed from Fig. 13(a). In addition, the standard deviation of the surge motion of the IFES is much smaller in the rated-around wind speed conditions. The standard deviation of the surge motion of the FOWT under LC10 and LC11 are 14.39m and 16.76m, respectively. The corresponding values of the IFES are respectively reduced to 6.17m and 5.90m. The wind speed in these two is over rated wind speed. The pitch control activated to reduce the aerodynamic efficiency for the regulation of generator torque. As a result, the fluctuation in the aerodynamic thrust is triggered, resulting a large standard deviation of surge motion. While the tidal turbines provide a hydrodynamic thrust that counteracts a certain of the fluctuations of the aerodynamic thrust. Therefore, the variation of the surge motion in these conditions is much smoother as evidenced by the significantly smaller standard deviation. In the LC14~LC23, the tidal turbines operate in the rated-above conditions. The pitch control is activated to maintain the generator power, resulting in a notable fluctuation in the hydrodynamic loads due to platform motions. Meanwhile, the aerodynamic thrust provided by the wind turbine is relatively small. The fluctuation in the hydrodynamic thrust of the tidal turbines significantly affects the platform surge motion. This implies that the coupling between the tidal turbines and the wind turbine must be considered for the control of the IFES, for improving the stability and safety of the system.

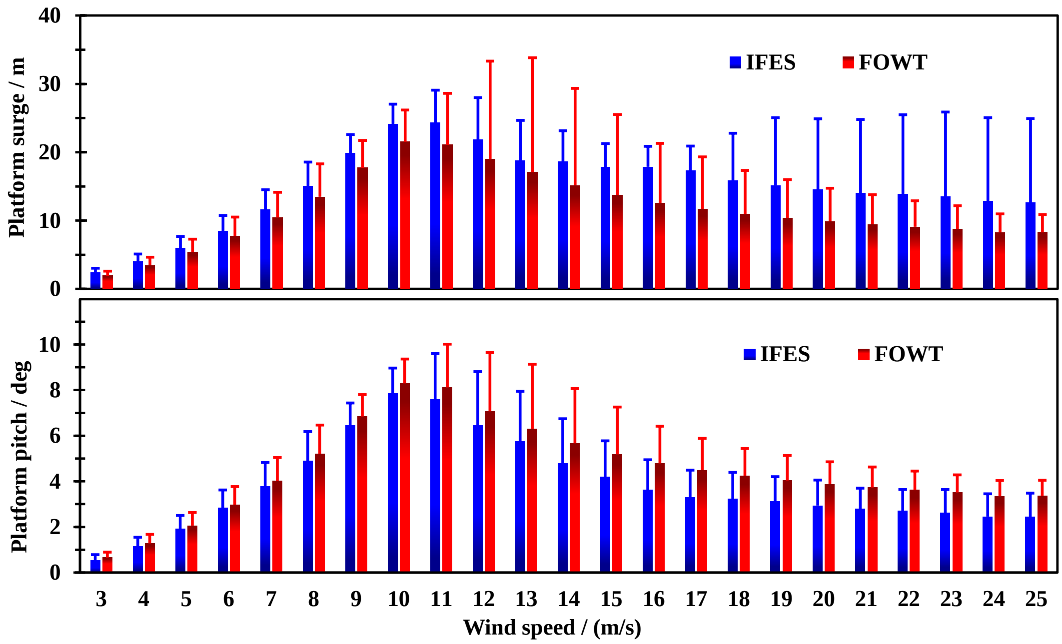

Fig. 13: Platform motion of the IFES and FPWT under load cases

Fig. 14 presents the average mooring tensions of the IFES and FOWT under all load cases.

Mooring line #1 is located in the downwind position, while moorings line #2 and #3 are situated in the windward position as shown in Fig. 1. In the IFES, the horizontal thrust generated by the tidal turbine causes a more significant longitudinal movement displacement of the platform, leading to a more significant stretching of the windward mooring. Thus, the tension in this mooring becomes notably high. When the wind speed is 17m/s, the corresponding current speeds are 2.12m/s. This leads to a decrease in the tension of mooring line #1 from 2.37MN to 1.97MN, resulting in a reduction rate of up to 16.88%. The reduction in tension of mooring line #1 in the IFES is greater than 10% compared to the average value in the FOWT under LC10 to LC18.

Furthermore, as the platform approaches the downwind mooring line anchor point, mooring #1 experiencing a relaxed state consequently has a less tension. It is worth noting that the reduction in tension of mooring #1 of the IFES is more substantial than that of the FOWT due to the presence of the tidal turbines. The results suggest that the installation of tidal turbines can result in significant differences in the mooring tension distribution, particularly in the windward moorings. Under LC10 and LC11, the mean value of mooring line #2 increased from 3.29MN and 3.27MN for the FOWT to 3.39MN and 3.28MN for the IFES, respectively. However, the increase ratios were only 3.04% and 0.31%, respectively. On the other hand, the mooring line #1 decreased significantly from 2.23MN and 2.35MN for the FOWT to 1.94MN and 2.04MN for the IFES, resulting in decrease proportions of 13.00% and 13.19%, respectively.

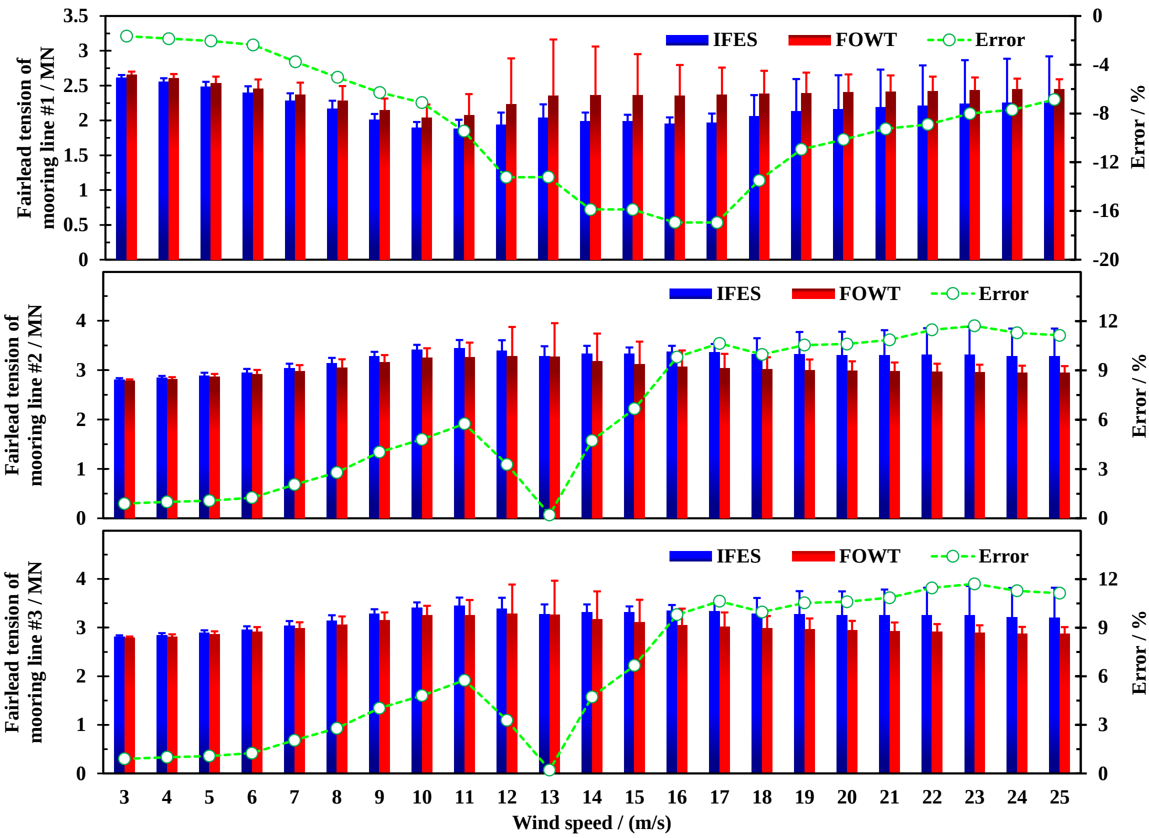

Fig. 14: Average of fairlead tension in the mooring lines under load cases

4.4 Tower fatigue damage

In this paper, the fatigue assessment is performed int the domain using the rainflow counting method for cycles. To ensure that the tower remains free from fatigue damage during its design service life, the estimation of the tower fatigue damage is required [60]. According to the Palmgren-Miner theory, individual stresses under cyclic loading are independent of each other, implying that the fatigue damage can accumulate linearly. Once the accumulated damage reaches a specific threshold value, fatigue damage occurs in the member [61]. The total fatigue damage is calculated by summing up the damage caused by each design sea state as given in Eq. (11). The damage for each sea state is computed by adding the damage for each stress or tension level using the rainflow counting method.

$$D = \sum_{j}^{N_{total}} \frac{n_j}{N_j} \tag{11}$$

where n_j is the number of cycles in the j^{th} stress range in the time history and N_j is the number of cycles to failure in the corresponding stress range according to the design S-N curve.

The fatigue damage at the tower base is evaluated. The stress at the tower base is converted from the bending moment and axial force as follows.

$$\sigma = \frac{M_y}{I_y} r \cdot \cos\theta - \frac{F_z}{A} - \frac{M_x}{I_x} r \cdot \sin\theta \tag{12}$$

where F_z is the axial force, M_x and M_y are the bending moments about the x-axis and y-axis, θ is the angle of the fatigue analysis point. A is the cross-section area. The coordinate system of the tower-base loads is presented in Fig. 15.

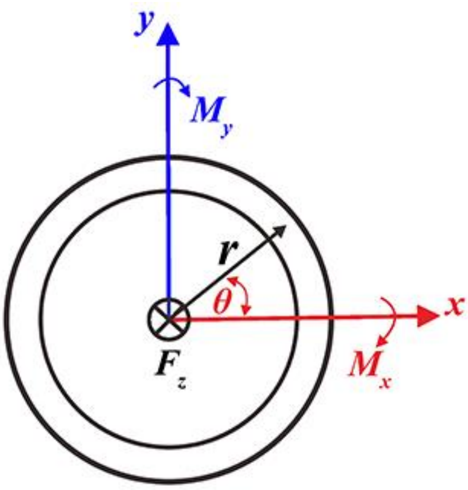

Fig. 15: Tower-base coordinate system

The S-N curve suggested in the DNV standard [62] for fatigue assessment of offshore steel structure is selected. The number of cycles to failure N is calculated using Eq. (13).

$$\log N = \log a - m \log\left(\Delta\sigma \left(\frac{t}{t_{ref}} \right)^k \right) \tag{13}$$

where $\Delta\sigma$ represents the stress range, and t is the thickness at the tower-base. Table 8 gives the values of other parameters for the fatigue assessment.

Table 8: S-N curve parameter for tower base

$N \leq 10^7$ cycles		$N > 10^7$ cycles		Fatigue time at 10^7 cycles [MPa]	k	t_{ref} [mm]
m	$\log a$	m	$\log a$			
3	12.164	5	15.606	52.63	0.2	25

As revealed in the above sections, the average value and standard deviation of the platform pitch motion are reduced by the tidal turbines. The installation of the tidal turbines is expected to reduce the loads at the tower-base, potentially decrease the fatigue damage. In order to quantitatively evaluate the effect of the tidal turbines on the tower fatigue damage, the equivalent stress of the tower is obtained using Eq. (13) for a specific orientation angle based on the bending moments and axial force eight orientation angles.

The equivalent tower-base stress at the 0° orientation (see Fig. 15) of IFES and FOWT under LC5, LC9 and LC18 are presented in Fig. 16. It is found that the mean stress of the IFES is lower than that of the FOWT for each of the load cases. At a wind speed of 7m/s, The maximum stress values of the FOWT and IFES under LC5 are respectively 3.48MPa and 3.42MPa. This indicates a stress reduction of 1.72% with the IFES model. Furthermore, the average stress value is reduced from 1.86MPa to 1.78MPa in the IFES model, meaning that a reduction of 4.30% is obtained. This stress reduction is attributed to the tidal turbines that alleviate the impact force of the current on the tower.

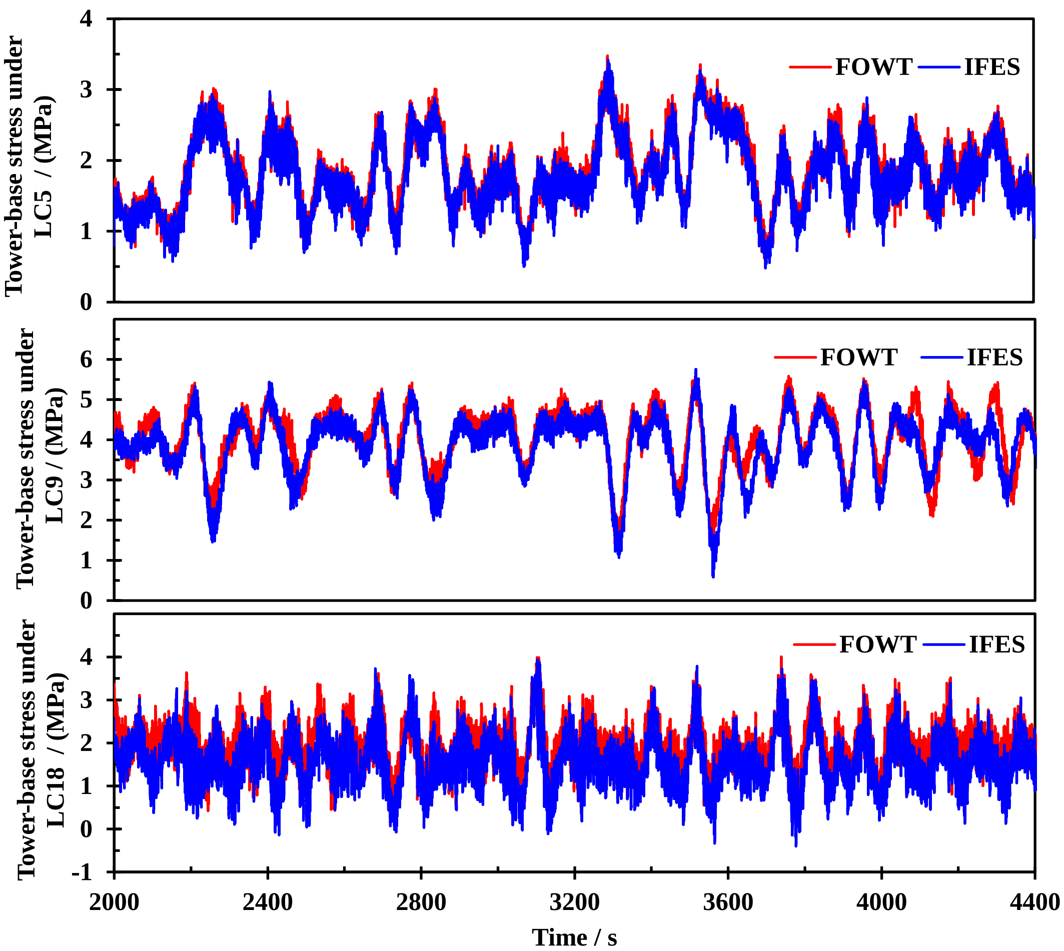

Fig 16: Tower-base stress at the 0° orientation under LC5, LC9 and LC18, respectively

Considering the occurrence probability, the weighting fatigue damage at the tower-base of the IFES and FOWT contributed by each of the load case is presented in Fig. 17. It is evident that the FOWT model experiences higher fatigue damage when the wind speed ranges between 12m/s and 15m/s. The IFES model exhibits significant reduction in the fatigue damage value. Notably, the fatigue damage decreases from 0.1447 to 0.0729 in IFES under the condition with a wind speed of 13m/s, denoting a remarkable reduction of 49.62%.

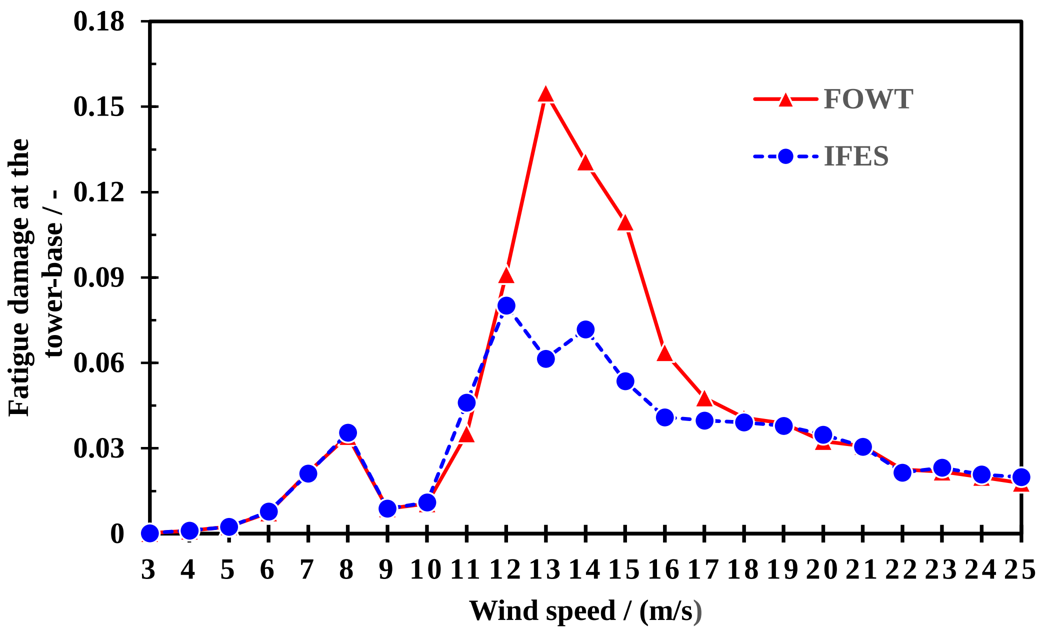

Fig. 17: Fatigue damage at the tower-base of the IFES and FOWT under all the load cases

The fatigue damage induced by each load case at the critical location is evaluated first and subsequently cumulated to obtain the total fatigue damage at the tower-base.

Fig. 18 presents the fatigue damage at the tower-base of the IFES and FOWT. It is evident that the FOWT experiences the highest fatigue damage at 0° and 180° orientations of the tower-base section with a value of 0.9345 and 0.9288, respectively. However, the introduction of two tidal turbines has led to a significant reduction in the corresponding damage for the IFES. The fatigue damage for IFES reduced by 13.91% and 14.14% at 0° and 180° orientations. Moreover, the IFES is successful in reducing the fatigue damage in other orientations at the tower-base section compared to the FOWT.

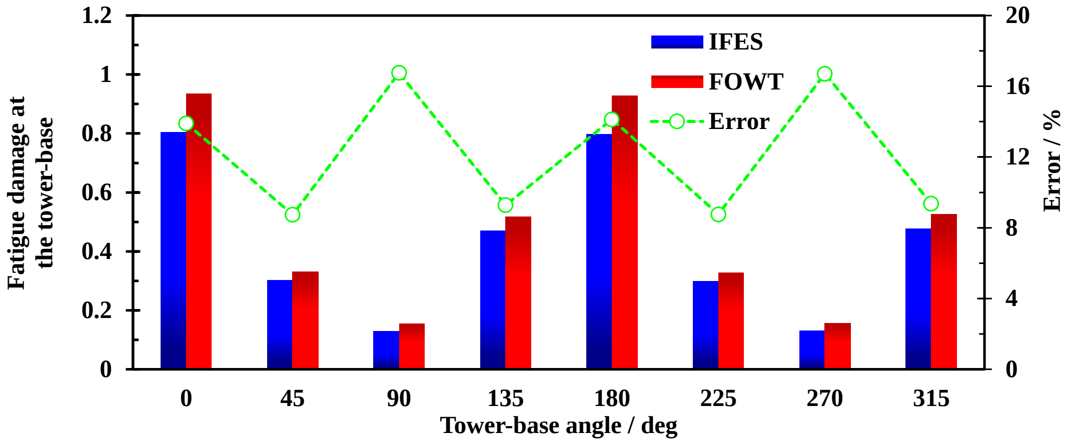

Fig. 18: Fatigue damage at the tower-base of the IFES and FOWT

5 Conclusions

This study investigates the performance and fatigue damage of an IFES consisting of a 10MW wind turbine and two 550kW tidal turbines. The validation against the OpenFAST and model test data confirms the suitability of CATIFES for multi-physics field coupled simulations of IFES. Integrating tidal turbines with a FOWT is able to improve the platform stability by introducing an additional reverse overturning bending moment. Consequently, the generator power of the wind turbine is improved in magnitude and smoothness.

Furthermore, the integration of tidal turbines into the FOWT significantly mitigates the tension fluctuation in the mooring lines by over 40.74%, primarily due to the narrower surge motion range. Compared to the FOWT, the maximum tension in each mooring line of the IFES is relatively smaller. Moreover, the fatigue damage at the tower-base of the IFES is significantly reduced compared to the FOWT. Specifically, the fatigue damage in the longitudinal points at the tower-base section decreased by around 14% due to the reverse bending moment produced by the tidal turbines.

It should be noted that the variable-speed-variable-pitch control of the wind and tidal turbines are examined separately, since developing a synergistic control strategy between the wind and tidal turbines is beyond the scope of this study. Future research can focus on developing a synergic control algorithm to improve the power production and motion performance of the whole system by incorporating additional control objectives into the conventional pitch-torque controllers. Another limitation of this paper is the omission of the structural flexibility of the tidal turbine's blades. Future studies can address this limitation by developing a fully coupled hydro-servo-elastic model to more accurately analyze the dynamic responses of the IFES.

Acknowledgements

The authors are grateful for the financial support from the National Key R&D Program of China (No. 2023YFE0102000), National Natural Science Foundation of China (Grant No.: 52101317), China Three Gorges Group Co., LTD (Contract No.: 202303059), Natural Science Foundation of Zhejiang Province (Grant No.: LQ22E090001), and the State Key Laboratory of Alternate Electrical Power System with Renewable Energy Sources (Grant No.: LAPS22009).

References

[1] Tahiri, F. E., Chikh, K., & Khafallah, M. (2021). Optimal management energy system and control strategies for isolated hybrid solar-wind-battery-diesel power system. *Emerging Science Journal*, 5(2), 111-124.

[2] Adanta, D., Sari, D. P., Syofii, I., Prakoso, A. P., Saputra, M. A. A., & Thamrin, I. (2023). Performance comparison of crossflow turbine configuration upper blade convex and curvature by computational method. *Civil Engineering Journal*, 9(1), 154-165.

[3] Council, G. W. E. (2022). Floating offshore wind—a global opportunity. *The Global Wind Energy Council*.

[4] Chen, Z., Wang, X., Guo, Y., & Kang, S. (2021). Numerical analysis of unsteady aerodynamic performance of floating offshore wind turbine under platform surge and pitch motions. *Renewable Energy*, 163, 1849-1870.

[5] Cheng, P., Huang, Y., & Wan, D. (2019). A numerical model for fully coupled aero-hydrodynamic analysis of floating offshore wind turbine. *Ocean Engineering*, 173, 183-196.

[6] Huang, Z., Qian, Y., Wang, Y., Mu, A., Yang, B., & Wang, J. (2022). Numerical analysis of floating wind turbines stability control strategy based on a novel tuned mass damper. *Journal of Renewable and Sustainable Energy,* 14(5).

[7] Chuang, T. C., Yang, W. H., & Yang, R. Y. (2021). Experimental and numerical study of a barge-type FOWT platform under wind and wave load. *Ocean Engineering*, 230, 109015.

[8] Fang, Y., Duan, L., Han, Z., Zhao, Y., & Yang, H. (2020). Numerical analysis of

aerodynamic performance of a floating offshore wind turbine under pitch motion. *Energy*, 192, 116621.

[9] Chen, J., Hu, Z., & Duan, F. (2018). Comparisons of dynamical characteristics of a 5 MW floating wind turbine supported by a spar-buoy and a semi-submersible using model testing methods. *Journal of Renewable and Sustainable Energy*, *10*(5).

[10] Zhou, Y., Xiao, Q., Peyrard, C., & Pan, G. (2021). Assessing focused wave applicability on a coupled aero-hydro-mooring FOWT system using CFD approach. *Ocean Engineering*, 240, 109987.

[11] Abdelbaky, M. A., Liu, X., & Jiang, D. (2020). Design and implementation of partial offline fuzzy model-predictive pitch controller for large-scale wind-turbines. *Renewable Energy*, 145, 981-996.

[12] Fleming, P. A., Peiffer, A., & Schlipf, D. (2019). Wind turbine controller to mitigate structural loads on a floating wind turbine platform. *Journal of Offshore Mechanics and Arctic Engineering*, 141(6), 061901.

[13] Kong, X., Ma, L., Wang, C., Guo, S., Abdelbaky, M. A., Liu, X., & Lee, K. Y. (2022). Large-scale wind farm control using distributed economic model predictive scheme. *Renewable Energy*, 181, 581-591.

[14] Kong, X., Wang, X., Abdelbaky, M. A., Liu, X., & Lee, K. Y. (2022). Nonlinear MPC for DFIG-based wind power generation under unbalanced grid conditions. *International Journal of Electrical Power & Energy Systems*, 134, 107416.

[15] Xue, W. (2016). *Design, numerical modelling and analysis of a spar floater supporting the DTU 10MW wind turbine* (Master's thesis, NTNU).

[16] Al, M., Fontanella, A., van der Hoek, D., Liu, Y., Belloli, M., & van Wingerden, J. W. (2020, September). Feedforward control for wave disturbance rejection on floating offshore wind turbines. *In Journal of Physics: Conference Series (Vol. 1618, No. 2, p. 022048).* IOP Publishing.

[17] Ahn, H., & Shin, H. (2020). Experimental and numerical analysis of a 10 MW floating offshore wind turbine in regular waves. *Energies*, 13(10), 2608.

[18] Zhao, Z., Shi, W., Wang, W., Qi, S., & Li, X. (2021). Dynamic analysis of a novel semi-submersible platform for a 10 MW wind turbine in intermediate water depth. *Ocean Engineering*, 237, 109688.

[19] Xing, Y., Wang, S., Karuvathil, A., Balakrishna, R., & Gaidai, O. (2023). Characterisation of extreme load responses of a 10-MW floating semi-submersible type wind turbine. *Heliyon*, 9(2).

[20] Wang, L. B., Zhang, L., & Zeng, N. D. (2007). A potential flow 2-D vortex panel model: Applications to vertical axis straight blade tidal turbine. *Energy Conversion and Management*, *48*(2), 454-461.

[21] Roc, T., Greaves, D., Thyng, K. M., & Conley, D. C. (2014). Tidal turbine representation in an ocean circulation model: Towards realistic applications. *Ocean engineering*, *78*, 95-111.

[22] Badoe, C. E., Edmunds, M., Williams, A. J., Nambiar, A., Sellar, B., Kiprakis, A., & Masters, I. (2022). Robust validation of a generalised actuator disk CFD model for tidal turbine analysis using the FloWave ocean energy research facility. *Renewable Energy*, *190*, 232-250.

[23] Diab, H., Amara, Y., Hlioui, S., & Paulides, J. J. (2021). Design and realization of a hybrid excited flux switching Vernier machine for renewable energy conversion. *Energies*, 14(19), 6060.

[24] Osman, P., Hayward, J. A., Penesis, I., Marsh, P., Hemer, M. A., Griffin, D., ... & Herzfeld, M. (2021). Dispatchability, energy security, and reduced capital cost in tidal-wind and tidal-solar energy farms. *Energies*, 14(24), 8504.

[25] Derakhshan, S., Moghimi, M., & Motawej, H. (2018). Development of a mathematical model to design an offshore wind and wave hybrid energy system. *Energy Equipment and Systems*, *6*(2), 181-200.
[26] Wan, L., Gao, Z., & Moan, T. (2015). Experimental and numerical study of hydrodynamic responses of a combined wind and wave energy converter concept in survival modes. *Coastal Engineering*, *104*, 151-169.
[27] Mohanty, A., Viswavandya, M., Ray, P. K., & Mohanty, S. (2016). Reactive power control and optimisation of hybrid off shore tidal turbine with system uncertainties. *Journal of Ocean Engineering and Science*, 1(4), 256-267.
[28] Michele, S., Renzi, E., Perez-Collazo, C., Greaves, D., & Iglesias, G. (2019). Power extraction in regular and random waves from an OWC in hybrid wind-wave energy systems. *Ocean Engineering*, *191*, 106519.
[29] Perez-Collazo, C., Pemberton, R., Greaves, D., & Iglesias, G. (2019). Monopile-mounted wave energy converter for a hybrid wind-wave system. *Energy Conversion and Management*, 199, 111971.
[30] Perez-Collazo, C., Greaves, D., & Iglesias, G. (2018). A novel hybrid wind-wave energy converter for jacket-frame substructures. *Energies*, 11(3), 637.
[31] Lee, H., Poguluri, S. K., & Bae, Y. H. (2018). Performance analysis of multiple wave energy converters placed on a floating platform in the frequency domain. *Energies*, 11(2), 406.
[32] Li L., Gao Y., Yuan Z., Day, S., & Hu, Z. (2018). Dynamic response and power production of a floating integrated wind, wave and tidal energy system. *Renewable Energy*, 116, 412-422.
[33] Li L., Cheng Z., Yuan Z., & Gao, Y. (2018). Short-term Extreme Response and Fatigue Damage of an Integrated Offshore Renewable Energy System. *Renewable Energy*, 126, 617-629.
[34] Li L., Yuan Z M., Gao Y., Zhang, X., & Tezdogan, T. (2019). Investigation on long-term extreme response of an integrated offshore renewable energy device with a modified environmental contour method. *Renewable Energy*, 132, 33-42.
[35] Chen, M., Xiao, P., Zhou, H., Li, C. B., & Zhang, X. (2022). Fully Coupled Analysis of an Integrated Floating Wind-Wave Power Generation Platform in Operational Sea-states. *Frontiers in Energy Research*, *10*, 931057.
[36] Tian, W., Wang, Y., Shi, W., Michailides, C., Wan, L., & Chen, M. (2023). Numerical study of hydrodynamic responses for a combined concept of semisubmersible wind turbine and different layouts of a wave energy converter. *Ocean Engineering*, 272, 113824.
[37] Yang, Y., Bashir, M., Wang, J., Yu, J., & Li, C. (2020). Performance evaluation of an integrated floating energy system based on coupled analysis. *Energy Conversion and Management*, 223, 113308.
[38] Bayati, I., Belloli, M. A. R. C. O., Bernini, L. U. C. A., Mikkelsen, R., & Zasso, A. L. B. E. R. T. O. (2016, September). On the aero-elastic design of the DTU 10MW wind turbine blade for the LIFES50+ wind tunnel scale model. *In Journal of Physics: Conference Series* (Vol. 753, No. 2, p. 022028). IOP Publishing.
[39] Shin, H. (2011, June). Model test of the OC3-Hywind floating offshore wind turbine. In *ISOPE International Ocean and Polar Engineering Conference* (pp. ISOPE-I). ISOPE.
[40] Topper, M. B., Olson, S. S., & Roberts, J. D. (2021). On the benefits of negative hydrodynamic interactions in small tidal energy arrays. *Applied Energy*, *297*, 117091.
[41] Jonkman, J., Branlard, E., Hall, M., Hayman, G., Platt, A., & Robertson, A. (2020). Implementation of substructure flexibility and member-level load capabilities for floating offshore wind turbines in OpenFAST *(No. NREL/TP-5000-76822). National Renewable Energy Lab. (NREL)*, Golden, CO (United States).

[42] Zhang, Z., & Høeg, C. (2021). Inerter-enhanced tuned mass damper for vibration damping of floating offshore wind turbines. *Ocean Engineering*, 223, 108663.

[43] Dinh, V. N., & Basu, B. (2013). On the modeling of spar-type floating offshore wind turbines. *Key Engineering Materials*, 569, 636-643.

[44] Molland, A. F., Bahaj, A. S., Chaplin, J. R., & Batten, W. M. J. (2004). Measurements and predictions of forces, pressures and cavitation on 2-D sections suitable for marine current turbines. Proceedings of the Institution of Mechanical Engineers, Part M: *Journal of Engineering for the Maritime Environment*, 218(2), 127-138.

[45] Yang, Y., Bashir, M., Michailides, C., Li, C., & Wang, J. (2020). Development and application of an aero-hydro-servo-elastic coupling framework for analysis of floating offshore wind turbines. *Renewable Energy*, 161, 606-625.

[46] Yang, Y., Li, C., Zhang, W., Yang, J., Ye, Z., Miao, W., & Ye, K. (2016). A multi-objective optimization for HAWT blades design by considering structural strength. *Journal of Mechanical Science and Technology*, 30, 3693-3703.

[47] Bahaj, A. S., Molland, A. F., Chaplin, J. R., & Batten, W. M. J. (2007). Power and thrust measurements of marine current turbines under various hydrodynamic flow conditions in a cavitation tunnel and a towing tank. *Renewable energy*, 32(3), 407-426.

[48] Doman, D. A., Murray, R. E., Pegg, M. J., Gracie, K., Johnstone, C. M., & Nevalainen, T. (2015). Tow-tank testing of a 1/20th scale horizontal axis tidal turbine with uncertainty analysis. *International Journal of Marine Energy*, 11, 105-119.

[49] Nicholls-Lee, R. F., Turnock, S. R., & Boyd, S. W. (2013). Application of bend-twist coupled blades for horizontal axis tidal turbines. *Renewable Energy*, *50*, 541-550.

[50] Bastankhah, M., & Abkar, M. (2019). Multirotor wind turbine wakes. *Physics of Fluids*, 31(8).

[51] Ghaisas, N. S., Ghate, A. S., & Lele, S. K. (2020). Effect of tip spacing, thrust coefficient and turbine spacing in multi-rotor wind turbines and farms. *Wind Energy Science*, 5(1), 51-72.

[52] Hebbar, U., Rane, J. D., Gandhi, F., & Sahni, O. (2020). Analysis of interactional aerodynamics in multi-rotor wind turbines using large eddy simulations. *In AIAA Scitech 2020 Forum* (p. 1489).

[53] Stewart, G. M., Robertson, A., Jonkman, J., & Lackner, M. A. (2016). The creation of a comprehensive metocean data set for offshore wind turbine simulations. *Wind Energy*, 19(6), 1151-1159.

[54] Lee, D. H., & Jeong, Y. J. (2011). Integrated analysis of hydrodynamic motions and structural behavior of large-scaled floating structures using AQWA-ANSYS coupling. *Journal of the computational structural engineering institute of Korea*, 24(6), 601-608.

[55] Zou, Q., Lu, Z., & Shen, Y. (2023). Short-term prediction of hydrodynamic response of a novel semi-submersible FOWT platform under wind, current and wave loads. *Ocean Engineering*, 278, 114471.

[56] Ding, Q., Li, C., Yu, N., Hao, W., & Ji, J. (2018). Numerical and experimental investigation into the dynamic response of a floating wind turbine spar array platform. *Journal of Mechanical Science and Technology*, 32, 1106-1116.

[57] Jeon, S. H., Cho, Y. U., Seo, M. W., Cho, J. R., & Jeong, W. B. (2013). Dynamic response of floating substructure of spar-type offshore wind turbine with catenary mooring cables. *Ocean Engineering*, 72, 356-364.

[58] Matha, D., Sandner, F., Molins, C., Campos, A., & Cheng, P. W. (2015). Efficient preliminary floating offshore wind turbine design and testing methodologies and application to a concrete spar design. *Philosophical Transactions of the Royal Society A: Mathematical, Physical and Engineering Sciences*, 373(2035), 20140350.

[59] Yang, Y., Bashir, M., Michailides, C., Li, C., & Wang, J. (2020). Development and

application of an aero-hydro-servo-elastic coupling framework for analysis of floating offshore wind turbines. *Renewable Energy*, 161, 606-625.
[60] Ismaiel, A. (2023). Wind turbine blade dynamics simulation under the effect of atmospheric turbulence. *Emerging Science Journal*, 7(1), 162-176.
[61] Ye, X. W., Ni, Y. Q., & Ko, J. M. (2012). Experimental evaluation of stress concentration factor of welded steel bridge T-joints. *Journal of Constructional Steel Research*, 70, 78-85.
[62] Veritas, D. N. (2004). Design of Offshore Wind Turbine Structure. O*ffshore Standard DNV-OS-J101*.